CELLULOSE NANOCRYSTAL REINFORCED THERMOPLASTIC POLYURETHANE NANOCOMPOSITES

KHAIRATUN NAJWA BINTI MOHD AMIN

MOHAMMAD DALOUR HOSSEN BEG

KAMAL BIN YUSOH

NURUL SA'AADAH BINTI SULAIMAN

AAINAA IZYAN BINTI NAFSUN

RESEARCH VOTE NO:

RDU1603128

Faculty of Chemical & Natural Resources Engineering

Universiti Malaysia Pahang

2019

ACKNOWLEDGEMENT

First of all, thank you to Allah the almighty for His blessing and strength throughout this journey. My special appreciation and thanks goes to my teammates, Assoc. Prof. Dr. Kamal, Assoc. Prof. Dr. Dalour, Dr. Sa'aadah and Dr. Izyan for their support, advice and valuable knowledge in this project. Many thanks to Faculty of Chemical and Natural Resources, (FKKSA), Centre of Excellence for Advanced Research in Fluid Flow (CARIFF) and Central Laboratory (CenLab) for helping the team in completing the experiments and characterisation. Infinity thanks also goes to Universiti Malaysia Pahang for the opportunity to conduct this research with the fund.

My fullest appreciation goes to my all the undergraduate (Raja, Hanif, Diyana, Fadhlullah, Ros Syazuin) and postgraduate (Muhammad Arif Fahmi) students which were supervised under this fund in helping, knowledge contribution and support through this study.

Thank You.

ABSTRACT

Thermoplastic polyurethane (TPU) is one of the most widely used thermoplastic elastomers (TPE) due to its high strength and tear resistance, good elasticity, flexibility and damping properties. Enhancement of TPU properties can be achieved by either varying the hard-soft segment composition ratio or by the reinforcement with micro or nanoscale fillers. In the last decade, cellulose nanocrystals (CNC) have gained an increasing degree of interest from both academics and industries as 'sustainable nanomaterials', as they have high-axial mechanical properties and reinforcing capability, abundance, low density, renewability and biodegradability. Contemporary research activities centred on the reinforcement of TPU with CNC have typically employed solvent-based fabrication methods (solution/wet casting). For the successful translation of this new class of nanocomposite materials from laboratory research to widespread applications, processing via scalable approaches has to be demonstrated. The utility of CNC as TPU reinforcers has also been limited by the poor thermal stability of CNC, which are typically isolated via acid hydrolysis, as well as the poor quality of dispersion achieved when more scalable methodologies are used (eg. melt compounding). Thus, this study firstly aims to explore, optimise and develop CNC with enhanced thermal stability, and secondly, to incorporate these more thermostable CNC into high performance TPU nanocomposites via scalable melt-compounding method. The report is presented in two main parts. The first part is focused on the production/isolation of CNC with enhanced thermal stability. CNC has been isolated via two methods, acid hydrolysis using mild acid and a scalable high energy bead milling process. Both processes have been optimised to isolate CNC with requisite thermal stability and dispersibility for TPU host polymers. The second part is focused on the processability of CNC into the TPU matrix via an intermediate-scale traditional twin screw extrusion melt compounding method as well as masterbatch process to improve the dispersibility of CNC in TPU. The main outcomes or observations from this study are:

- Isolation of CNC with enhanced thermal stability and dispersibility via mild, mixed acid hydrolysis and mechanical method.
- Improved dispersibility using masterbatch process in incorporating CNC and TPU which is suitable to be implied for industrial scale.

- The performance of the host TPU matrix, a “workhorse” aromatic polyether grade, is remarkably enhanced by the incorporation strategies reported, without negatively affecting the important elastic properties and compliance of the TPU.

ABSTRAK

Poliuretana termoplastik (TPU) adalah salah satu daripada elastomer termoplastik (TPE) yang paling banyak digunakan kerana kekuatan tinggi dan rintangan lusuh, keanjalan yang baik, fleksibiliti dan sifat redaman. Peningkatan sifat-sifat TPU boleh dicapai dengan mengubah nisbah komposisi segmen keras-lembut atau dengan tetulang dengan pengisi mikro atau nano. Pada dekad yang lalu, selulosa nanokristal (CNC) telah mendapat minat yang semakin meningkat dari ahli akademik dan industri sebagai bahan nano, kerana mempunyai ciri-ciri mekanikal yang tinggi dan keupayaan pengukuhan, kelimpahan, kepadatan yang rendah, dan keupayaan biodegradasi. Aktiviti penyelidikan kontemporari yang berpusat pada penguatan TPU dengan CNC biasanya menggunakan kaedah fabrikasi berasaskan pelarut. Untuk kejayaan terjemahan kelas bahan nanokomposit baru ini dari penyelidikan makmal ke aplikasi yang luas, pemprosesan melalui pendekatan berskala tingi perlu ditunjukkan. Kelebihan CNC sebagai penguat TPU juga telah dibatasi oleh kestabilan terma CNC yang rendah terutamanay yang dihasilkan melalui hidrolisis asid, serta kualiti penyebaran yang rendah dicapai apabila metodologi yang lebih berskala besar digunakan. Oleh itu, kajian ini bertujuan untuk meneroka, mengoptimumkan dan membangunkan CNC dengan kestabilan terma yang lebih baik, dan kedua, untuk memasukkan CNC yang mempunyai sifat terma yang lebih baik ini ke dalam nanokomposit TPU melalui kaedah biasa dan *masterbatch*. Laporan penyelidikan ini dirangka kepada dua bahagian utama. Bahagian pertama difokuskan pada penghasilan CNC dengan kestabilan haba yang dipertingkatkan. CNC dihasilkan melalui dua kaedah, hidrolisis asid menggunakan asid ringan dan proses mekanikal yang berskala besar. Kedua-dua proses ini telah dioptimumkan untuk menghasilkan CNC dengan kestabilan haba dan dispersibility terma bagi polimer tuan rumah TPU. Bahagian kedua difokuskan pada kebolehprosesan CNC ke dalam matriks TPU melalui kaedah pengkompaunan skru berkembar tradisional skala sederhana dan proses *masterbatch* untuk meningkatkan dispersibiliti CNC dalam TPU. Hasil atau pemerhatian utama dari kajian ini adalah:

• Penghasilan CNC dengan kestabilan haba dan *dispersibility* melalui hidrolisis asid ringan.

• Pengacakan yang lebih baik menggunakan proses *masterbatch* yang menggabungkan CNC dan TPU yang sesuai untuk digunakan untuk skala perindustrian.

• Prestasi matriks TPU dengan gred polyether aromatik "workhorse", dapat ditingkatkan dengan signifikan sekali oleh strategi penggabungan yang dilaporkan, tanpa memberi kesan negatif kepada ciri-ciri elastik asal TPU.

TABLE OF CONTENTS

LIST OF TABLES

LIST OF FIGURES

LIST OF SYMBOLS

℃	Degree Celsius
wt.%	Weight percentage
v/v	Volume/volume

LIST OF ABBREVIATIONS

ABS	Acrylonitrile butadiene styrene
ATR	Attenuated total reflectance
CNF	Cellulose nanofibre
CNF	Cellulose nanofibril
CNC	Cellulose nanocrystal
CNT	Cellulose nanotubes
DSC	Differential scanning calorimetry
FTIR	Fourier transform infrared spectroscopy
GNP	Graphite nano-platelets
MCC	Microcrystalline cellulose
TPU	Thermoplastic polyurethane
TPU/MCC-1.0	1.0wt. % of microcrystalline cellulose reinforced TPU
TPU/MCC-3.0	3.0wt. % of microcrystalline cellulose reinforced TPU
TPU/MCC-5.0	5.0wt. % of microcrystalline cellulose reinforced TPU
SEM	Scanning electronic microscopy
PP	Polypropylene
PU	Polyurethane
PLA-PHB	Polylactic acid/poly-hydrobutyrene
PVA/CNF	Polyvinyl alcohol/cellulose nanofibril

CHAPTER 1

INTRODUCTION

1.1 Background of Study

The invaluable properties of thermoplastic polyurethane (TPU) such as high elasticity, flexibility and damping ability have made TPU one of the most widely used thermoplastics for a wide range of applications.[1] The enhancement of certain properties of TPU can be achieved by the incorporation of various reinforcing fillers, such as carbon nanotubes, nanoclay, nanocellulose,silica,[2] either at microscale or nanoscale dispersion length scales. The incorporation of nanoscale fillers, even at low fractions (<5 wt. %), into TPU matrices has given rise to some remarkable improvements in the mechanical properties, thus sparking an interest in their further development with respect to cost and processing.[3] However, some of the remnant key issues associated with the incorporation of these nanofillers are discoloration or compromised appearance of the polymer composites[4] (black in the case of carbon nanotubes, and an earthy taint in the case of natural layered silicates) and their poor processability at commercial scale and at a cost acceptable to the market.

There has been a growing concern regarding the environmental impact and economy of fossil feedstock and a demand for products made from renewable and sustainable resources. During the last decade, nanoscale particles from renewable resources have been sought as sustainable nanofillers for reinforcing polymers. Cellulose, which is a homopolymer of D-glucose, is the most abundant polymer in nature, representing the main structural component of plants. Cellulose at the nanoscale level in native fibres possesses very high crystallinity, mechanical properties and transparency. By deconstructing to the nanoscale level different types of nanoparticles can be produced, including rod-like cellulose nanocrystals (CNC), which were previously known as cellulose nanowhiskers. CNC have high-axial mechanical properties and reinforcing capability, abundance, low density, renewability and biodegradability which make them ideal candidates for incorporation into polymer matrices.[5]

Recently, several researchers have reported some remarkable reinforcement of TPU through the incorporation of CNC. However, most of the polymer processing methods utilised in these studies have been solvent-based i.e. in-situ solution polymerisation and solution casting.[6] In order to achieve the widespread application of thermoplastic polyurethane nanocomposites at the industrial scale, processing has to be demonstrated either by conventional polymer processing techniques or new methods. To address this challenge, this research focuses on identifying the limitations, both with CNC nanofillers as well as TPU-CNC nanocomposite processing, and investigating new and different approaches for industrial scale processing of TPU/CNC nanocomposites. 1.3 Problem Statement

1.2 Problem Statement

Contemporary research activities regarding TPU/CNC nanocomposites are based mostly on the solution/wet casting method. The literature on the processing of TPU/CNC via the melt compounding method is very limited. We know that this poor processability using conventional processing methods (melt compounding, extrusion and moulding) is associated with low CNC thermal stability and non-optimised dispersibility or compatibility with TPU host polymers. The CNC produced via sulphuric acid hydrolysis exhibit low thermal stability, as the sulphate groups on the cellulose promote dehydration/degradation reactions. Hence the isolation of CNC with enhanced thermal stability is required using either a solvent or solvent-free method. CNC obtained using a mild acid hydrolysis or "acid-free" mechanical methods can be expected to retain thermal stability.

To fully exploit the reinforcement potential of CNC, high quality dispersion in the polymer matrix is vital and, for TPU, conventional solvent methods have been found to show a high degree of dispersion. Thus, in this work, approaches for improving the dispersibility of CNC using melt processing will be investigated. To obtain high performance in TPU nanocomposites, the interactions between CNC and TPU segments must be investigated. Hence, this study will focus on the comprehensive evaluation of the structure-property relationships of TPU/CNC nanocomposites. The outcomes of this work will demonstrate not only the potential of CNC with enhanced thermal stability and dispersibility as very attractive nanofiller candidates, but also that scalable processing of TPU/cellulose nanocomposites can potentially be used in various applications.

1.3 Objectives

This research aims to explore, optimise and develop cellulose nanocrystal (CNC) reinforced thermoplastic polyurethane (TPU) nanocomposites primarily via scalable melt compounding and reactive extrusion processing methods. In order to achieve this main objective, this project was divided into three specific objectives:

a) To isolate CNC with good thermal stability, dispersibility and high scalability suitable for melt compounding processing.
b) To achieve high quality dispersion of CNC in a TPU matrix and in the polyol precursors in the case of melt-compounding.
c) To demonstrate a full understanding of TPU/CNC nanocomposite processing-structure-property relationships.

1.4 Scopes of Study

The scope of the study for this research are:

i) CNC was isolated using acid hydrolysis and high energy bead milling method.
ii) Acids used were sulphuric acid and phosphoric acid.
iii) The parameters varied for acid hydrolysis is the ratio of two acids.
iv) The parameters varied for high energy bead milling method is concentration of MCC and milling time.
v) The weight percentage of CNC in TPU matrix was in the range of 0.5 to 5 wt.%.
vi) Characterization methods for CNC are SEM, TEM, FESEM and TGA.
vii) Characterization methods for TPU nanocomposite films are FESEM, DSC and mechanical testing.

CHAPTER 2

LITERATURE REVIEW

2.1 Thermoplastic polyurethanes (TPU)

Thermoplastic polyurethanes (TPU) are a unique category of plastics developed in 1937 as versatile polymers which are soft and processable when heated, hard when cooled and capable of being reprocessed multiple times without losing structural integrity. They have been used either as malleable engineering plastics or as replacements for hard natural rubber. Since TPUs offer the same mechanical properties as rubber and can be processed as thermoplastics, they also have been described as "bridging the gap between rubber and plastics" by the Alliance for the polyurethane industry. Other important attributes include their ability to resist oil, grease, solvents, chemicals and abrasion[7]. Hence, TPUs have been used for various applications such as medical devices, [8] coatings, [9] [10] automotive parts, cable insulation as well as toughening additives.[11] TPUs are multi-phase block copolymers that are obtained via classical chemical reactions between three basic components, polyols, diisocyanates and chain extenders. Figure 2.1 illustrates the typical chemical structure and the resulting morphology of a TPU made up of linear primary chains composed of alternating hard and soft segments connected end-to-end through strong, covalent urethane linkages.[12]

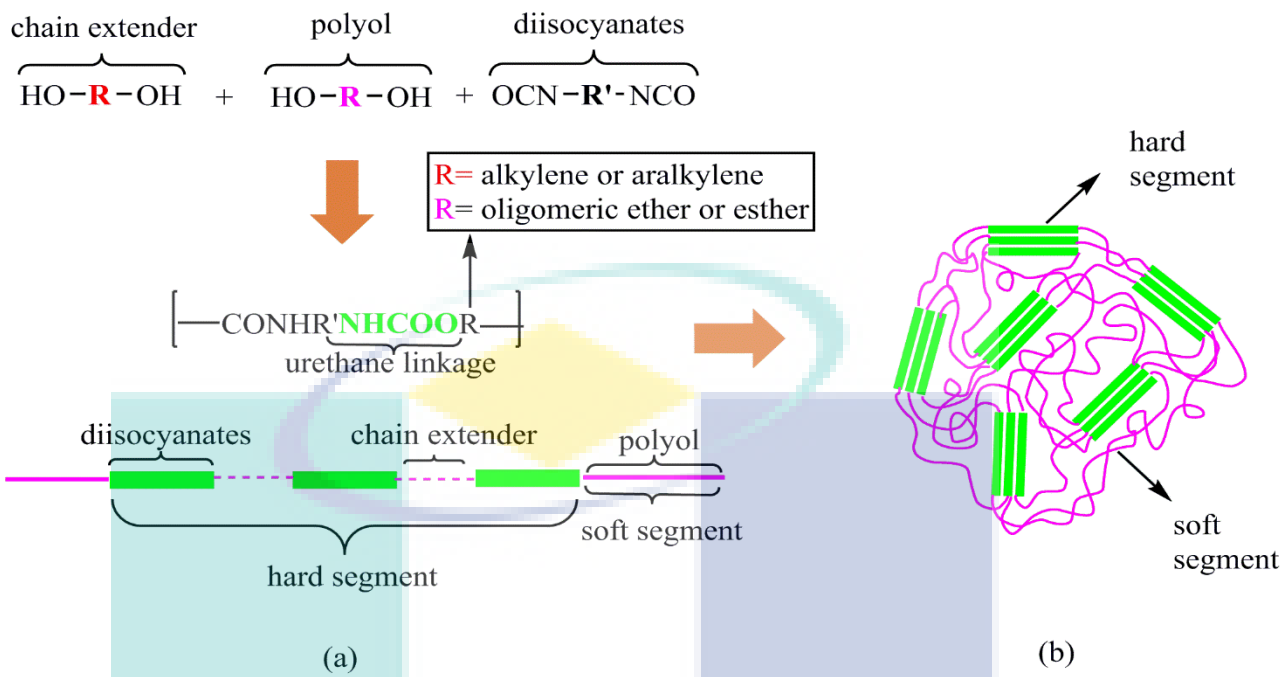

Figure 2.1. (a) General chemical structure and (b) morphology of thermoplastic polyurethane (TPU).

In TPU copolymers, hard segments which comprise alternating diisocyanate and short diol chain extender residues are responsible for imparting the stiffness and toughness to the material, while soft segments (polyols) impart the resilience, extensibility and flexibility.[13] In the hard segments, both aliphatic and aromatic diisocyanates can be used during the synthesis of TPUs. Aliphatic isocyanates, such as hexamethylene diisocyanates (HDI), are commonly used for PU applications as they display good biocompatibility and have the ability to degrade into non-toxic decomposition products.[14] Aromatic isocyanates used in TPU production include methylene diphenyl diisocyanates (MDI) and toluene diisocyanates (TDI). MDI is often preferred because of its symmetric structure and therefore potential to phase separate into reasonably stable crystalline or paracrystalline domains at a lower temperature.[15] The common polyols used are polyether and polyester polyols. About 90% of commercial polyurethane elastomers are polyether–based products due to their very good oxidative and hydrolytic stability, high tensile and tear strength, good abrasion resistance, ease of fabrication and low cost.[16] The most common chain extender used in polyurethane synthesis is 1, 4-butanediol (BDO).[17] BDO is able to confer superior tensile strength and rebound elasticity to the TPU matrix in the appropriate combination of isocyanates and polyol groups.[18]

Generally, polyurethanes are synthesised in the laboratory or small batch production runs using two approaches, namely, the prepolymer method and the 'one-shot' method.[19] In the prepolymer approach, isocyanates terminated 'prepolymer' will first be synthesised by reacting excess diisocyanates with the polyol and then a chain extension of the prepolymer will be performed through a reaction with a short organic diol to obtain a high molecular weight PU. By adjusting the pre-polymerisation conditions, it is possible to synthesise TPU with the range of desired properties. In the second approach, the 'one-shot' method, the polymerisation occurs by mixing all the reactants (diisocyanate, polyol, and chain extender) together in the desired stoichiometric ratio.[15a] Usually, this method is preferred when the use of any solvents is restricted. Sometimes, this method is limited as the precise control of the chain structure is difficult. [17] At large commercial scale the major TPU producers such as Lubrizol, Bayer Materials Science and BASF employ reactive extrusion. In this process temperature-controlled tanks of ultra-dry polyol, diisocyanate and chain extender are accurately metred into a twin screw extruder where the conditions of heat and shear can be carefully controlled to produce high quality TPU extrudates at high speed. One of the primary advantages of this process is the ease of incorporating micro or nano fillers, as will be exemplified in Chapter 8.

2.2. Performance enhancement by reinforcement of nanofillers

There are two main methods used to tailor the desired physical, mechanical and thermal properties of TPU. The first relies on the variation in the soft and hard segments by formulating different isocyanate/polyol ratios and altering the composition of the chain extender. Via this method, the phase separation strongly influences the resultant properties. The second method is based on classical reinforcement of TPU by incorporating different fillers at both micro- and/or nanoscale-levels.[13] A similarity between the reinforcing action of externally incorporated fillers in general purpose rubbers and the function of the rigid segments within polyurethanes has been highlighted, indicating that TPU can be regarded as self-reinforcing polymers.[20] However, by incorporating fillers it has been found that it is possible to further extend the typical property profiles of polyurethanes. For instance, the use of nickel zinc ferrite[21] was found to improve dielectric and magnetic properties. The (micro to nanoscale) particles of calcium carbonate,[22] aluminum hydroxide,[23] kaolin,[24] titanium dioxide,[24] zinc oxide,[25] silica,[26] carbon[27] and cellulose were reported to improve mechanical properties and similarly metallic fillers[28]

to improve acoustic properties. Due to their high surface area for interactions, stress transfer and very high individual mechanical properties, nanoscale fillers have been recently explored for polymer reinforcement. They can be obtained in different types and shapes, for instance, nanoparticles, nanofibres, nanotubes, fullerenes, and nanowires based on their physical dimensions and geometry as illustrated in Figure 2.2.[3]

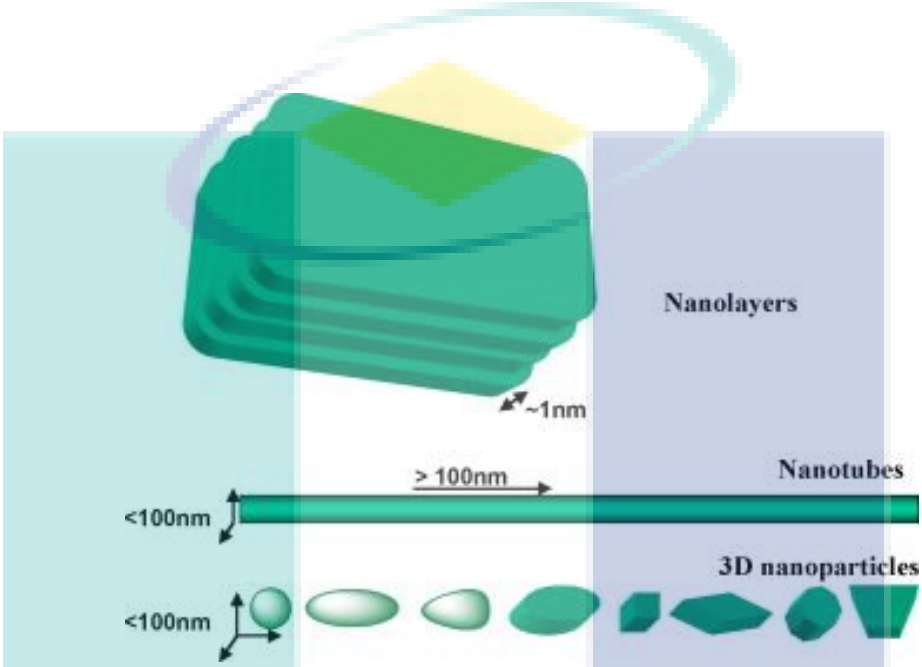

Figure 2.2 Different types of nanoscale particles for polymer reinforcement. Reproduction of image from[29] with permission from Elsevier.

Of the many nanoscale fillers, the most commonly used in TPU nanocomposites are carbon and clay. Carbon nanomaterials can be produced on a commercial scale and obtained from the market in different morphologies such as graphene/graphite nano-platelets (GNP), carbon nanofibres (CNF) and carbon nanotubes (CNT). Carbon nanomaterials are favoured for their unique mechanical properties, superior thermal conductivity and relatively low density.[30] This has been demonstrated by a few researchers who, by using low volume fractions (0.5 – 10 wt. %), managed to increase the conductivity properties of the TPU matrix and significantly improved the mechanical properties as well.[31]

Apart from carbon, clay is also one of the most common nanofillers used to reinforce the polymer matrix. By reinforcing polymers with clay minerals such as 2:1 layered silicates, different morphologies of polymer/clay nanocomposites can be produced, as illustrated in Figure 2.3. These clays can be combined with substances of a dissimilar type, such as

neutral, cationic, anionic organic molecules or biological molecules, to form materials with novel functions. Due to this attribute, clay has received much attention from the scientific and technological communities for use in the fabrication of polymer nanocomposites. Clays are able to improve mechanical, thermal, barrier and flame-retardant properties and are viewed as promising fillers in materials destined for the automotive, aerospace and packaging industries.[32]

Various types of clay have been used to reinforce TPU polymers, including montmorillonite, sepiolite and rectorite.[33] Since clay is an organophilic filler, it has always been modified with different surfactants or coupling agents before its incorporation with TPU. It has been claimed that TPU has a good affinity for the polar surface of silicate layers which may assist clay dispersion at different levels from immiscible to intercalated and exfoliated morphologies as illustrated in Figure 2.3(b). This has been found to significantly contribute to the improvement of properties (mechanical, gas barrier, thermal etc.) in TPU nanocomposites.[33a, 34]

In a nutshell, by incorporating nanofillers into TPU, it is possible to reduce the cost of production, increase the tensile strength and the stiffness of a material depending on processing methods. The increases in stiffness for conventional TPU composites are typically associated with compromising the elastic properties (reduced elongation, resilience and toughness) and optical properties (discoloration or opacity).[35]

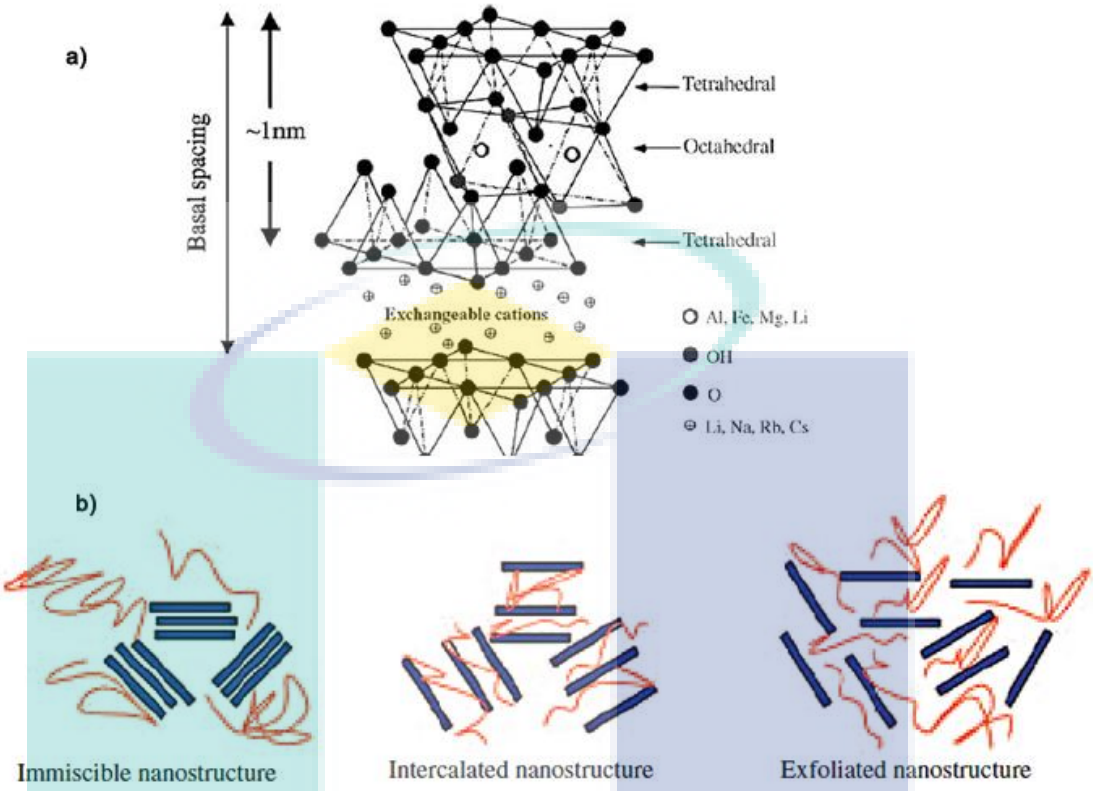

Figure 2.3. Schematic diagram of a) clay structure and b) nanoclay dispersion in a polymer matrix. Reproduction of image from[36] with permission from SAGE publications.

The key issues associated with the incorporation of the inorganic nanofillers are the discoloration or compromise in the appearance of the polymer composites[4] (black in the case of carbon nanotubes, and an earthy taint in the case of natural layered silicates) and poor processability at low cost. There has been growing concern about the environmental impact and economy of fossil feedstock and demand for products made from renewable and sustainable resources. Since the last decade, nanoscale particles from renewable resources have been sought as sustainable nanofillers for reinforcing polymers.

2.3 Cellulose nanocrystals – A sustainable nanomaterial

Cellulose which is a polysaccharide is the most abundant polymer in nature, representing the main structural component of plants. Cellulose can be found in the cell walls of plants, particularly in the stalks, stems, trunks and all woody portions.[37] In 1838, cellulose was first discovered and extracted by Anselme Payen.[38] Since then, extensive studies of its physical and chemical properties have been undertaken. Cellulose is a linear chain of

ringed glucose molecules and the repeat unit consists of two anhydroglucose rings $(C_6H_{10}O_5)_n$ where n = 10 000 to 15 000 depending on the cellulose source (Figure 2.4.).

Linear syndiotactic homopolymer of anhydroglucose are formed via β-(1→4) glycosidic linkage.[39] Due to the inter- and intra-molecular hydrogen bonding and the linearity of the chains, they form well packed and highly crystalline fibrillar structure at the nanoscale level in the native biomass.[40] A natural form of cellulose, *cellulose-I*, has a crystal structure consisting of two types of polymorph, cellulose Iα and Iβ, which vary in proportions depending on the source. [41] Cellulose Iα can be found predominantly in bacteria[42] and algae[43], whereas Iβ dominates in marine invertebrates (tunicates) and plant cell walls.[44] As illustrated in Figure 2.4, cellulose consists of regions that are highly ordered (crystalline - as fibrillar bundles, nanofibrils, nanocrystallites) and regions that are more disordered nano-domains (amorphous). [39b, 45] The portion of crystalline domains in the cellulose varies from 65 to 95 % depending on the source. [46]

These crystalline structures at nanoscale level in the native fibres possess very good mechanical properties and exhibit transparency. By deconstructing microfibres to the nanoscale, the different types of nanoparticles can be produced. Based on their dimensions, they can be classified as rod-like cellulose nanocrystals (CNC), which were previously known as whiskers and as filament-like nanofibres, (CNF), also called micro-/nano-fibrillated cellulose (MFC /NFC).

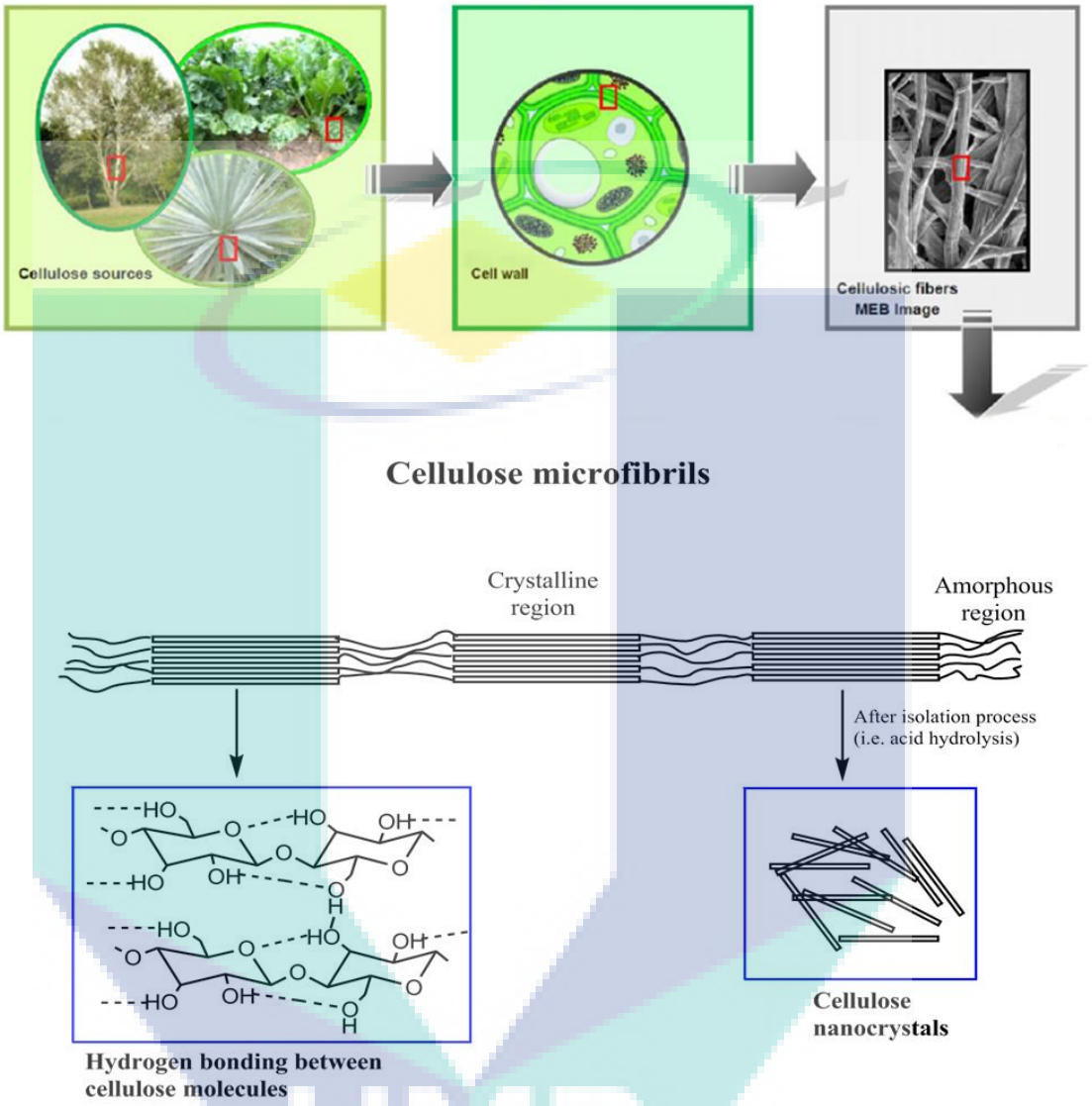

Figure 2.4. Schematic diagram of cellulose structure and cellulose microfibrils. Image reproduced from [47] with permission from Elsevier.

The rigid-rod like CNC can be typically extracted from plants like jute, cotton, ramie, and wood, and also from biomass residues such as agricultural crops. In addition, they also can be produced by bacteria and, in rare cases, found in sea creatures like tunicates.[48] The first colloidal suspension of cellulose was isolated in the 1950's via sulphuric acid-catalysed degradation of cellulose fibres.[49] Later, Marchessault et al.[50] found that a colloidal suspension of CNC took the form of a nematic liquid crystalline alignment after

optimisation using an acid hydrolysis process, and the dried suspension exhibited aggregates of needle-shaped particles.

Recent findings have proposed CNC to be among the most promising new nanoscale building blocks for next generation biomaterials and engineering applications due to their renewable origins, combined with low toxicity and unique physical properties.

2.3.1 Isolation of cellulose nanocrystal (CNC)

The isolation of cellulose nanocrystals from any lignocellulosic source or marine animals involves two steps. The first is to purify the source by regular pulping pre-treatments, and mechanical grinding and refining. In the pre-treatments for wood and plants, the removal of matrix materials like hemicellulose and lignin, completely or partially, is undertaken to obtain a pure form of cellulose. The second step is to isolate or liberate the crystalline domains as particles from the "purified" cellulose materials. This process can be performed in three different ways, namely, chemical/biological (for instance acid hydrolysis and enzymatic treatments), or mechanical treatment (such as ultrasonication,[51] homogenisation,[85, 86] refining, grinding, milling, and cryocrushing [52]) or the combination of these methods.

The most commonly reported method is acid hydrolysis using sulphuric acid, as the highly crystalline, rigid rod-like CNC are obtained in high production yield, which makes them suitable for polymer reinforcement applications. This method introduces sulphate charges on the surface of CNC and prevents agglomeration, thus promoting good dispersion in water.[53] A typical acid process involves acid hydrolysis reaction at controlled conditions (of time, temperature and concentration), centrifugation, dialysis process, ultrasonication and freeze drying of the suspension.[5a] In this process, amorphous and paracrystalline regions are preferentially hydrolysed. The crystalline parts of the cellulose, which have a higher resistance to acid attack, remain undamaged.[45b, 54] Similarly, acid hydrolysis using hydrochloric acid can generate a similarly shaped CNC as achieved using sulphuric acid, but its dispersibility is a limitation as the suspension tends to flocculate.[55] Other types of acids, for instance phosphoric,[56] formic,[57] and hydrobromic[58] acids, have also been used to isolate the CNC. However, the use of acid in the extraction process has disadvantages,

such as corrosivity and environmental hazards associated with a high energy demand, and can cause cellulose degradation.[51]

A range of CNC with different dimensions (aspect ratios) and morphology could be obtained depending on the source and the isolation methods used, as displayed in Table 2.1. The common cellulose source used to isolate the CNC, especially at the laboratory scale, is cotton, due to its high cellulose content.[59]

Table 2.1 Overview of the isolation method and the dimension of CNC obtained from different sources.

Source of Cellulose	Isolation method	Dimensions		Reference
		L (nm)	*w* (nm)	
Wood pulp	Acid hydrolysis	100-300	3-5	[60]
	Enzymatic hydrolysis	100-1800	30-80	[61]
	Chemical-mechanical	65	15	[62]
Cotton	Acid hydrolysis	70-160	15	[63]
	Microbial hydrolysis	120	40	[64]
Tunicates	Acid hydrolysis	1000-10000	3-20	[65]
Bacteria	Acid hydrolysis	250-1000	16-54	[66]
	Enzymatic hydrolysis	100-300	10-15	[67]
Agriculture crops (coconut husk fibres, rice straw, banana stem etc.)	Acid hydrolysis	177-200	5-7	[68]
	Chemical-mechanical	-	5-40	[69]
	Mechanical	-	3.5-60	[70]

Furthermore, various shapes of CNC can be produced, such as rods and spheres.[71]

2.3.2 CNC as potential reinforcing fillers

Early-stage developments on the polymer nanocomposites with cellulose nanocrystals and nanofibres have shown dramatic improvements in the mechanical properties of nanocomposites.[72] For the last 15 years, nanocellulose has been studied as a reinforcing element in nanocomposites.[46] One of the most desirable features of CNC is the hydroxyl groups on the surface of the nanocrystals. The abundance of OH groups favours the formation of hydrogen bonding, causing the cellulose chains to assemble into highly ordered structures. These reactive hydroxyl groups will interact with the functional groups of other molecules, and are valuable for tailoring the functional properties of CNC.[73] Moreover, the physical properties of CNC are superior to other engineering materials (Table 2.2) and, indeed, these features represent compelling criteria as advanced reinforcing or functional fillers for polymer nanocomposites. CNC also have a lower density with a high modulus.[74]

Table 2.2 Properties of various materials compared to cellulose.

Type of material	Modulus (GPa)	Specific modulus (GPa cm^3/g)	Density (g/cm^3)	References
Aluminium	62	23	2.7	[75]
Steel	200	25	7.8	[75b, 76]
Glass Fibre	73	28	2.6	[77]
Cellulose nanocrystals	110-220	138	1.6	[39b]

A good aspect ratio (length/diameter) value also contributes to its reinforcing abilities which enable a critical length for stress transfer from the matrix to the reinforcing phase.[2c] Furthermore, CNC are biologically renewable, sustainable, low cost, combustible, non-toxic and have biodegradable properties.[78] CNC was also used as a reinforcing filler for the composite in many other applications like barrier films, transparent films, flexible displays, biomedical implants, separation membranes, supercapacitors and templates for electronic components.[39b] Many researchers have demonstrated the potential of CNC by incorporating it into various polymer matrices (polypropylene,[79] polyethylene,[80]

polyvinyl alcohol,[81] poly(lactic acid)[82]). The nanocomposites obtained demonstrated improvements in mechanical properties. In particular, CNC also display an outstanding potential in for increasing the composite material properties at low concentrations.[83] CNC is also unique in their capacity to maintain the transparency of the host material.[84]

2.4 Cellulose reinforced polymer nanocomposites

2.4.1 Processing of cellulose reinforced polymer nanocomposites

The successful processing of polymer nanocomposites depends heavily on the chemical, physical and thermal properties of the polymer matrices, polymer-filler interactions and the processing methods. Nanocomposites with cellulose nanocrystals (CNC) can be processed via four different pathways as illustrated in Figure 2.5.[85] The first and most common is the '*solution method'* or *'solvent casting method'* in which CNC is first dispersed in a solvent in which the host polymer is also soluble or dispersible in latex form, followed by casting and drying (evaporation of solvent).[46, 86] However, this method has disadvantages with respect to production speed, production costs and film quality (CNC tends to re-aggregate).[87]

In the second, '*in-situ polymerisation'*, CNC is dispersed well in the monomers (with or without the use of solvent) and subsequently polymerised/cured further to obtain the nanocomposites.[88] The presence of cellulose in the pre-polymerisation state of TPU encourages a chemical bonding with the polymer matrices.[89] Cao et al.[90] prepared waterborne polyurethane with nanocellulose via an *in-situ* polymerisation method and managed to obtain a significant improvement in overall stiffness and strength. Despite the improvement in mechanical properties, it was found that the nanofiller could negatively impact upon on the polymer molecular weight and crosslink density, thereby offsetting the potential benefits from the addition of nanofillers.[91]

The third method is based on a solvent exchange *sol-gel process*, where a template of CNC through percolating network is first formed from a homogeneous dispersion of CNC by successive solvent exchange with the solvent in which CNC are not dispersible and the polymer/monomer is then imbibed into it.[92] This method is commonly used with the purpose of reducing the surface energy of nanofillers, thus improving their dispersibility/compatibility with non-polar media.[93] It is versatile and becomes very

important for achieving a high level of dispersion (even in hydrophobic polymers) and transport properties where the percolating network of CNC plays a vital role. However, solvent exchange is a relatively slow processing method and requires a large energy recovery expenditure in order to recover the solvents.[94] Furthermore, it is not an environmentally friendly method.[95]

The fourth method is a conventional '*melt blending*' method where CNC can be melt blended with any polymer whose softening or melting temperature is below the degradation temperature of the CNC used. To alleviate the poor dispersion, surfactants or compatibilisers are very often used, especially with most common non-polar, hydrophobic polymer matrices.[96] This method is preferred by the industry as it is economically viable and environmentally friendly (almost zero usage of solvents). The melt compounding method simplifies TPU fabrication compared with other methods, which are complex and time consuming. Despite the remarkable improvements in the field of cellulose reinforced polymer nanocomposites, the transition from laboratory to widespread application can be achieved only through industrial scale production at a favourable cost/performance ratio.

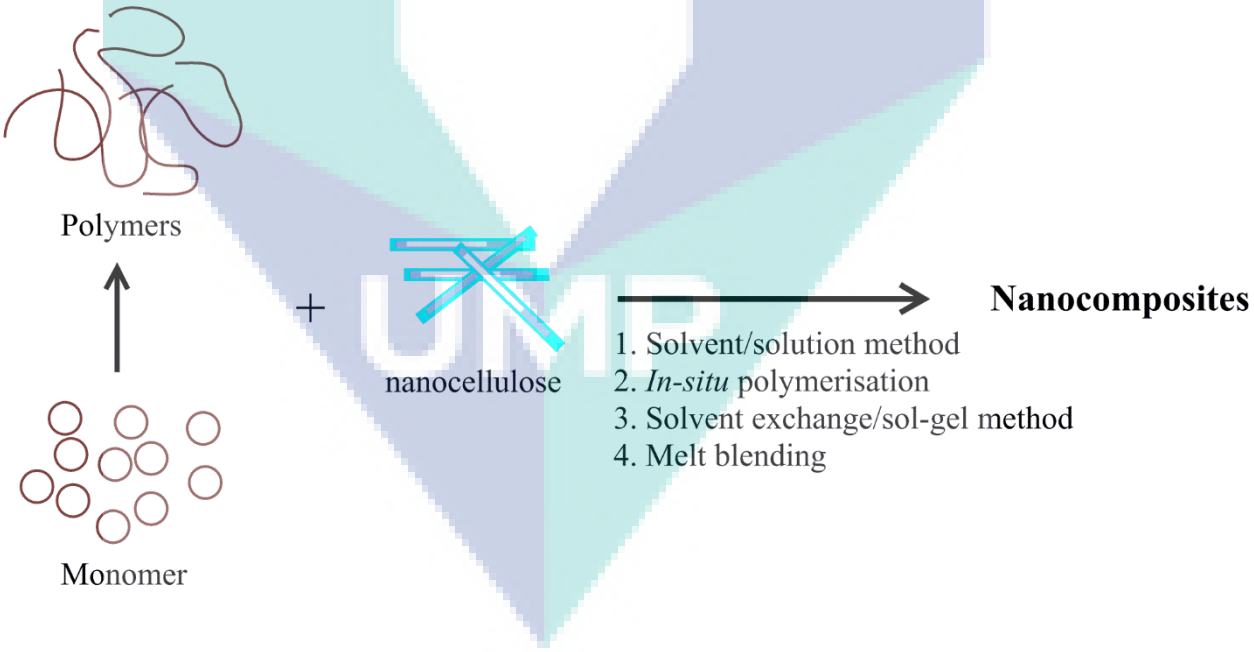

Figure 2.5 General schematic diagram of processing of TPU nanocomposites.

In reactive extrusion, an extruder is used as a chemical reactor for the polyurethane synthesis or polymerisation process. The main advantages of the reactive extrusion method, are that it is a continuous process, has a large heat transfer area and it is economic,

as devolitilisation of the reaction product in the extruder makes it possible to recycle unreacted components. However, instabilities during polymerisation due to large viscosity changes may result in very low conversion or fluctuating throughput. Furthermore, as the extruder is acting as a reactor, it is desirable for the residence time of the reaction to be short, though inadequate residence time will negatively impact upon the reaction conversion.[97] Nonetheless, it can be considered as one of the best methods for the production of TPU/CNC nanocomposites on a large scale due to their low environmental impact and processing time. No studies related to CNC via reactive extrusion have yet been undertaken. However, other studies using polyurethane and prepared via reactive extrusion have demonstrated the benefits of this method. For instance, Cai et al.[98] reported the production of TPU via reactive extrusion reinforced with nanoclay. The TPU nanocomposite obtained displayed an increase in tensile strength of 25% and showed good nanoclay dispersion in the TPU matrix. A study by Imre et al.[99] of poly(lactic acid)/polyurethane blends prepared by reactive extrusion also showed favourable results, supporting the notion that reactive extrusion is a convenient, cost-effective and environmentally friendly method for achieving blends with improved properties.

2.4.2 Cellulose nanocrystal reinforced thermoplastic polyurethane nanocomposites

Wu et al.[100] reported that polyurethane (PU) nanocomposites reinforced with microcrystalline cellulose (MCC) particles were prepared via in-situ solution polymerisation. This study demonstrated that significant improvements in stiffness, strain-to-failure, and strength are possible with the assistance of "pre-swelling" in a DMF solvent combined with two-step solution polymerisation. For example, at an optimum concentration (5 wt. %) of MCC, the tensile strength was improved three-fold, albeit from a very modest baseline, from 8 MPa to 24 MPa, whereas the 'conventional' solution polymerised cellulose composite failed to significantly improve tensile strength (8 MPa to 9 MPa), but still resulted in significant stiffening.[100] These contrast results were attributed to the differences in solution processing affecting the degree of in-situ defibrillation of MCC (bundles) into nanofibres and, in turn, enhanced the stress transfer because of the nano-scale reinforcement.

In another study, nanocomposites using rod-like or elongated rice-like CNC were prepared by dispersing them in a waterborne polyurethane host polymer,[101] or dispersing the

organogel of CNC in a thermoplastic polyurethane solution.[6b] These nanocomposites demonstrated remarkable improvements in stiffness, for example the nanocomposites via waterborne methods showed an improvement in the Young modulus from 0.5 to 344 MPa with 0-30 wt.% CNC, whereas, the organogel based TPU/CNC nanocomposites showed an improvement in tensile storage modulus from 14 to 1076 MPa with high loadings of 2 – 20 % v/v of CNC. However, they failed to demonstrate improvements in tensile strength, due to the high loading of nanoparticles that sacrifice the rubbery properties of TPU materials. An analysis performed by Marcovich et al.[102] on nanocellulose reinforced polyurethane suggested that percolation occurs at 1 wt.% of CNC loading. Above that volume fraction, well-dispersed nanocrystals can touch each other and form large percolating structures of H-bonded "rods", which can be easily destroyed by shearing the sample outside the analysed linear viscoelastic range.[103] With high aspect ratio (> 100) filament-like cellulose nanofibrils, the nanocomposites were usually developed by compression moulding of the stacks comprising polyurethane films and mats of cellulose nanofibrils.[104] They have also shown improvement in the stiffness of nanocomposites. Table 2.3 presents a summary of significant research using CNC as reinforcing filler in a polyurethane matrix.

Table 2.3 Polyurethane nanocomposites reinforced with CNC.

Type of polyurethane	Key Findings	References
Polyurethane	Improvement of mechanical properties due to strong filler-matrix interaction between the crystals and the isocyanates component.	[105]
	Addition (1-5 wt. %) of CNCs increased thermal degradation while maintaining mechanical properties of neat polyurethane.	[106]
Shape memory polyurethane	At 1 wt. % of the CNC, the tensile modulus was increased around 53%.	[107]
	Cellulose nanocrystals (0-30 wt. %) content in WPU matrix increased Young's modulus and	[6c]

waterborne polyurethane (WPU)	tensile strength from 0.5 to 344 MPa and 4.3 to 14.9 MPa respectively.	
	Tensile strength of resin-based WPU increased from 28.2 to 52.3 MPa with increasing amount of CNCS (0-20 wt. %).	[108]
	Incorporation of 1 wt. % starch nanocrystals and 0.4 wt. % cellulose nanocrystals resulted in a remarkable improvement in tensile strength (135%) and Young's modulus (252%) while elongation at break remained the same compared to neat WPU matrix.	[109]
Polyurethane elastomer (PU)	1 wt. % of cellulose nanocrystals reinforced in PU matrix able to achieve an 8-fold increase in tensile strength and 1.3-fold increase in strain-to-failure.	[110]
Bio-based polyurethane	Castor oil-polyol based polyurethane reinforced by CNC's increased tensile strength, modulus as well as the storage modulus shows filler worked effectively in the PU matrix.	[1b]
Polyurethane foam	0.5 wt. % of cellulose nanocrystals increased tensile modulus of PU significantly.	[111]
	CNC up to 5 wt. % reinforced into rigid polyurethane foam have shown significantly improved mechanical and thermal properties.	[112]

In reading these particular studies some pragmatic questions must be posed: what is the point of turning a thermoplastic elastomer into a plastic, and would there be more utility in trying to engineer a TPU-nanocellulose nanocomposite with maximum strength, toughness, compliance and resilience? It appears that others are pursuing this objective. When the nanocomposites were prepared via in-situ polymerisation using a low concentration of CNC (1 % v/v), these nanocomposites achieved an eight-fold increase in tensile strength with only a small increase in the tensile modulus. This improvement

indicates that at a low volume fraction, these low aspect ratio rod-like nanocrystals can enhance the stress transfer dramatically between polymer and filler particles due to the high interfacial surface area and a reduced number of complex agglomerates or bundles.[113]

However, all of these studies rely on solvent-based, solvent exchange and in-situ polymerisation methods. The melt compounding process, which involves high processing temperatures, becomes less favourable for the fabrication of cellulose based TPU composites due to the low degradation temperature of cellulose. However, by considering industrial demand, the melt compounding process was the best method to produce a TPU/cellulose nanocomposite in order to achieve high scale production. For large scale production, wet processing methods are limited by the use of large amounts of solvents, causing environmental issues and greatly increasing the nanocomposite production-cost to unacceptable levels.

2.5 Key limitations in industrial scale processing of TPU/CNC nanocomposites

The TPU nanocomposites with rod-like CNC have to date been processed via i) dispersion of CNC or organogel of CNC in a TPU solution or waterborne polyurethane, ii) dispersion of microcrystalline cellulose (MCC) particles or CNC in solvent (N,N-dimethyl formamide) and monomers followed by in-situ polymerisation, subsequently by solvent evaporation. The main issue with the processing of TPU/CNC nanocomposites via a scalable manufacturing method are the ***thermal stability*** of CNC at elevated processing temperatures and the ***dispersibility*** in the polymer matrix. Usually the processing temperature of TPU is above 180 °C which is close to the onset degradation temperature of CNC obtained via acid hydrolysis.[114] This behaviour is typically associated with sulphate groups as they can promote dehydration reactions and thereby decrease the thermal stability of cellulose. [114],[115]

The limitation of ***dispersibility*** relates to the surface chemistry (hydrophilicity) of CNC, which affects the molten-processability and the interfacial interactions between the polymers and fillers.[2c] The strong hydrogen bonding between the fillers subsequently provides a strong tendency for aggregation and poor dispersion in the polymer matrix during solvent-free processing.[92a, 116] Therefore, this work focuses on:

- The isolation of the CNC with a higher thermal stability and good dispersibility;
- The investigation on the processability of TPU/CNC nanocomposites via melt processing methods such as melt compounding and reactive extrusion.

In addition, the possibilities for isolating CNC at a larger scale via mechanical methods are also being investigated in order to increase their commercial scale usage. It is noteworthy that to-date, there are no published reports which detail the melt processing (melt compounding and reactive extrusion) of TPU with CNC.

CHAPTER 3

MATERIALS AND METHODS

The overview of the whole process of the work as illustrated in Figure 3.1.

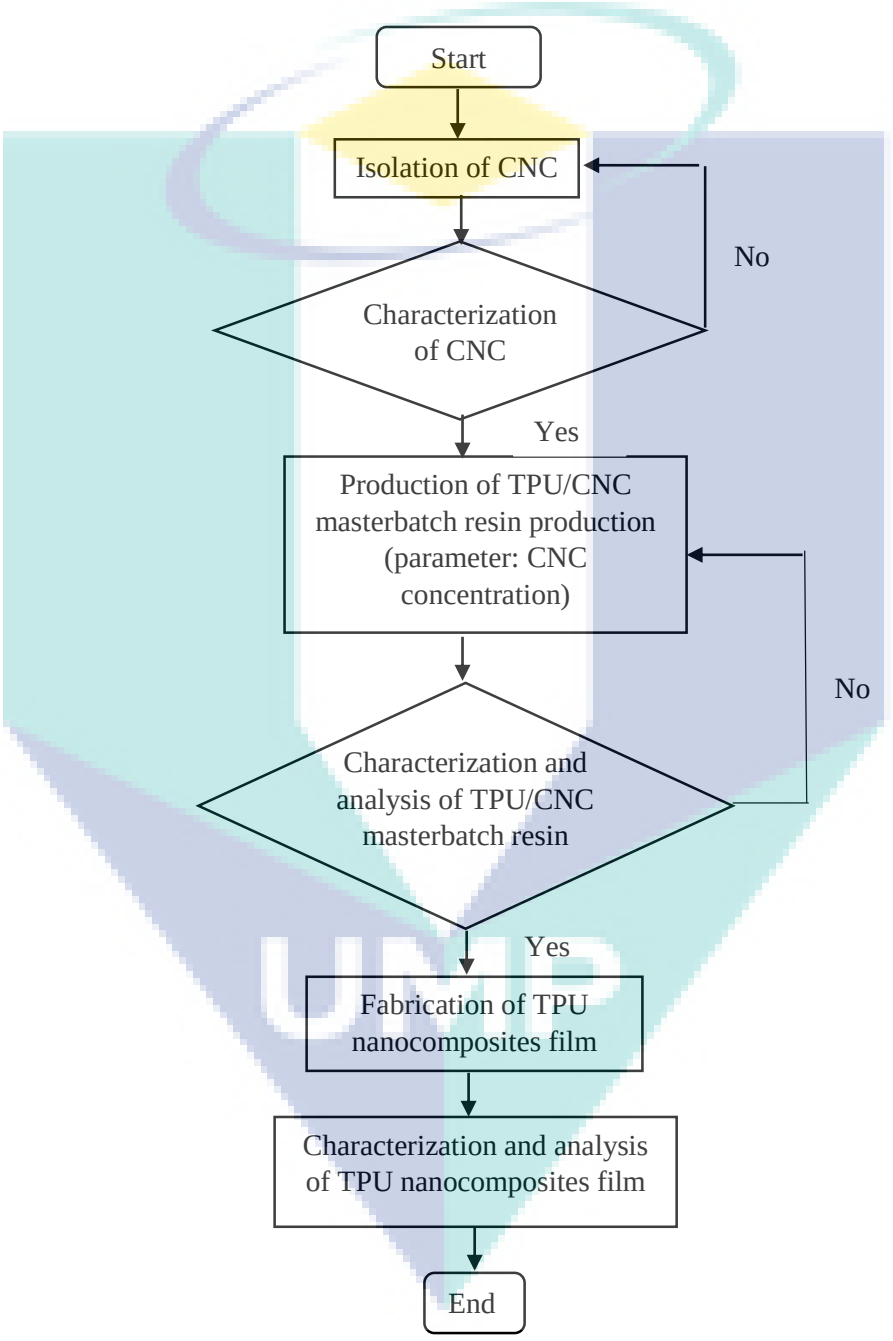

Figure 3.1: Process Flow Chart of Experiment

3.1 Materials

Microcrystalline cellulose(MCC) was used in this work purchased from Sigma Aldrich. The TPU Texin 990 from Bayer. Sodium chloride (NaCl), sulphuric acid, phosphoric acid and pyridine from Sigma Aldrich were used in acid hydrolysis and solvent exchange process.

3.2 Methods

3.2.1 Isolation of CNC

3.2.1.1 Isolation of CNC via single acid hydrolysis

The isolation process using sulphuric acid was adapted from Capadona et al. 2007[92a] with some modifications. The solid to liquid ratio for this isolation process was 1:75. Filter paper was blended with deionised water. The sulphuric acid was added slowly under vigorous mechanical stirring to the cooled filter paper until the final solution reached an acid concentration of 32%. Since the acid hydrolysis process is exothermic, while adding acid, ice bath is used to keep the temperature below 20 °C. After the acid addition is complete the reaction is set at 50 °C or higher for a stipulated time. The mixture was then heated to 50°C for 3.5 hours. The cellulose suspension was cooled to room temperature and was subsequently centrifuged four to five times at 4750 rpm until it became turbid. The cellulose suspension was then dialysed (dialysis tubing with MW cut-off = 14000) against deionised water until the suspension reached the neutral state (pH ~7). Then the cellulose suspension was ultrasonicated using high intensity ultrasonication (QSonica ultrasonicator) for 30 minutes at an output of 500 W, a frequency of 20 kHz, and 20% amplitude. Finally, the cellulose suspension was lyophilised using liquid nitrogen and was vacuum freeze dried.

Meanwhile, the extraction of CNC using phosphoric acid hydrolysis was undertaken using the procedure of Camarero Espinosa et al. 2013[56]. The solid to liquid ratio for this isolation process was 1:185. Filter paper was added to deionised water. Phosphoric acid was added slowly until an acid concentration of 62% was reached. The mixture was heated for 1.5 hours at a temperature of 100°C. The following processes were similar to that used in the sulphuric acid hydrolysis process. The phosphoric acid hydrolysis using MCC was performed using a similar procedure, except that the solid to liquid ratio was reduced to 1:75 and the hydrolysis process temperature was reduced to 50°C for a period of 1 h.

In the optimisation of the isolation process via phosphoric acid with MCC, the solid to liquid ratio was 1:77. A similar procedure for the isolation of CNC using filter paper was used with variations in the time (30 and 60 min) and the temperature (30 and 70°C) of the reaction.

3.2.1.2 Isolation of CNC via mixed acid hydrolysis

2.6g of MCC was weighed and immersed in 115ml of deionized water for 24 hours before the isolation process is began. Next, the isolation experimental was set up as shown in Figure 3.2. MCC solution was stirred under constant speed about 1 hour before the experiment started. By maintaining the ratio of mixed acid at 1:3 of sulphuric to phosphoric acid (v/v), 20ml of sulphuric was dropped slowly in the MCC solution.

After hydrolysis process was done, the solution was cooled under room temperature and undergo acid removal through centrifugalizing with deionized water at 5,000 rpm for 10 minutes until it reached the neutral state. This process is repeated for about four to five times depending the acidity of the suspension. The acidity of suspension was determined using pH paper. Figure 3.3 shows the suspended CNC after centrifugation process.

The CNC were further treated using was sonicated using Q Sonica ultrasonicator for 30 minutes at an output of 500 W, frequency of 20 kHz and amplitude of 20 % (Amin et al., 2016). This treatment is necessary to agitate particles in sample to ensure evenly dispersing of CNC in liquid (Deora N.S, 2013). Finally, the CNC suspension is going through freeze-dry process using liquid nitrogen for two days. The liquid nitrogen was used to ensure rapid freezing and avoid settling of CNC at the bottom of flask. The powder form was collected and the CNC yield was recorded.

3.2.1.3 Isolation of CNC via high energy bead milling

Isolation of CNC via high energy bead milling (HEBM) with deionised water has been provided in section 3.2.2.2 of Chapter 3. The resulting CNC were designated as follows: CNC-M*An* where *A* is MCC concentration (0.5, 1, 2 wt. %) and *n* is the milling time utilised (15, 30, 60 min).

To evaluate the effect of mild phosphoric acid on the milling process, MCC was dispersed in dilute 1wt. % H_3PO_4 for one hour before the milling process. After milling, the CNC were separated from the liquid by centrifugation. The supernatant was decanted and replaced by an equal amount of deionised water and the mixture

was centrifuged again until the supernatant reached neutral pH. Finally the CNC suspension obtained was freeze-dried. The CNC produced via milling with H_3PO_4 was coded as CNC-MP*An*, where P denotes the acid pre-treatment, and *A* and *n* are the same as above.

3.2.2 Preparation of TPU nanocomposites

3.2.2.1 Solvent casting

TPU resin and CNC were individually dissolved in dimethylformamide (DMF). 0.5 wt. % of CNC in TPU was prepared by mixing the desired amounts of CNC and TPU solution in DMF. The mixture was stirred vigorously for 1 hour at room temperature. The mixture was then sonicated for 2 minutes at 20 kHz. Subsequently, further stirring was undertaken after the sonication process and immediately cast onto a Teflon petri dish. The films were dried under nitrogen purged for 24 hours and subsequently annealed in a vacuum condition at 80°C for 12 h.

3.2.2.2 Melt compounding

Initially CNC and PU resin were mixed physically. PU and cellulose was melt compounded with a ThermoHaake twin screw extruder. The barrel temperature used was between 175 and 225°C and a screw speed of 120 rpm was employed to extrude the material. The extrudates were pelletised and dried overnight at 70°C before being compression moulded. The samples were compressed using a water-cooled hydraulic press at 175 -180°C for 1 minute and then cooled to room temperature using a controlled water flow. The samples were pressed using brass plates with 1 mm machined rectangular cavities. To prevent the polymer from sticking to the plates, glass fibre reinforced Teflon sheets were placed between extrudates and the plates. Subsequently, the samples were annealed under vacuum conditions at 80°C for 12 hours.

3.2.3 Preparation of TPU/MCC nanocomposites via masterbatch process

3.2.3.1 Solvent exchange

MCC aqueous suspension was undergoing solvent-exchange in pyridine by added a small amount of NaCl in order to allow the precipitation of MCC. The mixtures of TPU

and MCC were prepared by mixing the pyridine based MCC with TPU solution (5 g/ 150ml solvent mixture) in a mixture of pyridine-NaCl 9:1 (w/w).

3.2.3.2 Coating MCC with polyurethane

The MCC suspension in pyridine was diluted with extra pyridine and the desired amount of TPU was added to obtain the weight ratios of 5/1 (pyridine/TPU) and 4/1 (TPU/MCC). The system was let under magnetic stirring at room temperature until the complete dissolution of TPU. The suspension was syringed into water under a gentile magnetic stirring to precipitate the TPU/MCC mixture. The formed solid particles were collected, washed with distilled water and dried at room temperature until no evidence of residual solvent detected. Precipitation in water accelerated the production of TPU/MCC capsules because it eliminates the necessity of solvent evaporation and facilitates the recovery of the solvent if needed.

3.2.3.3 Preparation of TPU/MCC nanocomposites film

The MCC reinforced TPU nanocomposites were prepared by solvent casting method. The resultant composites were denoted as TPU/MCC1.0, TPU/MCC3.0, and TPU/MCC5.0. The numbers represent weight percentage of MCC in the composites. Next, the TPU films were dried for 24h in oven at 70 °C for annealing process.

3.3 Characterisation

3.3.1 Determination of production yield

Total yield percentage (Y) of the acid-treated cellulose including yields of the insoluble and regenerated parts of cellulose is calculated using equation (Alemdar et al., 2008): -

$$(Y)\% = \frac{dry\ weight\ of\ CNC}{dry\ weight\ of\ MCC} \times 100\% \qquad (3.1)$$

3.3.2 Scanning electronic microscopy

Scanning electron microscopy (SEM) was carried out to investigate the morphology of MCC before and after acid hydrolysis. A few milligrams of sample in powder form was put on the plate metal and the surface of the sample was coated with gold

under vacuum before analysed in Carl Zeiss/ EVO 50 at 15kV, and image were captured. The masterbatch sample was cut with a razor blade and gold coated. The inner structure of TPU and TPU/MCC nanocomposites after tensile testing were compared.

3.3.3 Field Emission Scanning Microscope (FESEM)

FESEM (JEOL) with an accelerating voltage of 30kV was employed to investigate the structure and the aspect ratio of the CNC. It capable to capture up to 300,000 magnificent. Thus, it is suitable in capturing nano-sized particles. A few milligrams of samples are coated with gold before observation is made to avoid charging

3.3.4 Thermogravimetric Analysis (TGA)

The thermal stability of isolated CNC was analyzed using TGA measurement carried out on Mettler Toledo TGA/DSC1. The heating process is done under nitrogen atmosphere. Before analysis, approximately 2 mg of each sample is placed in an aluminum pan and heated from room temperature to 110°C at heating rate of 10°C/min. Then, the sample is isothermally held for 10 minutes before it was heated up to 500°C at heating rate of 5°C/min.

3.3.5 Fourier Transform Infrared (FTIR) Spectroscopy Analysis

FTIR Spectroscopy was employed to examine the changes in the functional groups induced by the various treatments using a Nicolet TM iS™ 5 FT-IR Spectrometer. All the spectra were an average of 16 scans from 525 to 4000cm^{-1} at a resolution of 2cm^{-1}. The powder form CNC is placed on the diamond crystal of an attenuated total reflectance (ATR) accessory.

3.3.6 Dispersion Studies

The dispersibility of CNC was investigated by dispersing CNC in deionized water. The dispersions were prepared at concentration of 2mg/mL and stirred continuously for 1 hour. Photographs were taken immediately after preparation and subsequently after 5 minutes, 15 minutes, 30 minutes, 1 hour and 5 hours.

3.3.7 XRD analysis

The crystallinity of the raw fiber, steam exploded fiber, cellulose and CNF were monitored using Broker D8 Advance X-ray diffractometer with Ni-filtered CuKα radiation. The fibers were scanned within a 2θ angle range from 5°to 60°at 2 per minute. The crystallinity index Crl value was calculated using the following Equation 3.2:

$$Crl(\%) = \frac{I_{002} - I_{am}}{I_{002}} \times 100\% \qquad 3.2$$

Where:

I_{002} = peaks intensity of crystalline fraction

I_{am} = intensity of amorphous fraction.

3.3.8 Diffrential scanning calorimetry (DSC analysis)

Nanocomposte film was analysed using DSC (TA/Q 1000 DSC Series, New Castle), under heat/cool/heat method. Approximately 2-3 mg of sample is sealed into an aluminium pan and lid. Sample was analysed at heating and cooling rate of 10 °C/min from -100 °C to 500 °C. Meanwhile, the nitrogen gas flow rate purging to the system is maintained at 10 mL/min.

3.3.9 Mechanical analysis

The mechanical properties of the composites were measured at room temperature using an Instron model 5543 universal testing equipped with a 500N load cell. The tensile tests were cut into dumbbell shapes according to ASTM D-638-14. The tests were performed with the thickness of 14mm. For each sample, five strips for the tensile tests were tested. Modulus was determined from the slope of initial low strain and toughness were determined by integrating the area under the curve.

CHAPTER 4

RESULTS AND DISCUSSIONS

4.1 Isolation of CNC

4.1.1 Isolation of acid hydrolysis via single acid hydrolysis

4.1.1.1 Morphology and dimension of CNC from filter paper (cotton)

Figure 4.1 shows CNC obtained from filter paper (cotton) via single acid hydrolysis using sulphuric acid and phosphoric acid. It can be seen that CNC has rod-like/needle-like shape for both acid hydrolysis processes. The production yield and dimensions of CNC from both processes are also summarised in Table 4.1. The average aspect ratios of rod-like CNC obtained via hydrolysis are 13 and 10 for CNC-S and CNC-P respectively, which are similar to those achieved in earlier reports.[56, 92a] The production yield (%) of CNC (with respect to the initial mass of cellulose) produced via single acid hydrolysis was 81 and 62% using sulphuric and phosphoric acids respectively. A low production yield of CNC-P may be attributed to phosphate groups attached to the cellulose, which can be converted back to free phosphoric acid and amorphous cellulose, and thus reduce the potential for recrystallisation.[117]

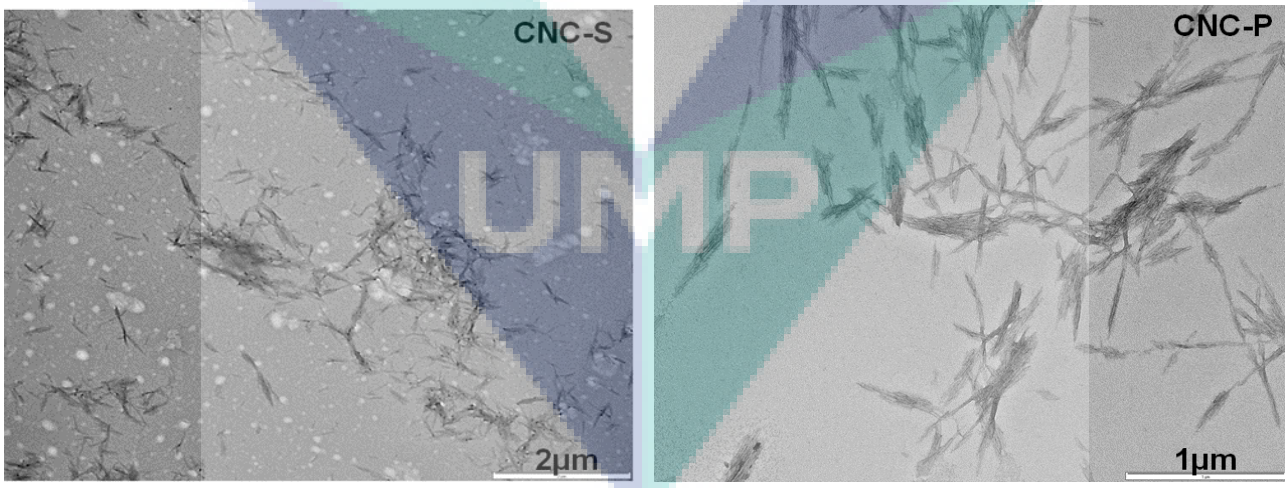

Figure 4.1 TEM images of CNC from cotton produced via acid hydrolysis using sulphuric acid (CNC-S) (left) and phosphoric acid (CNC-P) (right).

Table 4.1 Dimensions and production yield of CNC isolated from cotton.

Sample	Length (nm)	Diameter (nm)	Aspect Ratio	Production yield (%)	Volume (mL) of concentrated acid per gram of CNC
CNC-S	213 ±50	16 ±3	13	81	33
CNC-P	270 ±135	26 ±13	10	62	218

4.1.1.2 Thermal stability of CNC from filter paper (cotton)

Figure 4.2, shows the thermograms of CNC obtained via single acid hydrolysis using sulphuric and phosphoric acids. It shows that CNC-S starts to degrade at 200°C with maximum decomposition at 348°C. The low thermal stability can be attributed to the surface functionalisation with sulphate charges which promote dehydration reactions.[56, 92a] A significant improvement in thermal stability can be observed for the CNC-P which does not begin to degrade until a temperature 255°C, with maximum decomposition at 341°C. An enhanced thermal stability can be attributed to the absence of highly reactive functional groups like sulphates which can promote dehydrations and the introduction of phosphate groups which may reduce the rate of dehydration reactions while maintaining the dispersion stability of CNC.

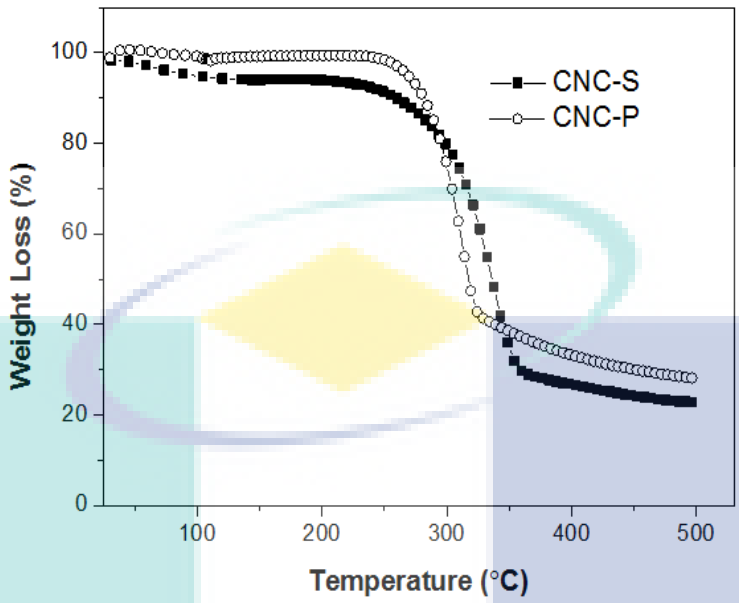

Figure 4.2 TGA thermograms of CNC-S and CNC-P obtained from cotton.

Though, the phosphoric acid hydrolysis [56] was able to increase the thermal stability of CNC, its consumption was remarkably high. As shown in Table 4.1, it required 218 mL/g of phosphoric acid to produce per gram CNC whereas it requires lesser (33 mL) sulphuric acid according to the above-mentioned lab-scale protocols. The following section was designed to overcome this problem while sustaining the good thermal stability and crystallinity of CNC.

4.1.1.3 Isolation of CNC from microcrystalline cellulose (MCC) via single acid hydrolysis

Commercial grade pure cellulose powder, microcrystalline cellulose (MCC), was used to isolate CNC using phosphoric acid under similar conditions to those in sulphuric acid hydrolysis from cotton. An initial reduction in size of the raw materials (millimetre to microns) allows us to work towards reducing the time and acid consumption to isolate CNC. The micrograph of MCC in Figure 4.1 shows cellulose particles are smaller (20-40 µm). For microcrystalline cellulose (MCC) powder, hydrolysis was performed using

H_3PO_4 (32% acid concentration at 1:75 solid to liquid ratio) following the protocol of sulphuric acid hydrolysis at hydrolysis temperature of 50°C for 1 hour.

4.1.1.4 Morphology, dimension and thermal stability of the CNC from MCC

Figure 4.3 shows TEM image and TGA thermogram of cellulose nanocrystals (mCNC-P) produced via acid hydrolysis.

The CNCs produced under this protocol (32%, 1h at 50°C) did not show any distinct rod-like shape. The reason is still unclear, however, it may be attributed to the low acid concentration with short resident time. At low concentration, presumably the phosphoric acid may penetrate into both amorphous and crystalline domains but slower in liberating/separating the crystalline domains from the amorphous domains of cellulose particles, resulting in cellulose without any distinct shape. Therefore, further optimisation has been carried out using H_3PO_4 (see section 4.1.1.6) in order to obtain CNCs with distinct shape and high production yield.

Meanwhile, results from TGA measurements have shown improved thermal stability with onset degradation temperatures for MCC and mCNC-P are 270°C and 250°C, respectively (Figure 4.3). In a comparison of sources, CNC obtained from MCC demonstrated higher thermal stability than CNC obtained from cotton (i.e. CNC-P, Figure 4.4).

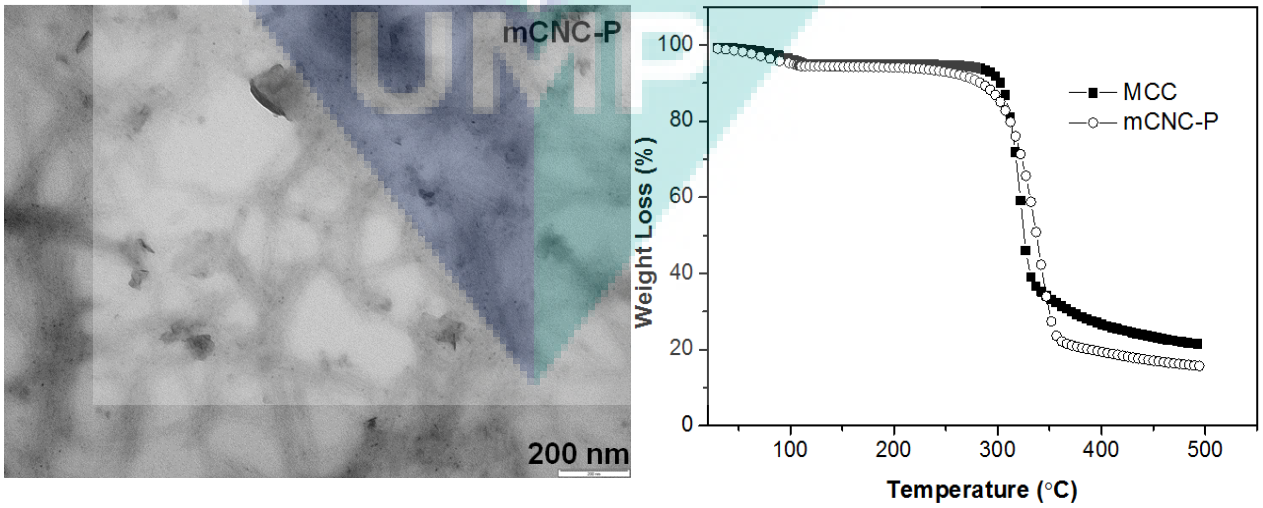

Figure 4.3 TEM image (left) and TGA curve (right) of cellulose nanocrystals (mCNC-P) produced via phosphoric acid hydrolysis.

4.1.1.5 Optimisation of the phosphoric acid hydrolysis process to obtain CNC from MCC

Following from the previous section, the hydrolysis process was optimised by maintaining the solid to liquid ratio at 1:75, with acid concentration being increased to 63% in addition to varying the time (30, 60 and 120 min) and the temperature (30, 70°C). They are coded as CNC-P***Xn*** where '***X***' is A and B for 30 and 70 °C, respectively, and '***n***' is 1 and 2 for 30 and 60 min.

4.1.1.5.1 Morphology and dimensions of CNC from the optimisation of phosphoric acid hydrolysis

Figure 4.4 illustrates the shape of CNC and Table 4.2 lists the dimensions measured resulting from the optimisation of H_3PO_4 hydrolysis. A rod-like shape can be found in all samples and CNC-PB1 has the most distinctive shape, whereas the remaining samples show heavy agglomeration. CNC-PB1 measurements were 168 nm in length, 9.6 nm in diameter with an aspect ratio of 20. The production yield (weight of product over initial weight of raw material) of CNC-PB1 achieves a level of 85%, which is higher than CNC obtained from filter paper (76-80%).[56] Figure 4.4 illustrates the TEM images of CNC obtained from this isolation process. It is observed that the CNCs with a rod-like shape and high yield can be isolated from acid hydrolysis using phosphoric acid in a shorter reaction time (30-60 min) and at a higher temperature (70°C). Significantly CNC-PB1 has reduced acid consumption by approximately 71% (Table 4.2) when compared with the phosphoric acid hydrolysis procedure using cotton, and the hydrolysis time was reduced by 30 minutes.

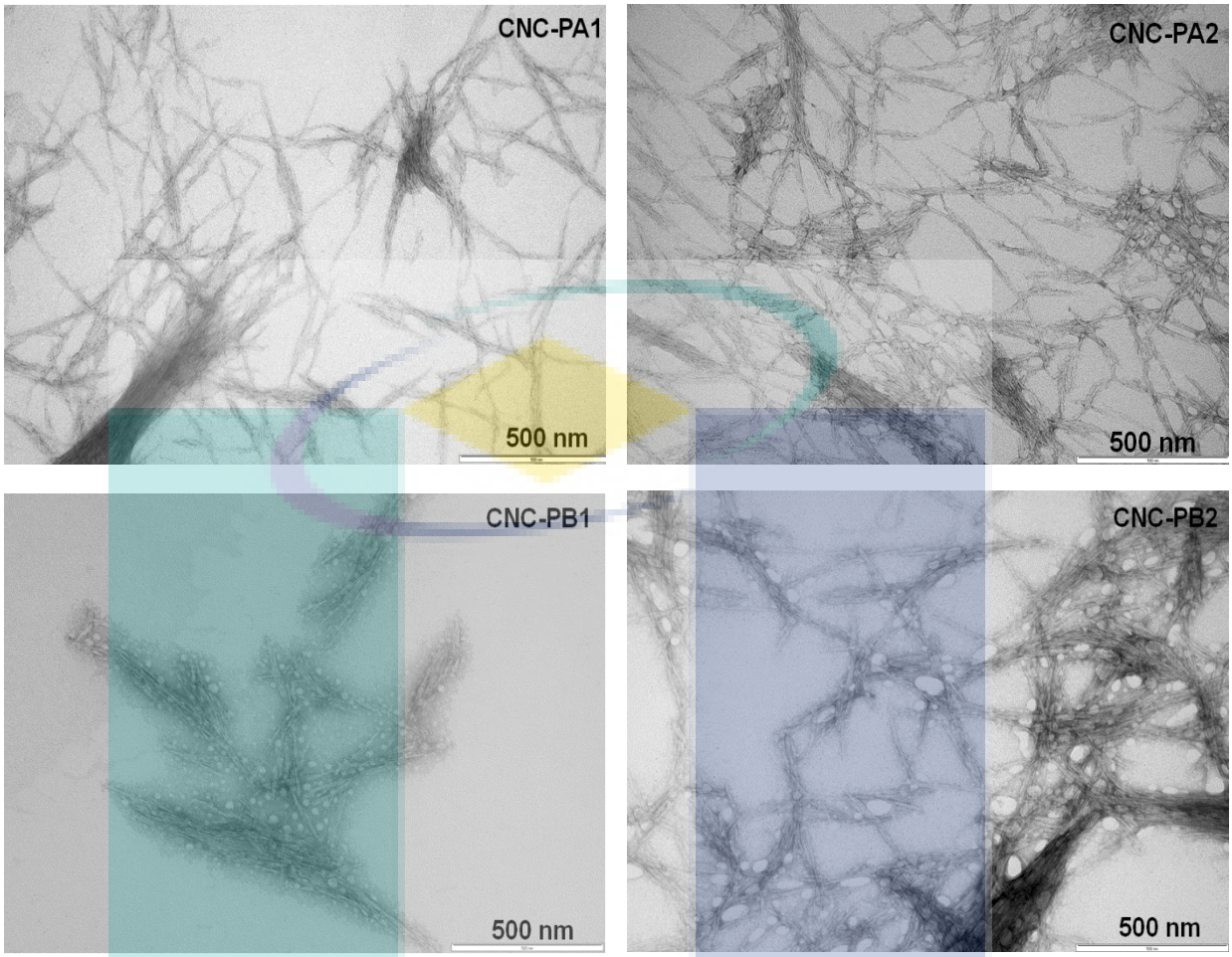

Figure 4.4 TEM images of CNC from phosphoric acid optimisation CNC-PA1, CNC-PA2, CNC-PB1 and CNC-PB2.

Table 4.2 Dimensions of CNC isolated using phosphoric acid and yield percentage from MCC.

Sample codes *	Length (nm)	Diameter (nm)	Aspect Ratio	Production Yield (%)	Acid required (ml) / CNC production (g)	Degree of Crystallinity (%)
CNC-PA1	336.9 ±13	10.0 ±3	37.4 ±22	81	71	89.7
CNC-PA2	190.4 ±32	8.6 ±2	23.3 ±7	60	96	89.8
CNC-PB1	168.6 ±18	9.6 ±4	20.0 ±8	85	64	91.2
CNC-PB2	189.6 ±50	10.1 ±5	20.2 ±5	52	111	88.4

*CNC-P***Xn** where '***X***' is A and B for 30 and 70 °C, respectively, and **'*n*'** is 1and 2 for 30 and 60 min.

4.1.1.5.2 Thermal stability of CNC from MCC of optimised phosphoric acid hydrolysis

As seen in Figure 4.5, all CNC samples from the optimisation of H_3PO_4 hydrolysis had a small weight loss at a low temperature (<120°C) corresponding to the water absorbed. The onset degradation temperature ranged from 259°C to 275°C. The thermal behaviour of CNC increases significantly compared to the CNC produced from sulphuric acid hydrolysis which was at approximately 150°C.[56] Examining the derivatives peak from the TGA traces for all CNC samples reveals one clear peak, with CNC-PB1 having an obviously broader peak that stretches from a temperature of ca. 270°C to 360°C.

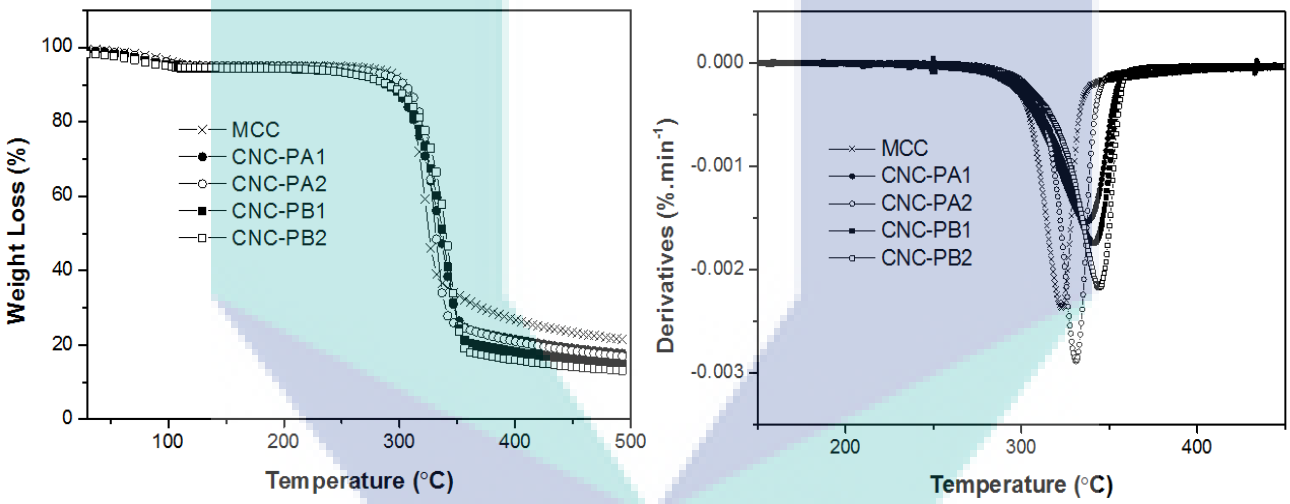

Figure 4.5 TGA curves (left) and derivatives (right) show the weight loss upon decomposition of MCC and CNC obtained from optimisation of phosphoric acid hydrolysis.

4.1.1.5.3 Crystallinity of CNC optimisation of phosphoric acid hydrolysis

The obvious intensity peak from the x-ray diffractogram in Figure 4.6 is at a 2θ value of 22° which represents the crystalline structure of cellulose I, whereas the amorphous background was characterised by a peak at a 2θ value of 18°.[118] The overall degree of crystallinity of the CNC obtained from the optimisation of H_3PO_4 hydrolysis was determined as having a value in the range of 88 – 91 %. The characteristic peaks at 2θ = 15 (101), 16.5 (10$\bar{1}$), 20.8 (021), 22.5 (002) and 34.3 (040) show the crystalline polymorph I cellulose for MCC. This acid hydrolysis process indicates it was able to sustain a high degree of crystallinity in the cellulose structure.

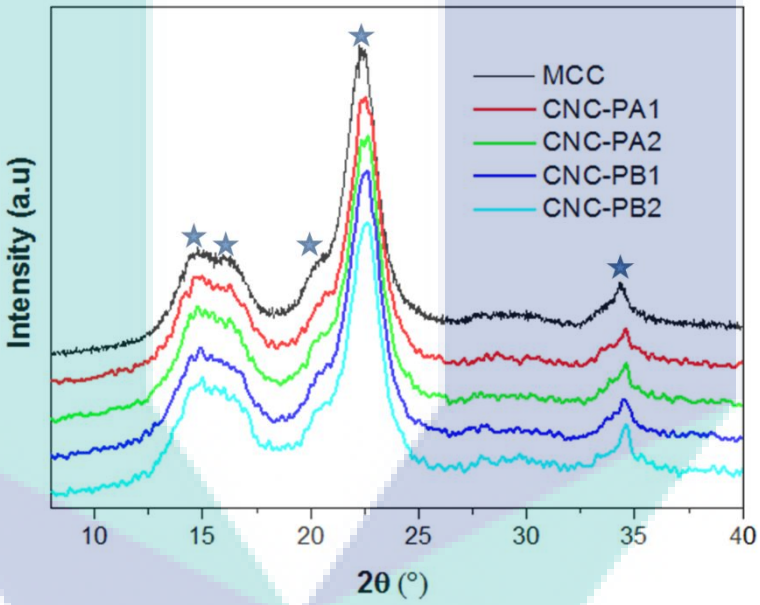

Figure 4.6 XRD pattern of microcrystalline cellulose (MCC) and cellulose nanocrystals from optimised phosphoric acid hydrolysis (CNC-PA1, CNC-PA2, CNC-PB1 and CNC-PB2).

4.1.2 Isolation of acid hydrolysis via mixed acid hydrolysis

4.1.2.1 Percentage of yield

Table 4.3 shows the relationship between parameters and percentage of yield produce by maintaining other conditions such as types of acid used, acid ratio, solid-liquid ratio and ultrasonication time. Initial weight of MCC was fixed at 2.6 g.

Table 4.3 Production yield of CNC isolated from MCC

Sample		Production Yield (%)
Hydrolysis time, min	**Temperature,** °C	
30	50	90.4
	70	85.8
	90	83.7
60	50	83.4
	70	85.9
	90	88.9
90	50	82.9
	70	70.9
	90	-

Based on yield tabulated in Table 4.2, highest percentage of CNC is produce at condition of 50°C/30min. As the temperature increased to 90°C, the production yield is lesser because it closer to degradation condition. Hence, this condition is not suitable in producing better properties of CNC. The lowest percentage which is at condition 90°C/60 min. As it further the reaction time to 180 min, degradation of MCC began to occur. Thus, no further characterization has been made to the sample at 90°C/180 min.

4.1.2.2 Morphology of CNC

The morphology of CNC and MCC was observed using SEM and FESEM. Figure 4.7 shows the difference in morphology of MCC and CNC with its dimension that obtained after acid hydrolysis. It can be seen that acid hydrolysis altered the morphology of MCC. Under the same magnificent, CNC produced is smaller and have bigger aspect ratio (D/L) while MCC in raw material display aggregated irregular shaped fibrils and rough surface with lower aspect ratio (D/L). From experimental result, it was proven that temperature and reaction time affect the aspect ratio of CNC. The aspect ratio is increasing as the temperature and reaction time increase. However, longer reaction time gives more impact

to the aspect ratio as shown in the difference of ratio at 50°C/ 30 min (7.15) and 50°C/ 60 min (12.44) compared to ratio 21 at 70°C/ 30 min (7.80). Based on previous study made by Espinosa (2013)[119], it shows the aspect ratio of CNC from mixed acid relies in range of CNC-S and CNC-P. This aggregation is composed of strong hydrogen bonding between the cellulose.[120]. Obviously, the mixed acid hydrolysis has successfully isolated the CNC as shown by the reduction of the particle size and higher aspect ratio.

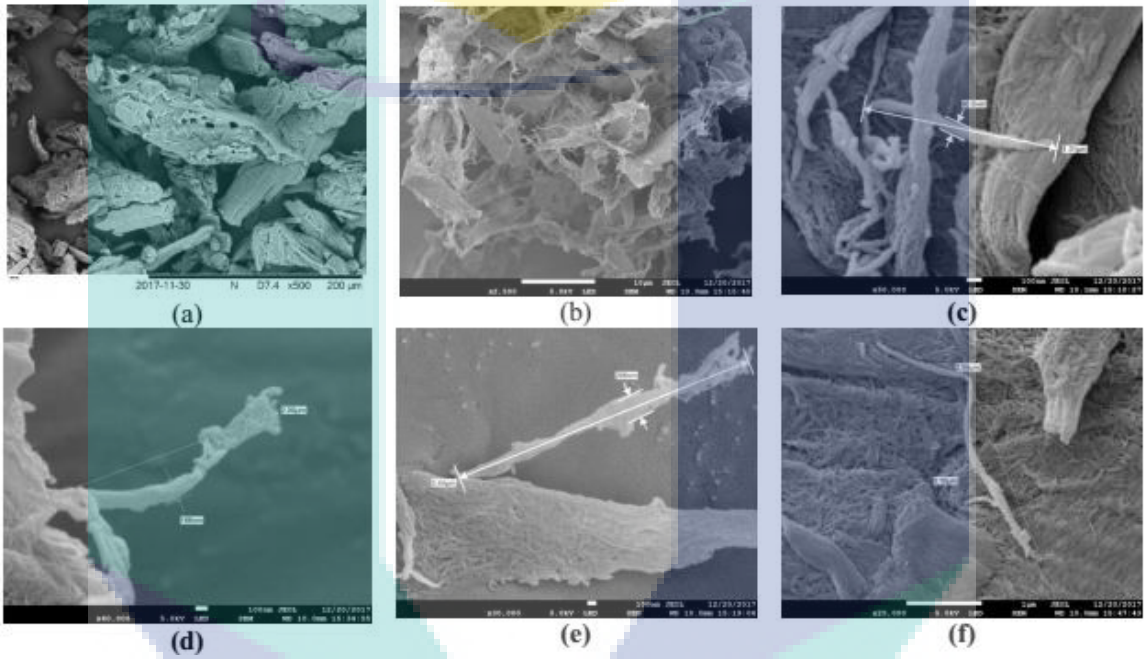

Figure 4.7 SEM image of commercial MCC (a); FESEM image of CNC after acid hydrolysis (b); CNC at 50°C/30 min (c); CNC at 50°C/60 min (d); CNC at 70°C/30 min (e); CNC at 70°C/60 min (f)

4.1.2.3 Fourier Transform Infrared (FTIR) Spectroscopy Analysis

FTIR spectra were used to characterize the functional groups presence on the surface of CNC. Figure 4.8 shows the differences of spectra between commercialized MCC with the CNC produced after acid hydrolysis. As shown in figures above, all conditions show the changes in chemical behaviour that occurred in response to acid hydrolysis of MCC. The broad absorption spectrum located between 3700 to 3000 cm^{-1} contains fundamental stretching modes of hydroxyl groups (-OH) due to carbohydrates and vibration of the hydrogen bonded between hydroxyl groups.[121] Based on Figure 4.8(a), there is significant difference at peak between 3700 to 3000 cm^{-1} where it shows

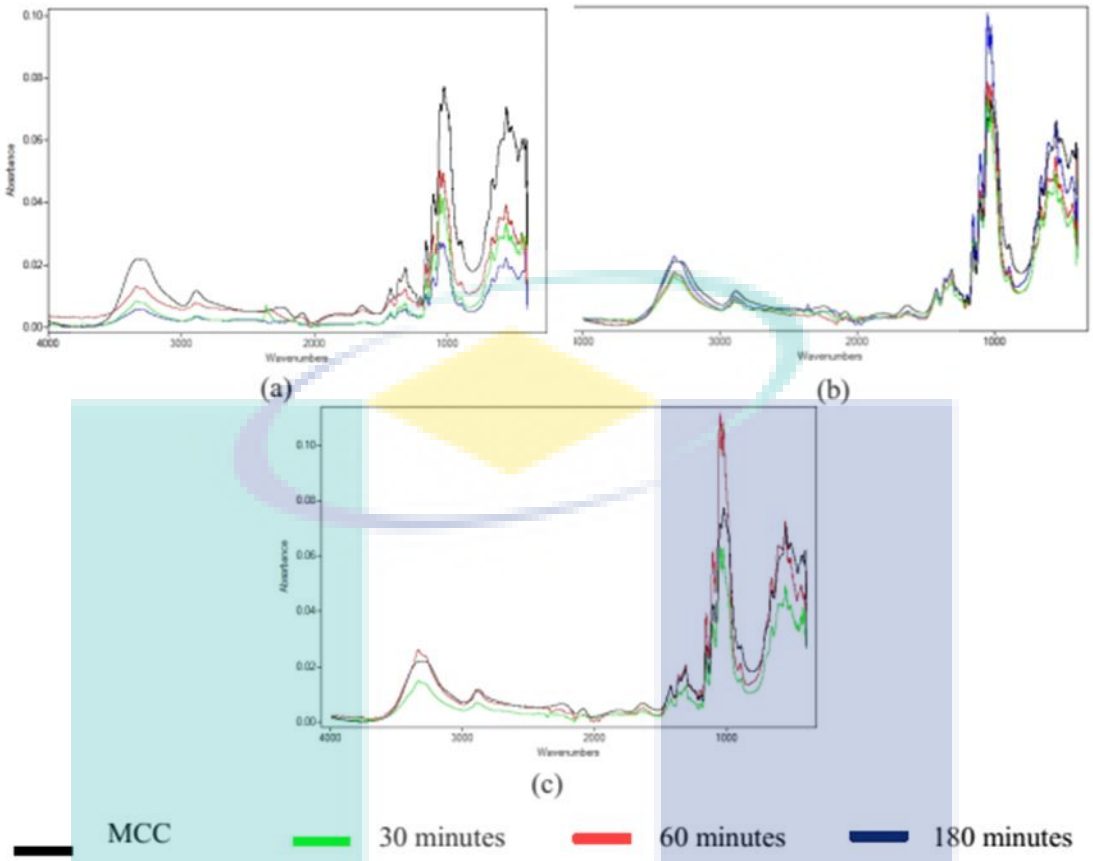

Figure 4.8 FTIR Spectra for MCC and CNC at 50°C (a); 70°C (b); 90°C (c)

higher amount of hydroxyl group detected at MCC compared to CNC. It might due to sulphate group that attached at the surface of CNC which lowering the amount of hydroxyl detected. The spectrum around 2900 to 2800 cm^{-1} identified to be attributable to the symmetric and anti-symmetric stretching modes of -CH in methyl (CH_3) and methylene (CH_2) functional groups.[122] According to previous study, the peak that lies between 1700-1600 cm^{-1} indicate to the bending mode of water molecules due to strong interaction between cellulose and water.[123] Furthermore, the peaks at around 1150, 1,104 and 663 were attributed to the stretching vibration intermolecular ester bonding, stretching vibration of CO) and C-OH.[124] A small, sharp peak at 896 cm^{-1} corresponded to the glycosidic -CH deformation with ring vibration contributions and -OH bending, which is characteristic of glycosidic linkages between the glucose in cellulose.[120] However, this peak is decreased with the increased of hydrolysis time as shown in Figure 4.8 (a); (b); (c). Based on FTIR spectra, the intensity most of the peaks was found to be significantly lower than MCC. This was considered to result from the oxidation of cellulose during acid hydrolysis reaction.[125] In contrast, these peaks essentially showed similar pattern of

spectra as MCC. Hence, it is concluded that molecular structure of cellulose remains unchanged in the presence of mixed acid.[126] This indicates that the chemical functional groups cellulose was stable and no strong reaction occurred.

4.1.2.4 Thermal stability

Figure 4.9 shows the thermal behaviors of MCC and CNC produced after acid hydrolysis. Based on data from Figure 4.9, it shows higher onset degradation temperature of MCC after acid hydrolysis compared to the raw material. While temperature of MCC originally, 70°C/30 min, 70°C/60 min and 90°C/30 min remain constant. Besides that, at 70°C/180 min shows decreasing thermal behavior compared to MCC. This might due to the closer to degradation condition. However, Figure 4.9(c) showed significantly different degradation behavior by having a two-step degradation process as revealed by DTG curve in Figure 4.10 where the higher temperature stage at 334.1°C may be related to the breakdown of the interior of unsulfured crystals similar to that reported by Li et al. (2009)[127].

As reported in previous study, thermal behaviour of CNC produced from sulphuric acid approximately 150°C.[119] On the other hand, CNC produced from experimental of mixed sulphuric-phosphoric acid shows higher onset degradation temperature which around 270°C to 289°C. Thus, this proved that mixed acid hydrolysis able to overcome the limitation of single acid. The higher decomposition temperature obtained was attributed to the greater crystallinity of cellulose material.[128] The high thermal stability of CNC has large potential applications.[122, 127]

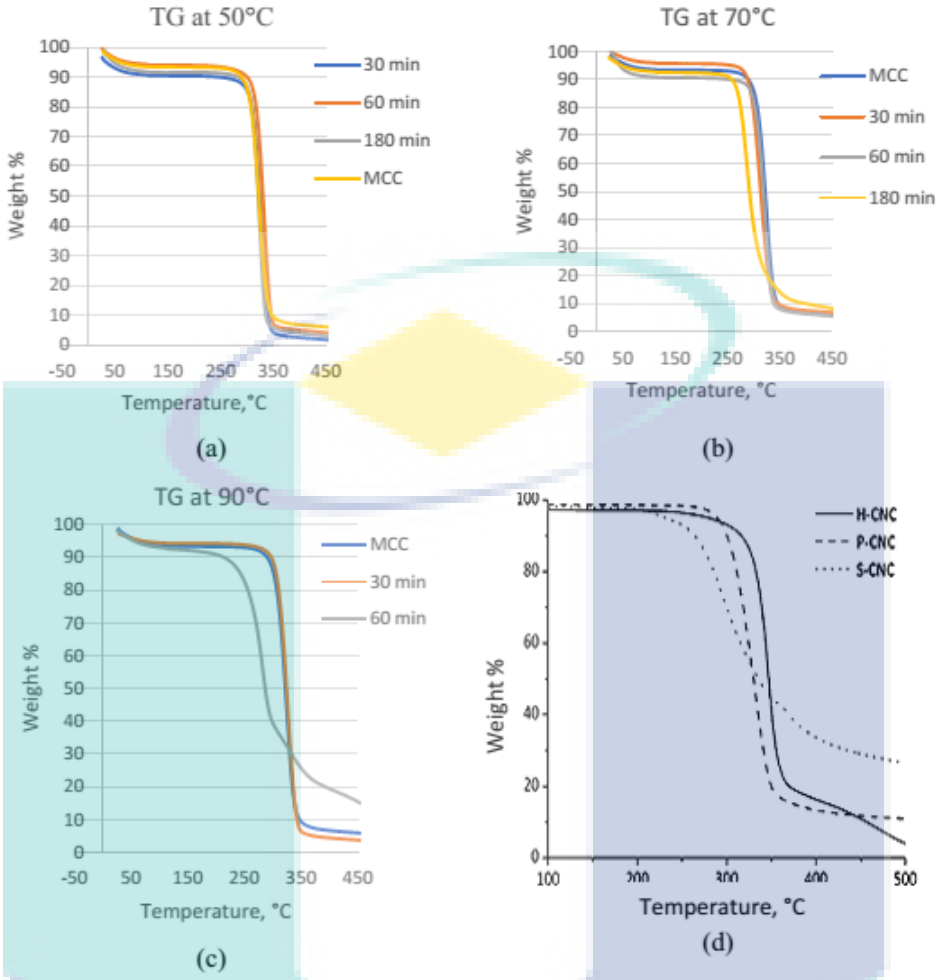

Figure 4.9 Thermogram for MCC and CNC at 50°C (a); 70°C (b); 90°C (c); CNC from single acid (d)[119].

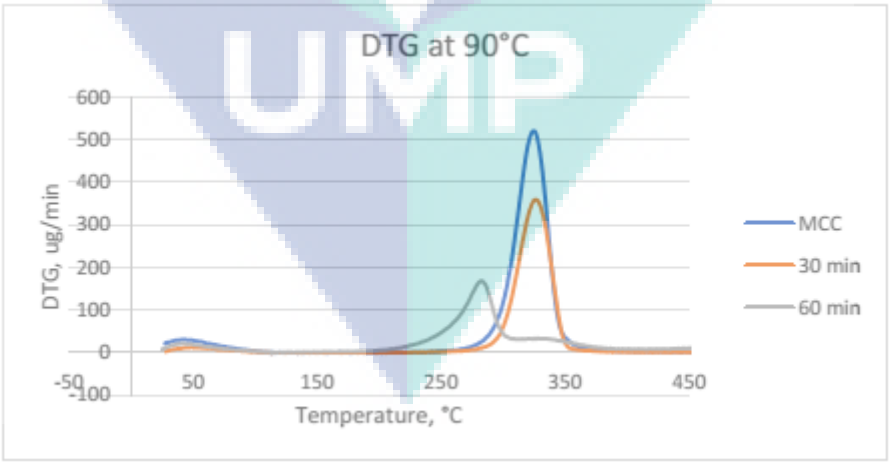

Figure 4.10 DTG curve at 90°C.

4.1.2.5 Dispersion stability

Dispersion is one of the factor that contribute in good properties of CNC. However, it is main challenge to nanoparticles due to interaction of surface of hydroxyl group of omnipresence. In this study, dispersibility was investigated by dispersing them in deionized water and observing the stability of dispersion over some period. Photograph was taken immediately after stirring for 1 hour and at 5 minutes, 15 minutes, 30 minutes, 1 hour and 5 hours.

Based on Figure 4.11, CNC at all conditions shows the decreasing in dispersbility at 1 hour as the solvent becomes clearer compared to after stirrer. However, it is observed that CNC produce at 90°C have rapid sedimentation as shown in photograph taken at 1 hour. As compared to other, the solvent turns clearer at 5 hours. Based on previous study, dispersion stability is done by sonication method before it was observed. As a results, CNC produced after acid hydrolysis have very stable dispersion in water as it can withstand up to 10 days.[129] The dispersibility of CNC depends strongly on their aspect ratio, surface functionalization and the ability of solvent and surface groups to counterbalance the attractive hydrogen-bond interactions exerted by the abundant of hydroxyl groups.

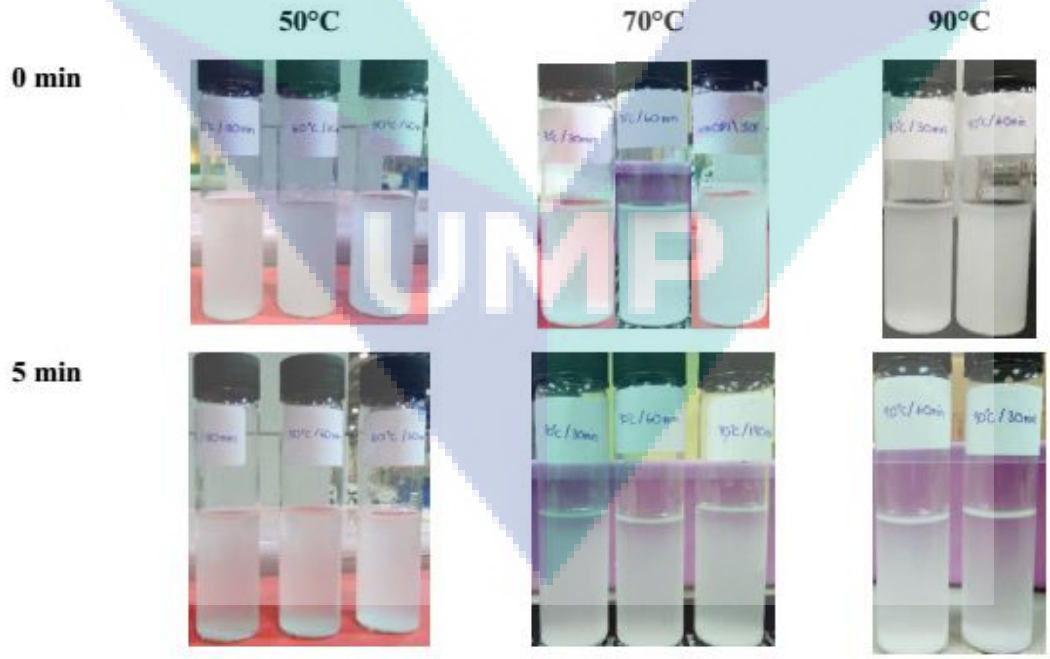

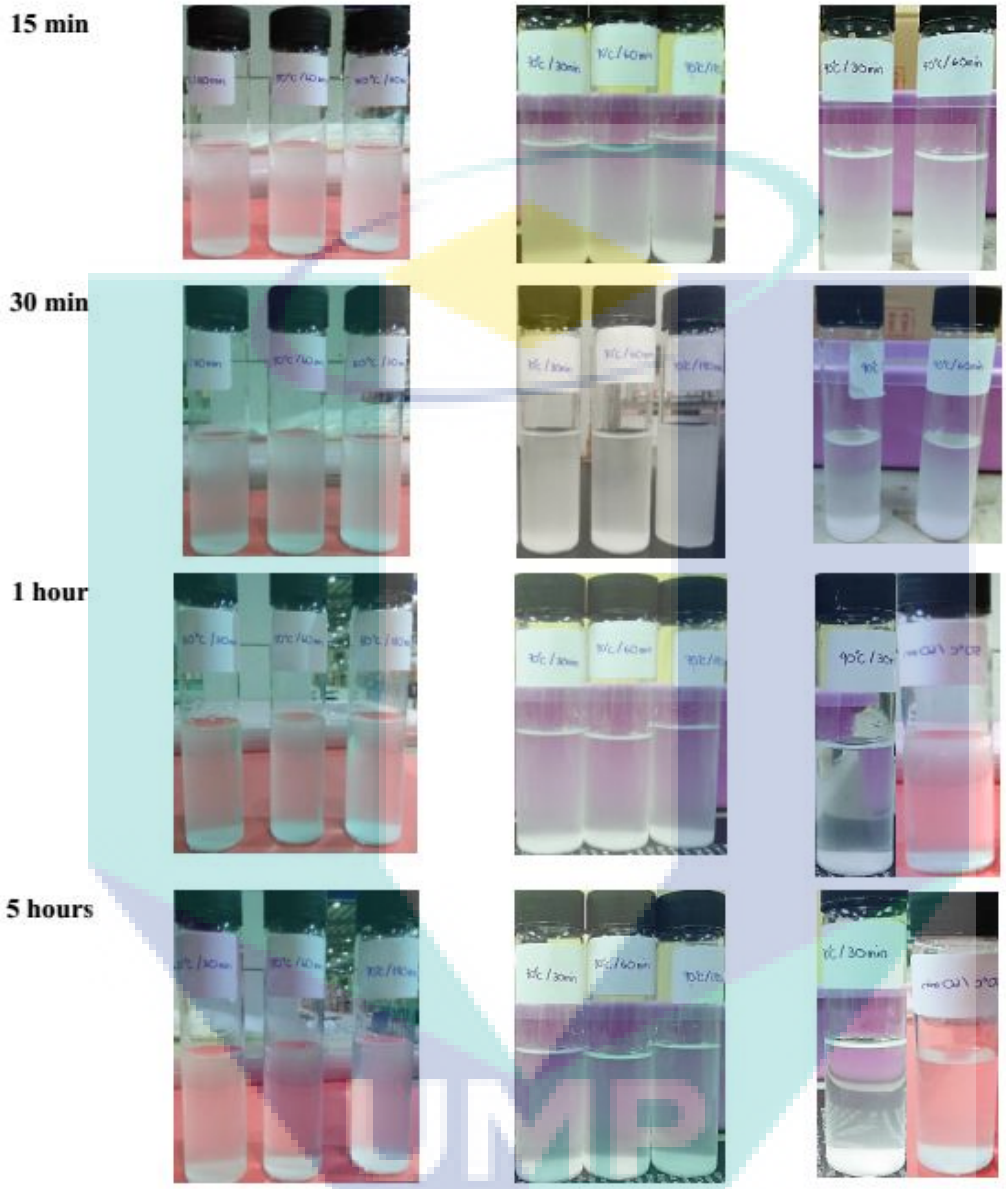

Figure 4.11 Photographs of CNC isolated via mixed acid hydrolysis system at 50°C, 70°C, and 90°C were dispersed in deionized water at 5 min, 15 min, 30 min, 1 hour and 5 hours.

4.1.3 Isolation of CNC via mechanical method (high energy bead milling)

4.1.3.1 Morphology and dimensions

Transmission electron microscopy (TEM) was carried out to investigate the dimensions and morphology of CNC. The dimensions were measured using ImageJ software by magnifying the images to identify the rice-like particles end to end with at least 10 particles measured. From the TEM images in Figure 4.12 and 4.13, it can be seen that MCC was successfully fibrillated and deconstructed into nanocrystals via the HEBM process. Unlike other mechanical processes[130] reported, including a similar ball milling process[131] (with softwood pulp sheet and alkaline solutions) where only micro- and nano-fibrillated cellulose (MFC/NFC) were observed. Here, the nanoparticles produced via our HEBM investigation exhibited rod-like or long rice-like morphology. As listed in Table 4.4, the aspect ratio of CNC products ranged from 20 to 26. Interestingly, the morphology and the aspect ratio values are actually quite similar to that of the CNC produced via acid hydrolysis.[132] Furthermore, we found that the changes to morphology and dimensions were not significantly affected by the duration of milling (between 15 and 120 min) and the concentration (between 0.5 and 2 wt. %) of the suspension used in this study. It implies that even at 15 minutes of milling, rod-like cellulose nanocrystals can be obtained. However, according to the TEM images, the interaction between the individual CNC is slightly altered, for example, the CNC obtained from higher concentrations (eg. 2 wt. %) tend to interact through edges of the particles indicating the electrostatic interactions between the CNC. The production yield (%) (product weight over raw material weight) of CNC from the suspension of MCC ranged between 57 and 76 %. It is to be noted that some yield reduction can be attributed to material losses occurring during handling, including withdrawal of the suspension from the mill, and filtering plus washing of the balls after the milling process. The yield % values are relatively higher than the reported yield of CNC obtained via acid hydrolysis (22 – 52%) depending on sources.[64, 132a, 133]

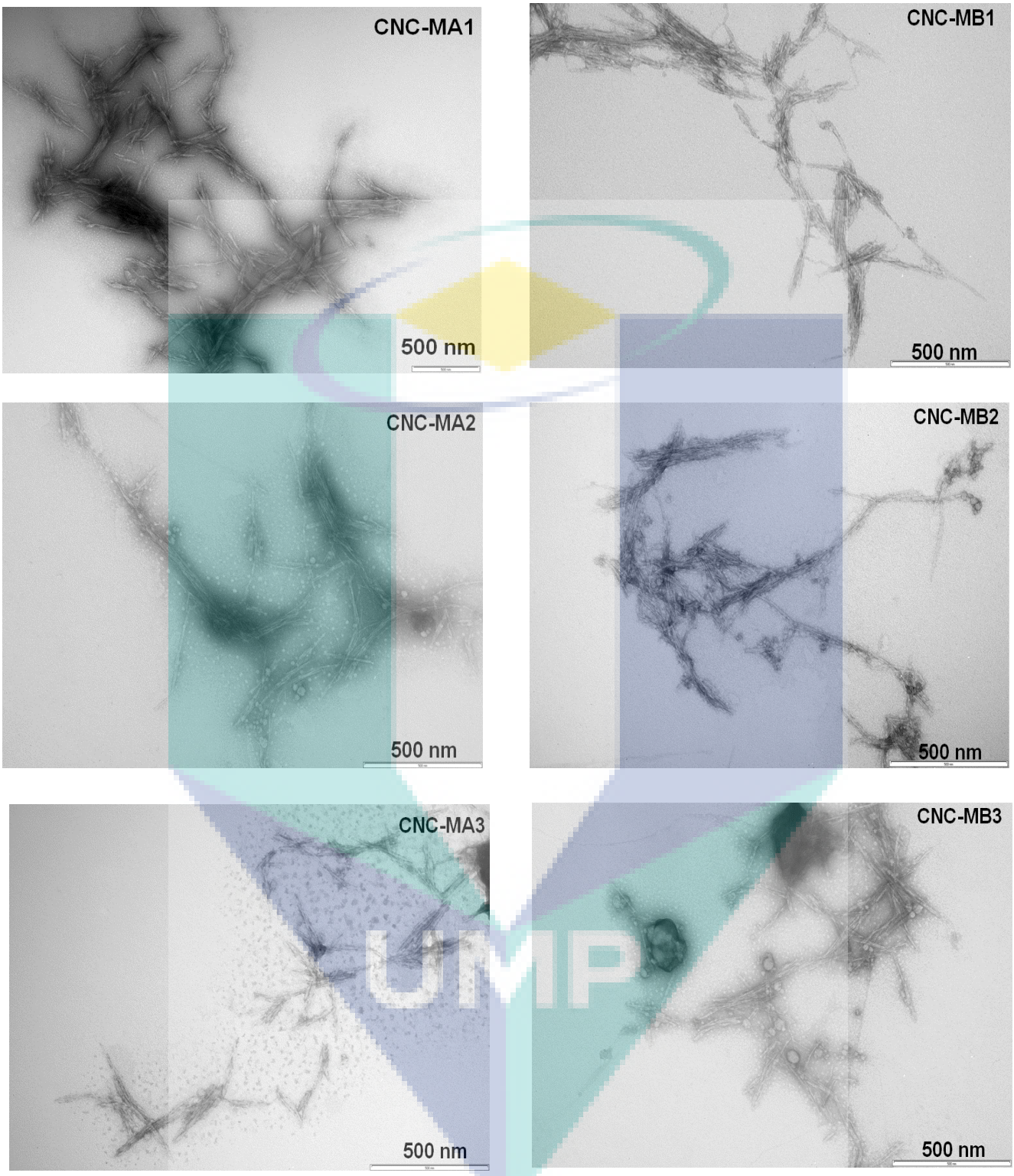

Figure 4.12 TEM images of CNC obtained via HEBM from the dispersion of 0.5 wt.% (left) and 1 wt.% (right) of MCC obtained via HEBM process.

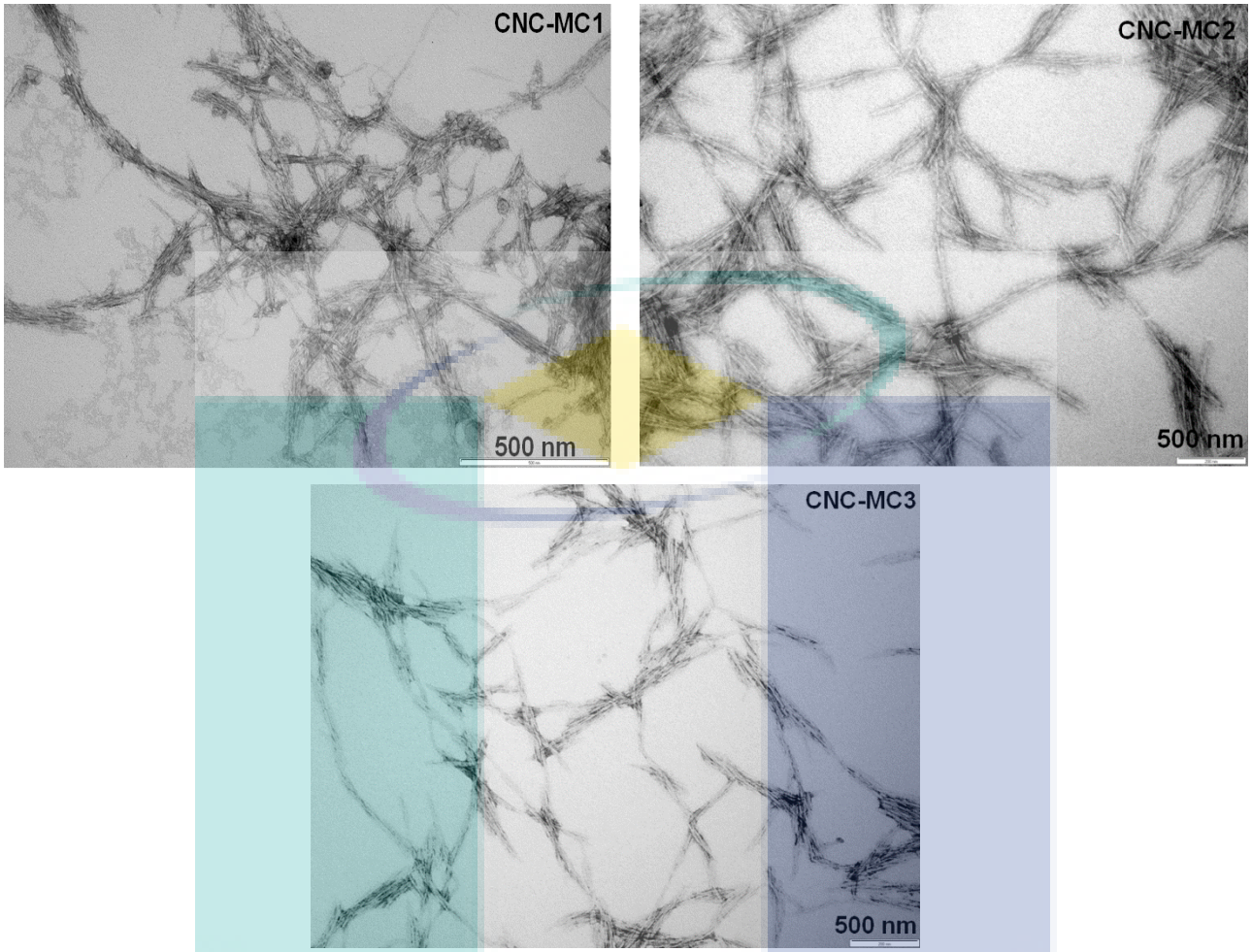

Figure 4.13 TEM images of CNC obtained via HEBM from the dispersion of 2 wt. % MCC in deionised water.

Table 4.4 Dimensions and the production yield of CNC isolated using high energy bead milling.

Sample	Conc. (wt.%)	Milling time (min)	Length (nm)	Width (nm)	Aspect Ratio	Yield (%)
CNC-MA1	0.5	15	320 ±53	15 ±3	21	69
CNC-MA2	0.5	30	351 ±90	18 ±5	20	57
CNC-MA3	0.5	60	317 ±63	18 ±4	23	65
CNC-MB1	1	15	286 ±100	13 ±5	23	64
CNC-MB2	1	30	301 ±115	13 ±7	24	66
CNC-MB3	1	60	371 ±71	14 ±5	26	76
CNC-MC1	2	15	431 ±138	20 ±9	23	67
CNC-MC2	2	30	387 ±83	15 ±3	26	58
CNC-MC3	2	60	424 ±90	17 ±4	25	76

As a comparison, CNC was also obtained via an ultrasonication method following previously reported protocols[134] with some slight modifications. Figure 5.4 shows the TEM images of CNC obtained from the top layer of the suspension obtained after ultra-sonication (CNC-U) of the MCC. They also showed 'rod-like' or 'rice-like' nanocrystals with an average aspect ratio of 15 (165 ±23 nm length and 11 ±2 nm in width). However, the production yield (%) of CNC from top layer suspension was very low, i.e. 8-10 % of the initial weight. Meanwhile, the bottom layer had clusters or agglomerates of cellulose particles with dimensions of 100 nm to 500 nm (Figure 5.4).

4.1.2.6 Thermal stability

Thermal stability of CNC obtained via milling was measured by thermogravimetric analysis (TGA). Figure 4.14 compares the thermograms of MCC and CNC. A slight weight loss in the low temperature region (<110°C) can be attributed to the residual adsorbed water in the cellulose particles, even after vacuum drying. The onset degradation temperature (T_{onset}) for MCC was 270°C, whereas a slight decrease in T_{onset} was observed for CNCs (230 - 263°C) obtained after the milling process. This slight

decrease can be attributed to either the increase in the cellulose surface area, fragmentation or decrease in crystallinity caused by the milling process.

The degradation of CNC-U starts from 250°C which is slightly lower than the onset degradation temperature of MCC. This decrease may be associated with the increase in free cellulose chains and fragmentations brought about by ultrasonication.[56] The CNC variants obtained via the HEBM process all show a higher thermal stability when compared to the thermal stability of the CNC obtained via typical sulphuric acid hydrolysis, which typically start to decompose at 150°C.[56, 114] It is to be noted that the processing temperature of many thermoplastic polymers falls within the range of thermal stability exhibited by CNC obtained via HEBM process.

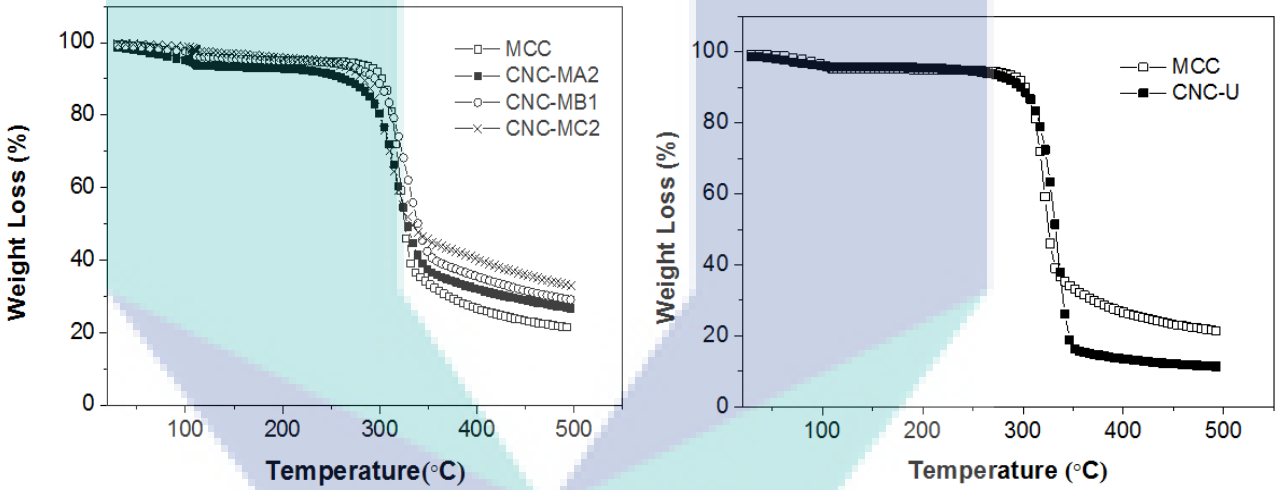

Figure 4.14 TGA thermograms of CNC obtained via HEBM (right) and ultrasonication (left) obtained from MCC, retainment of thermal stability.

4.1.2.7 Crystallinity of CNC

The effect of milling on the crystalline structure of MCC particles was investigated by X-ray diffraction analysis. The characteristic peaks at 2θ= 15 (101), 16.5 (10$\bar{1}$), 20.8 (021), 22.5 (002) and 34.3 (040) of crystalline polymorph I cellulose for MCC[135] can be seen in Figure 4.15. These peaks can be still observed for the CNC obtained via milling process. The crystallinity index (I_{Cr}) expressed as a percentage was calculated from the ratio of the crystalline peak ($I_{002} - I_{am}$) and the total peak of 002 lattice plane. The I_{Cr} of the initial MCC was about ~ 95 %.

CNC obtained by the milling process showed a degree of crystallinity in the range between 85 – 95% with no significant trend observed upon varying concentration (0.5 - 2 wt. %) and milling time (15-60 min). The crystallinity for CNC obtained via ultrasonication was within this range, ~ 90%, indicating a similar crystalline structure. The crystallinity range observed in this study is still higher than the earlier reported values (67 - 82%) for CNC obtained via acid hydrolysis.[56, 136] It is also higher than the crystallinity (~32%) reported for CNC obtained after prolonged dry milling (1-6 days) and dilute acid hydrolysis.[137] Nevertheless, the maximum milling time was only 60 minutes via the wet milling conditions used in this study lead to less destruction of the crystal structure than seen with extensive dry milling.

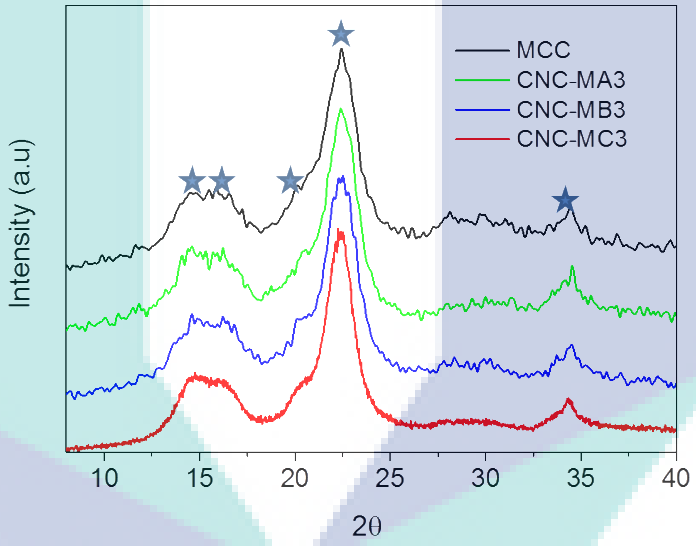

Figure 4.15 XRD patterns of commercial MCC and CNC obtained (after 60 min of milling) via HEBM method showing the retainment of crystalline domains of cellulose at 2θ = 15 (101), 16.5 (10ī), 20.8 (021), 22.5 (002) and 34.3 (040).

4.2 TPU nanocomposites

4.2.1 TPU/CNC nanocomposites

4.2.1.1 Physical appearance of TPU nanocomposites

The influence of different thermal stabilities and surface chemistry of CNC on processing can be clearly observed in Figure 4.16 from the physical appearance of compression

moulded nanocomposite films produced via melt compounding and solvent casting. The TPU/CNC nanocomposite films produced via solvent casting retained the transparency of the host TPU at low 0.5-1 wt. % loading levels for all types of CNCs, and at the higher 5 wt. % loading the nanocomposites with CNC-S and CNC-MC showed just some feint discolouration. The solvent cast nanocomposites with CNC-P were able to retain the transparency of the host TPU even at 5 wt. %. However, very obvious and commercially-unacceptable colour changes (darkening) for nanocomposites obtained via melt-compounding can be seen from Figure 4.16, and the order of extent of discolouration is as follows: TPU control (MC-TPU Control) < Nanocomposites using phosphoric acid hydrolysed CNCs (MC-TPU/CNC-P) << Nanocomposites using micronised CNCs (TPU/CNC-MC) < Nanocomposites using conventional sulphuric acid hydrolysed CNCs MC-TPU/CNC-S. Even at 0.5 wt. % of CNC-S loading, the light brown colour of nanocomposite films was noticeable. As the processing temperature employed in the extruder was about 225°C, the CNC isolated from sulphuric acid hydrolysis showed degradation behaviour and darkened. As reported previously, sulphate $(SO_4)^{2-}$ groups, which are present on the surface of CNC might promote the dehydration reactions.[114, 124, 138] The onset degradation temperature of CNC-P and CNC-MC stated in previous section show 255 and 258 °C respectively However, the dispersibility of CNC-P (where phosphate groups assist in achieving superior colloidal suspension stability) is better than CNC-MC, which also gives rise to the discolouration of nanocomposites incorporating CNC-MC. This strongly suggests that this discolouration in melt compounded TPU nanocomposites is due to relative CNC thermal stability and degradation, which in-turn leads to the aggregation of the less thermally stable nanocellulose.

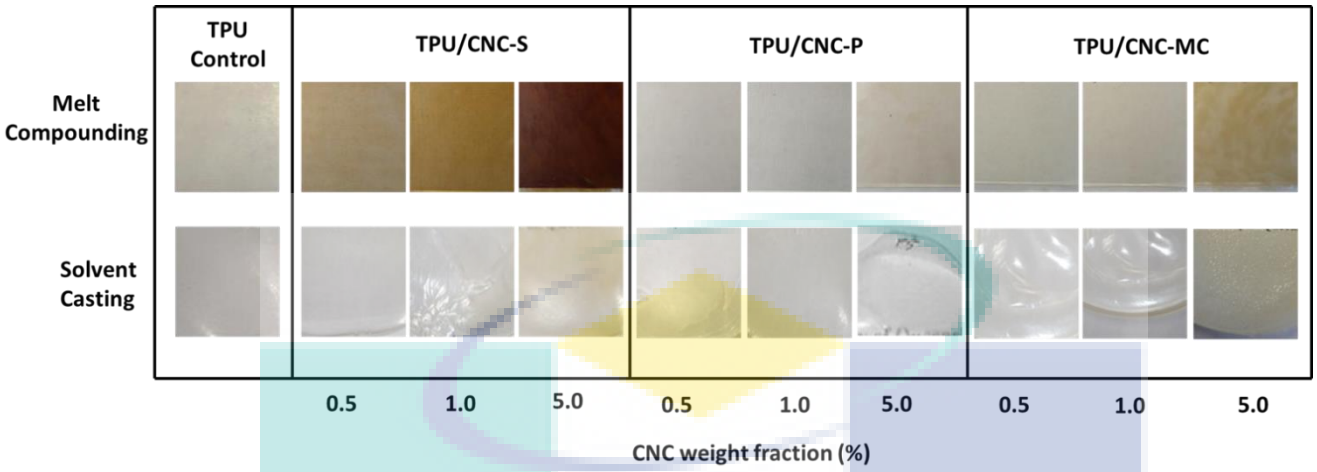

Figure 4.16 Photographs of TPU control and TPU/CNC nanocomposites processed via solvent casting (bottom) and melt compounding (top).

4.2.1.2 Spectroscopic characterisation of TPU/CNC nanocomposites

Fourier transform infrared (FTIR) spectroscopy was used to identify the network bonding of TPU and the effect of CNC presence in TPU nanocomposites. It can be expected that the hydroxyl groups and any other ionic charges available on the surface of CNC may play a critical role in dispersion and physical appearance of nanocomposite films. The hydroxyl groups on the surface of CNC may interact with polyurethane matrix chains by reacting with any free isocyanate groups and/or via hydrogen bonding through N-H and C=O groups. Their influence on the network formation was further followed by determining the association of N-H bonding quantitatively from the intensities and area of corresponding peaks. The 'free' N-H bond denotes the N-H covalently connected with C=O groups in the urethane linkage (represents for elastic behaviour), whereas the 'associated' N-H represents the N-H bonds further associated with C=O via hydrogen-bonding (which represents the association in hard domains and physical network formation).[139], [140], [141]

Figure 4.17 and 4.18 shows the FTIR spectra of TPU control and its nanocomposites obtained via solvent casting and melt compounding methods, respectively. The peak at 3450-3454 cm^{-1} represents the stretching vibration of 'free' N-H bonding and the degree of association can be further calculated by a shift in frequency (wavenumber) to low energy region as in equation (3) described in Chapter 3.[142] Table 4.4 shows the frequency shift (Δv) (from 3451 cm^{-1}) of the N-H stretching mode values, peak area of N-H and C=O

groups of TPU control and its nanocomposites. In comparison of process, the nanocomposites processed via melt compounding have shown higher frequency shift than that processed via solvent casting. The shearing force in melt compounding, probably increase the potential of hydrogen bonding formation. Moreover, the peak at 3300 cm^{-1} which represents 'associated'/'bonded' N-H groups has sharply increased for melt compounded samples. This may be related to the formation of more N-H bonding through degradation and transurethanisation reactions[143] in nanocomposites and the TPU control itself showed a decrease in molecular weight probably due to chain scission upon melt compounding. TPU/CNC-S nanocomposites also show a decreasing trend in frequency shift and bonded N-H due to thermal degradation occurred in the presence of cellulose. Furthermore, an additional peak between 1620 cm^{-1} and 1650 cm^{-1} can be seen in TPU nanocomposites via melt compounding method which may represents an amide (N-H) functional group. Again, this may indicates TPU nanocomposites melt compounded had a sign of degradation and transurethanisation reactions at elevated temperature. This has been discussed by several authors who investigated model compounds with MDI/BDO hard segments and observed that the dissociation of the free isocyanate and hydroxyl end-groups was the primary degradation mechanism. For instance Yang et al.[144] and Martin et al.[145] showed significant TPU degradation and the existence of free isocyanate at the processing temperature above 200°C and 150°C respectively.

The peaks at 1729 cm^{-1} and 1700 cm^{-1} were assigned to the "free" C=O and hydrogen bonded C=O respectively.[142, 146] Table 4.5 shows the area of the absorbance peak of 'free' C=O, and 'associated' C=O for TPU nanocomposites reinforced with CNC, processed via both solvent casting and melt-compounding methods. The increase of "free" C=O in melt compounded samples may also indicates the chain scission occurred which decreased the potential of network formation between functional group therefore shows insignificant changes in bonded C=O. Comparison based on types of CNCs shows that CNC-S incorporated TPU via solvent casting shows significant decrease for C=O group linearly with CNC loading.

The influence of CNC incorporation in TPU matrix was further studied in terms of degree of phase separation (DPS) and degree of phase mixing (DPM).[147] The degree of the carbonyl groups participation in hydrogen bonding can be defined by the carbonyl hydrogen bonding index, R. The obtained values of R and DPS of TPU/CNC

nanocomposites are given in Table 4.6 for TPU nanocomposites fabricated by solvent casting and melt compounding methods, respectively. Overall, the DPM of melt compounded materials was not significantly influenced by cellulose addition, whereas the DPM values for solvent cast samples showed quite a bit of variability. This may indicate that the quality of TPU/CNC dispersions and some variation in, for example, rate of solvent evaporation depending on positioning in the purged casting oven may have affected the association of polymer sequences (hard segments) with CNC (for the solvent cast nanocomposites), whereas, the high shear and temperature control employed in melt compounding results in nanocomposites with (a) better distributive and dispersive mixing, and (b) more well-controlled thermal history.

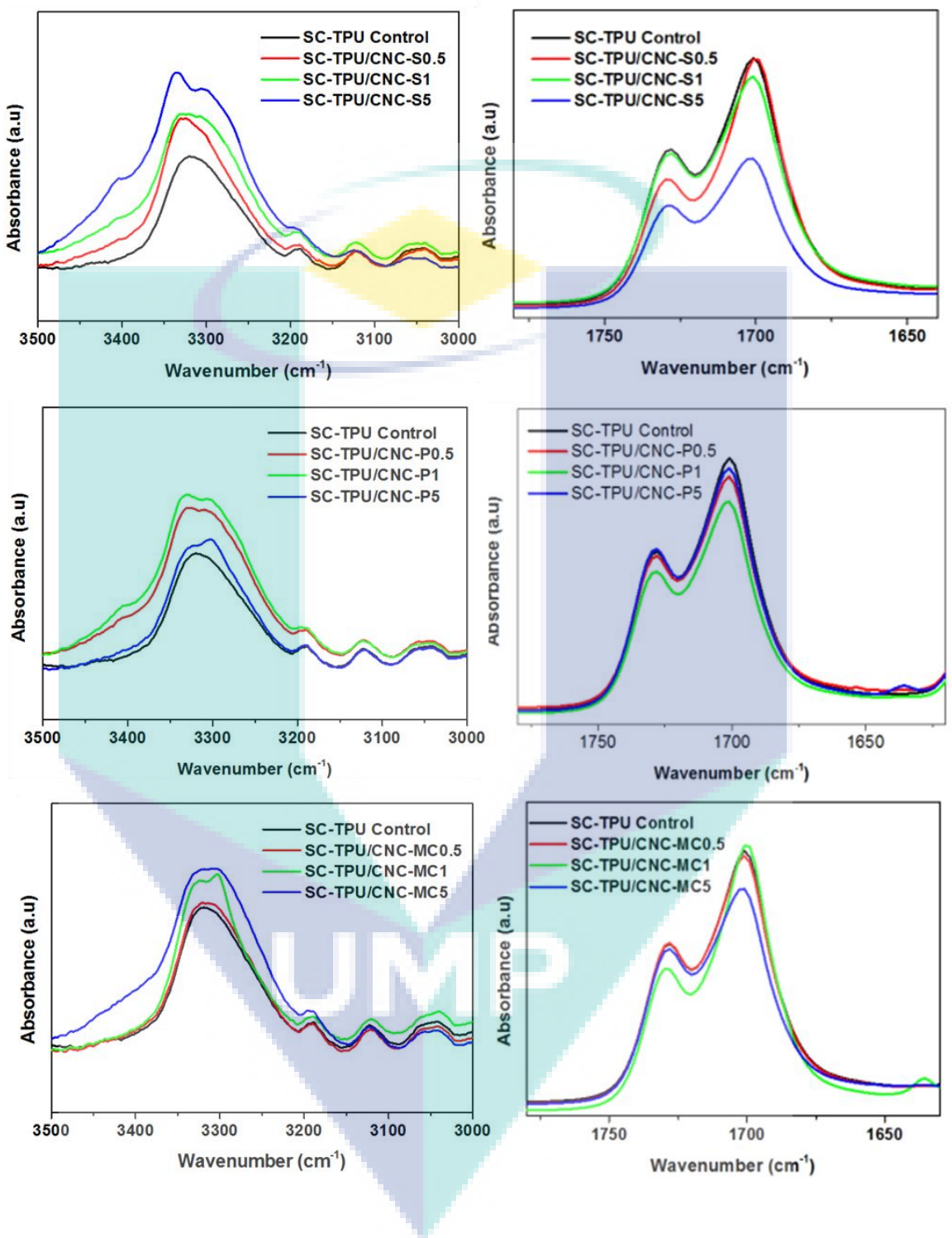

Figure 4.17 FTIR spectra of the N-H stretching region (3350 cm^{-1}) and C=O (1700 and 1729 cm^{-1}) stretching region of TPU nanocomposites fabricated via the solvent casting method.

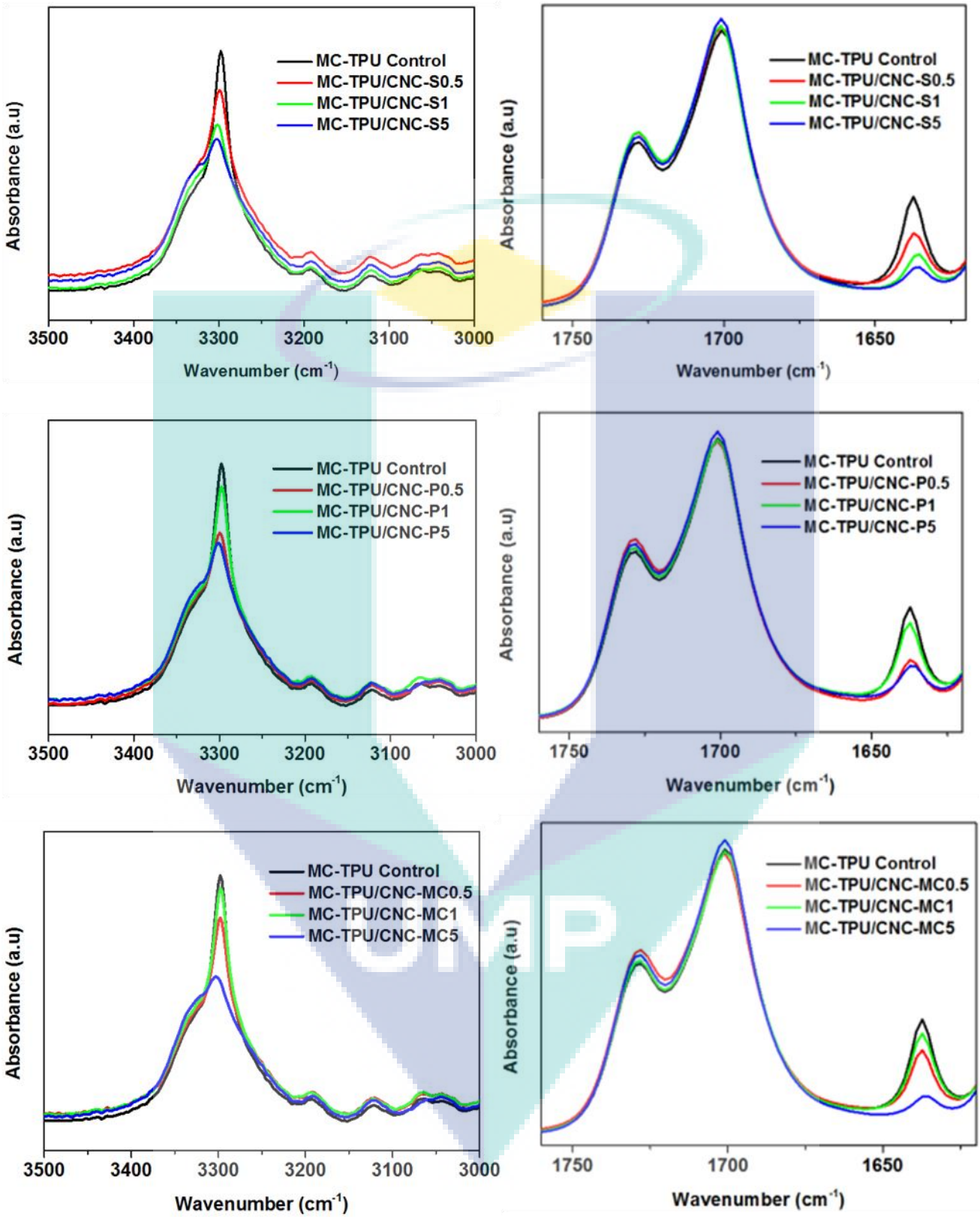

Figure 4.18 FTIR spectra of the N-H stretching region (3350 cm^{-1}) and C=O (1700 and 1729 cm^{-1}) stretching region of TPU nanocomposites fabricated via the melt compounding method.

Table 4.5 Frequency shift of the N-H stretching mode, and peak area of N-H and C=O groups of the TPU nanocomposites via solvent casting (SC) and melt compounding (MC) method.

Sample	Δv (cm^{-1})		Bonded N-H		"Free" C=O (1729 cm^{-1})		Bonded C=O (1700 cm^{-1})	
	SC	MC	SC	MC	SC	MC	SC	MC
TPU Control	130	153	17.2	14.9	8.6	7.8	20.7	19.0
TPU/CNC-S0.5	123	153	21.1	17.5	6.8	8.4	20.0	19.9
TPU/CNC-S1	125	150	25.0	15.2	8.7	8.2	19.6	19.5
TPU/CNC-S5	116	149	30.2	15.5	5.9	8.0	12.5	19.8
TPU/CNC-P0.5	135	152	25.3	15.2	8.8	8.3	18.2	19.4
TPU/CNC-P1	134	153	25.1	16.2	7.8	8.1	17.7	19.3
TPU/CNC-P5	136	150	19.4	15.7	9.1	8.2	20.2	19.6
TPU/CNC-MC0.5	134	153	18.0	15.5	8.8	8.1	20.4	19.7
TPU/CNC-MC1	135	154	19.7	16.1	6.7	7.9	19.2	19.5
TPU/CNC-MC5	136	149	23.8	14.7	8.6	8.4	18.3	19.7

Table 4.6 The carbonyl hydrogen bonding index, the degree of phase separation (DPS) and the degree of phase mixing (DPM) in TPU/CNC nanocomposites via solvent casting (SC) and melt compounding (MC) method.

Sample	R		DPS		DPM	
	SC	MC	SC	MC	SC	MC
TPU Control	1.68	1.68	62	63	38	37
TPU/CNC-S0.5	1.63	1.63	66	62	34	38
TPU/CNC-S1	1.62	1.62	60	62	40	38
TPU/CNC-S5	1.68	1.68	62	63	38	37
TPU/CNC-P0.5	1.54	1.54	61	60	39	40
TPU/CNC-P1	1.65	1.65	60	62	40	38
TPU/CNC-P5	1.63	1.63	60	62	40	38
TPU/CNC-MC0.5	1.54	1.54	61	60	39	40
TPU/CNC-MC1	1.65	1.65	66	62	34	38
TPU/CNC-MC5	1.64	1.64	58	62	42	38

4.2.1.3 Thermal properties

The thermal transition behaviour of TPU controls and TPU/CNC nanocomposites was analysed by differential scanning calorimentry (DSC). The associated thermograms in Figure 4.19 shows at least five transition temperatures for the series of samples due to the disruption and fusion of different segmental phases. This indicates the classical multiphasic morphology of segmented polyurethanes.[148]

These endothermic transitions can be divided into four parts as follows;

T1 (50-70°C): The ordering of hard segments containing single MDI.
T2 (100-180°C): The glass transition of hard-segments and disruption of various degrees of short-range hard segments (HS) composed of MDI_2BDO, MDI_3BDO_2 blocks
T3 (190-210°C): Higher melting hard microphase.
T4 (211-217°C)*:* The disruption of predominantly MDI_4BDO_3 and MDI_5BDO_4 hard segment structures.

Table 4.7 and 4.8 summarise the transition temperatures, the glass transition temperature (T_g) and the ethalpy for the fusion of the hard segments in TPU fabricated via solvent cast and melt compounding. In general, the TPU systems and nanocomposites shows diffuse and clear differences in the classical thermal transition signatures that typically found in DSC and DMA as commercial of TPU (Texin 990) was used. The T_g of TPU control via both solvent cast and melt compounding are 50 and 51°C, respectively, indicating no significant change in soft domain is observed upon processing conditions. However, after the incorporation of CNC, the T_g of TPU nanocomposites was increased slightly shows the limitation in mobility of polyether sequences which attributed to the presence of CNC in the structure.

T1 endotherm is evident in all materials at the temperature recorded in the range between 58°C and 68°C. T1 endotherm in materials prepared from melt compounding is slightly lower shows that material has fewer short hard segments[148b] compared to solvent cast samples. T2 endothermic transitions can be seen in all TPU and nanocomposites as well, with temperature range between 94°C to 169°C. Significant difference between fabrication method was observed at T3 and T4 endotherm peak segments. These peaks exhibit distinctively in TPU nanocomposites processed via melt compounding method. This indicates the formation of crystal structure with long range orders [149] in melt compunded material.

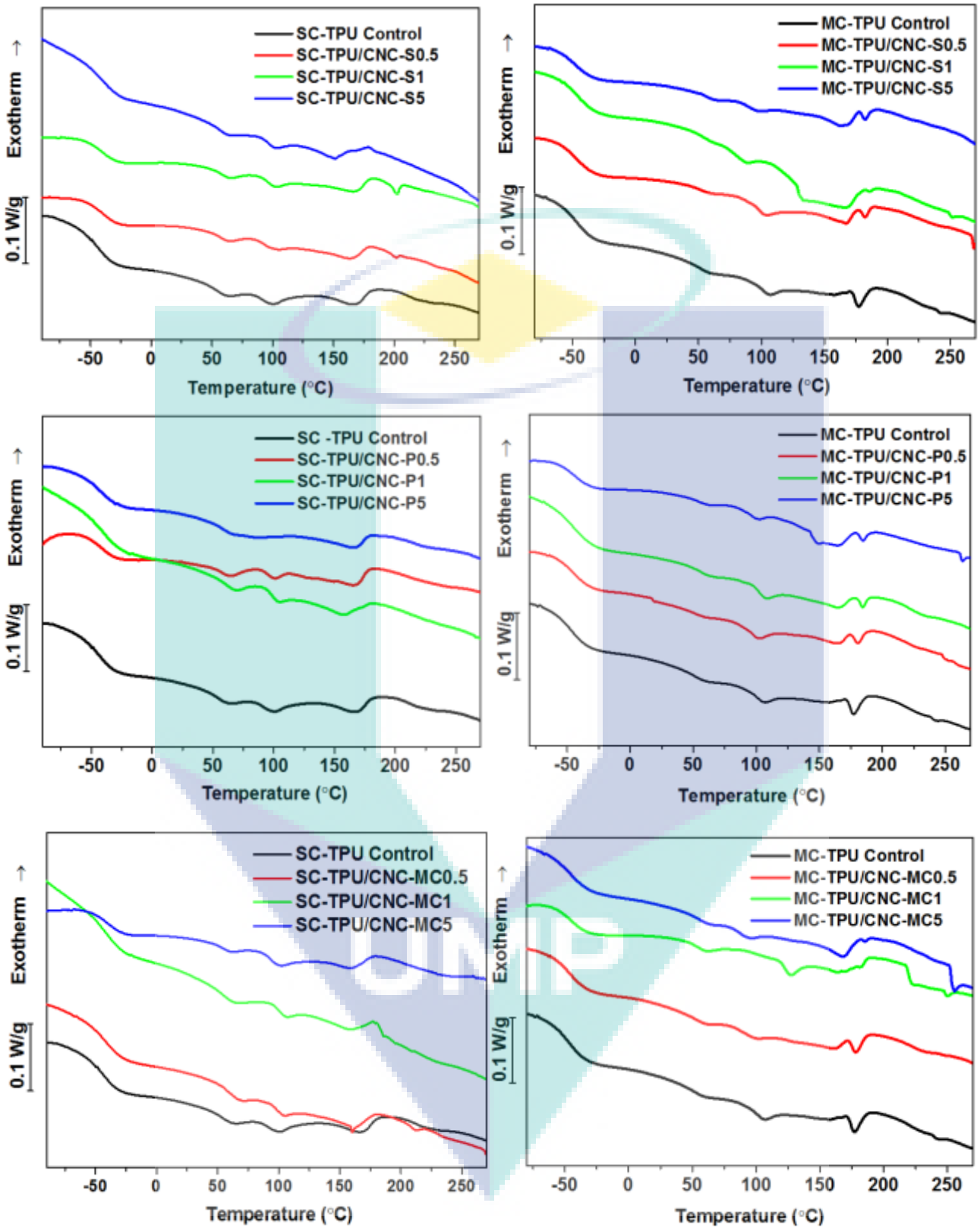

Figure 4.19 DSC thermograms of TPU/CNC nanocomposites processed via solvent casting (left) and melt compounding (right).

Table 4.7 Transition temperatures for TPU/CNC nanocomposites processed via solvent casting.

Sample	$T_{g\ (soft)}$ (°C)	Endotherm Peaks				Hard Phase ΔH (J/g)
		T1(°C)	T2(°C)	T3(°C)	T4(°C)	
SC-TPU Control	-50	62	101 166	-	-	6.54
SC-TPU/CNC-S0.5	-40	64	103 165	201	-	4.45
SC-TPU/CNC-S1	-41	65	102 169	202	-	5.07
SC-TPU/CNC-S5	-42	64	103 152	-	-	5.84
SC-TPU/CNC-P0.5	-43	64	100 168	-	-	4.90
SC-TPU/CNC-P1	-45	67	103 159	-	-	5.76
SC-TPU/CNC-P5	-41	66	167	-	-	3.71
SC-TPU/CNC-MC0.5	-46	68	104 160	-	211	5.94
SC-TPU/CNC-MC1	-45	66	105 160	201	-	6.71
SC-TPU/CNC-MC5	-40	61	101 141	-	-	6.01

The cumulative enthalpy (ΔH) which is sum of the enthalpies of all transitions observed for samples are also tabulated. In comparison of control samples, TPU processed via solvent casting showed higher enthalpy indicating the solvent-induced ordering of polymer chains (hard-segments). In addition of cellulose there was no significant trend was observed in the enthalpy of TPU nanocomposites.

As it was not possible to perform synchrotron SAXS on these systems for this project, as we have done previously, this study would be the most sensitive approach to resolve statistical morphological differences (eg average interdomain spacings, hard domain

textures, effect of the addition of CNC nanofillers on the hard-soft microdomain interphase region).[150]

Table 4.8 Transition temperatures for TPU/CNC nanocomposites processed via melt compounding.

Sample	$T_{g\,(soft)}$ (°C)	Endotherm Peaks				Hard Phase ΔH (J/g)
		T1(°C)	T2(°C)	T3(°C)	T4(°C)	
MC-TPU Control	-51	59	106	176	238	3.83
MC-TPU/CNC-S0.5	-49	60	103 168	183	269	4.86
MC-TPU/CNC-S1	-45	68	105 170	188	251	9.91
MC-TPU/CNC-S5	-50	64	97 164	183	-	4.57
MC-TPU/CNC-P0.5	-46	58	102 166	176	250	4.45
MC-TPU/CNC-P1	-46	62	107 166	184	232	4.45
MC-TPU/CNC-P5	-44	62	101 160 164	185	263	6.87
MC-TPU/CNC-MC0.5	-46	60	99 162	178	231	3.94
MC-TPU/CNC-MC1	-49	61	127 164	182	249	4.10
MC-TPU/CNC-MC5	-47	63	94 169	186	255	5.62

4.2.1.4 Thermo-mechanical properties

The dynamic mechanical analysis (DMA) has been done to analyse the mechanical properties upon temperature dependence. DMA for every sample was carried out at least times to obtain consistent curve. Figure 4.20, 4.21 and 4.22 show the storage modulus (*E′*) and tan δ as a function of temperature for nanocomposites reinforced with CNC-S, CNC-P and CNC-MC, respectively. In the glassy region (below -60°C), the storage modulus for all samples has high value around 1-3 GPa which typically shows by multi-phasic elastomers material. By incorporating CNC at lower loading (0.5 and 1 wt. %), the *E′* of TPU nanocomposites were minimally affected. However, at 5 wt. %, the *E′*of TPU nanocomposites was increased greatly. Overall, the *E'* at room temperature of TPU control and TPU nanocomposites is higher when prepared by melt compounding and increased linearly with CNC loading. This probably due to the hard microdomains is more cohesive inducing their filler-like reinforcement and physical crosslinking.[151] The storage modulus (*E′)* in the rubbery region (0 to 100°C) of TPU control and nanocomposites samples shows different relaxation behaviour depending on the processing method. Overall, in melt compounded samples, the storage modulus decreased linearly probably represent well dispersed of CNC and hydrogen bonded/ associated system in the structure. Meanwhile,

solvent cast samples display solvent-induced morphology (depending on the dispersion of CNC and crystallisation behaviour).

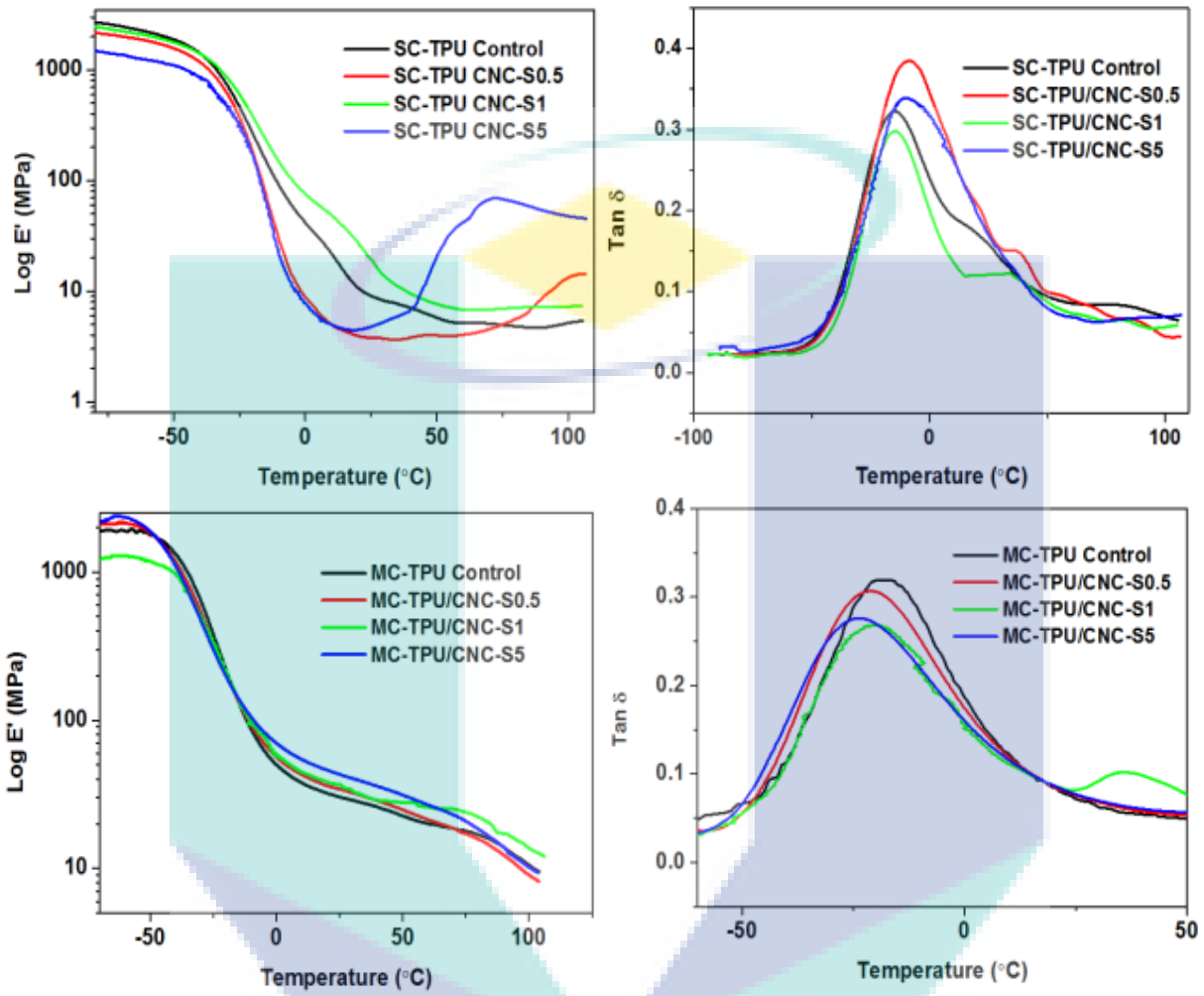

Figure 4.20 Storage modulus (left) and tan delta (right) of TPU/CNC-S nanocomposites processed via solvent casting (top) and melt compounding (bottom).

In comparison of CNC types, obviously TPU nanocomposites incorporated with acid hydrolysed CNCs (CNC-S, CNC-P) display a strange trend of curve especially in solvent casting process. This may be probably due to residual of solvent (N,N-dimethyformamide (DMF)) which has been used as dispersion medium. However, this phenomenon was not observed significantly in TPU/CNC-MC nanocomposites. It looks like the acid hydrolysed CNCs have perhaps adsorbed or bound solvent, or are otherwise affected in some way by the swelling in DMF.

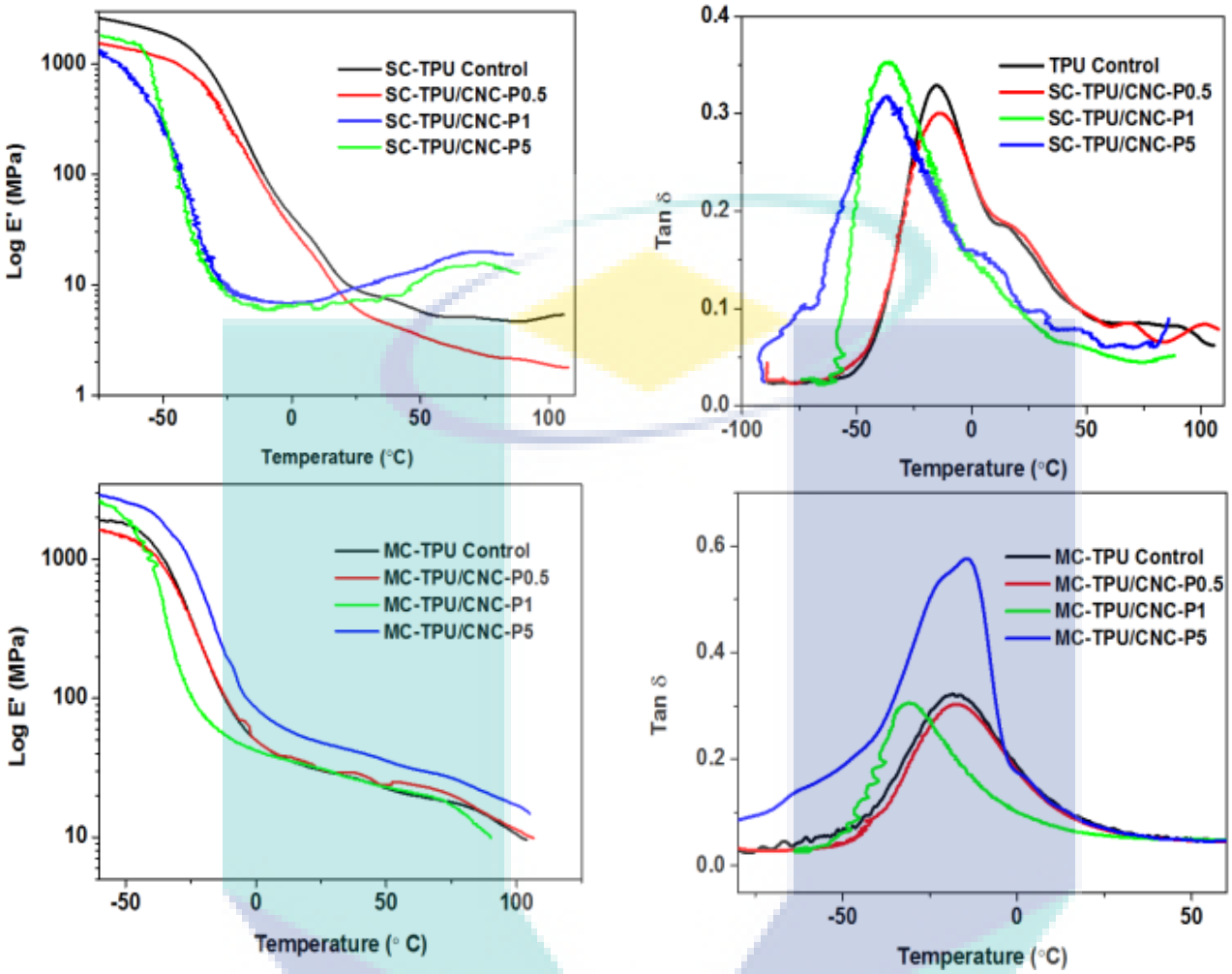

Figure 4.21 Storage modulus (left) and tan delta (right) of TPU/CNC-P nanocomposites processed via solvent casting (top) and melt compounding (bottom).

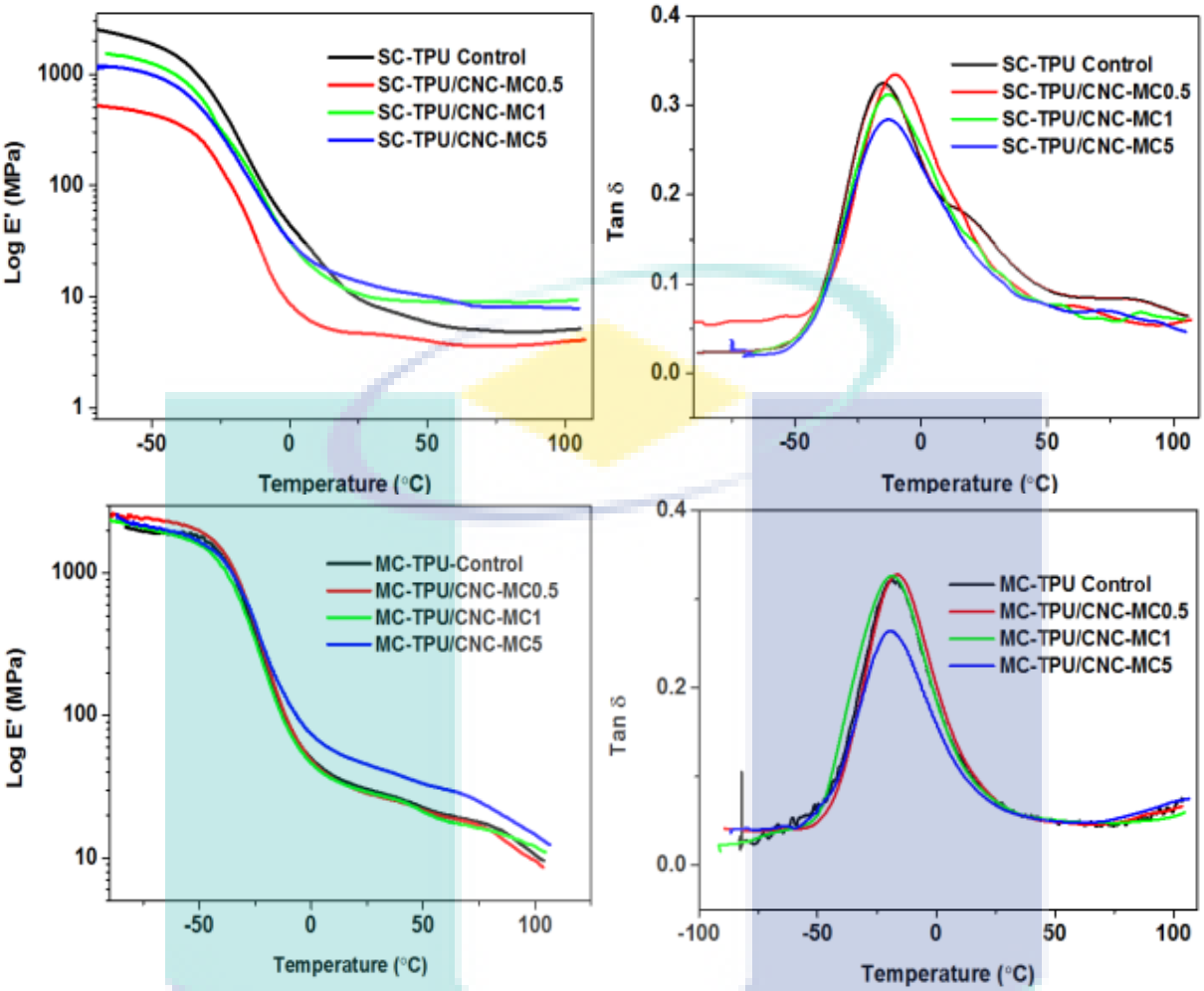

Figure 4.22 Storage modulus (left) and tan delta (right) of TPU/CNC-MC nanocomposites processed via solvent casting (top) and melt compounding (bottom).

The tan δ peak represents the soft segment glass transition temperature (T_g) and the peak values are given in Table 48. T_g measured via DMA is shifted to higher temperature with respect to T_g via DSC analysis due to its dependency on frequency. Overall the T_g value is in agreement with the results of DSC which was increased slightly after the incorporation of cellulose at low volume fraction. However, there is a decrease of T_g in some samples like TPU/CNC-P by solvent casting and CNC-S incorporating TPU via melt compounding probably cause by the CNC agglomeration and degradation.

Table 4.9 Tensile storage modulus (*E'*) and glass transition temperature (T_g) of TPU and nanocomposites.

Sample	Storage modulus at 25 °C (MPa)		Damping peak (°C)	
	SC	MC	SC	MC
TPU Control	9.0	30.7	-15.5	-18.3
TPU/CNC-S0.5	3.8	34.1	-8.0	-17.5
TPU/CNC-S1	19.1	36.2	-14.8	-19.7
TPU/CNC-S5	5.0	47.2	-10.7	-23.8
TPU/CNC-P0.5	6.1	31.3	-14.3	-17.1
TPU/CNC-P1	7.2	30.8	-36.5	-31.1
TPU/CNC-P5	10.4	48.7	-37.0	-17.1
TPU/CNC-MC0.5	4.7	28.3	-10.3	-16.3
TPU/CNC-MC1	10.7	29.6	-13.1	-19.0
TPU/CNC-MC5	13.3	44.7	-13.4	-19.3

4.2.1.5 Mechanical properties

In the development of polyurethane nanocomposites with nanoparticles, a significant improvement in tensile strength is important without compromising the elastic properties such as elongation and toughness. The reinforcement effect of the CNCs was investigated by measuring the tensile properties, tear strength, creep behaviour and hysteresis of the TPU control and its nanocomposites, at room temperature.

Figure 4.23 shows the stress-strain curves of TPU control and nanocomposites produced via both processes and the values determined are summarised in Table 4.10. Obviously, no significant changes in tensile strength upon 0 to 300% of tensile strain were observed for melt compounded material, whereas solvent cast nanocomposites show the increase difference immediately after 50% of strain. The solvent cast TPU control obtained higher tensile strength than melt compounded materials. The reduction mostly contributed by transurethanisation reaction occurred due to the harsh environment in the extrusion process.

The tensile strength of TPU reinforced with CNC-S, CNC-P and CNC-MC shows 18%, 16% and 14% of improvement respectively upon host polymer via melt compounding

method. The increase was recorded at CNC loading of 0 to 1 wt. %, as it reached 5 wt.% mechanical properties of the composites was declined. Regarding percolation model related to volume fraction of filler, the percolation threshold for CNC previously has been determined at 1- 2 volume % [46, 152] for CNC to form network with polymer matrix which most probably linked by the hydrogen bonding. Thus, in this work, CNC loading at 5 wt. % have been assumed ineffective as reinforcing element to the TPU matrix.

Moreover, elongation and stiffness at the optimum value of tensile strength were also unaffected indicating the soft-segment domain (rubbery property) of TPU was not disrupted by the cellulose addition. Furthermore, the reinforcement of CNC was also can be seen from the improvement in toughness and tear strength of TPU nanocomposites. These results indicate that CNCs able to work as an efficient stress transfer medium without disrupting the original function of the TPU microstructure (hard segment and soft segment). Indeed, preventing the undesired stiffening with soft domain was able to maintain the elongation of the TPU composites.

The strength of the material fabricated via melt compounding is competent by comparing it with solvent casting process. This also proved that cellulose (CNC-P and CNC-MC) able to be processed with high processing temperature method.

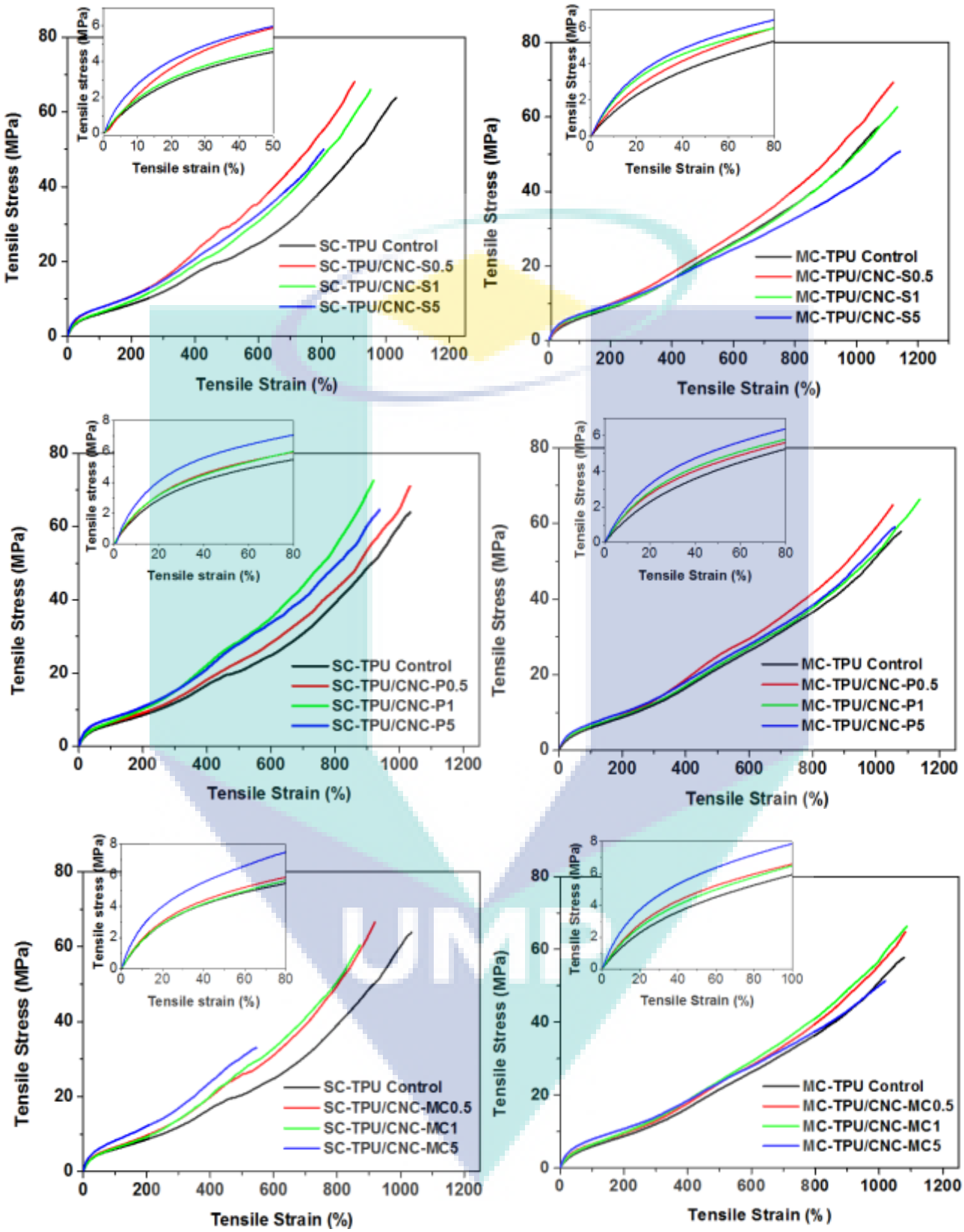

Figure 4.23 Stress-strain curves TPU nanocomposites fabricated via solvent casting (left column) and melt compounding (right column).

Table 4.10 Summary of tensile properties of TPU nanocomposites processed via solvent cast (SC) and melt compounding (MC) method.

Sample		Tensile Stress (MPa)	Tensile Strain at break (%)	Modulus (MPa)	Toughness (MPa)	Tear Strength (N/mm)
TPU Control	**SC**	64.7 ±1	954.6 ±33	13.6 ±1	258.9 ±7	69.4 ±15
	MC	57.7±3	1041.3 ±39	11.3±1	261.5 ±18	119.9 ±4
TPU/CNC-S0.5	**SC**	67.1 ±8	925.7 ±27	17.4 ±3	255.1 ±35	88.6 ±8
	MC	67.9 ±3	1115.7 ±29	14.3 ±1	319.3 ±21	118.7±4
TPU/CNC-S1.0	**SC**	65.8 ±3	964.6 ±35	16.5 ±3	261.9 ±14	96.8 ±5
	MC	62.1 ±2	1115.4 ±26	15.0 ±1	295.8 ±12	123.2±1
TPU/CNC-S5.0	**SC**	49.4 ±4	809.2 ±49	21.6 ±4	183.9 ±17	73.7 ±11
	MC	51.3 ±1	1137.5 ±19	17.2 ±1	281.6 ±9	129.1 ±4
TPU/CNC-P0.5	**SC**	66.0 ±7	994.8 ±55	11.3 ±4	256.2 ±39	70.5 ±27
	MC	65.9 ±2	1062.4 ±24	13.5 ±1	296.9 ±13	121.7±5
TPU/CNC-P1.0	**SC**	66.2 ±6	924.1 ±21	14.0 ±1	243.4 ±20	88.6 ±3
	MC	66.8 ±1	1108.8 ±29	14.0 ±1	295.8 ±12	120.9±2
TPU/CNC-P5.0	**SC**	64.5 ±7	950.8 ±62	20.7 ±2	271.2 ±40	78.9 ±16
	MC	59.9 ±2	1063.6 ±25	16.2 ±1	280.8 ±8	123.5 ±7
TPU/CNC-MC0.5	**SC**	66.9 ±8	956.0 ±46	14.9 ±2	256.3 ±33	85.7 ±16
	MC	64.0 ±2	1062.6 ±30	12.6 ±1	290.2 ±15	113.1±6
TPU/CNC-MC1.0	**SC**	60.4 ±4	822.4 ±70	14.6 ±2	210.3 ±24	81.6 ±21
	MC	65.6 ±2	1084.7 ±5	12.4 ±1	305.9±7	125.2±7
TPU/CNC-MC5.0	**SC**	33.2 ±3	583.7 ±75	22.4 ±4	103.3 ±19	83.1 ±12
	MC	51.2 ±1	1005.6 ±20	21.1 ±1	247.2 ±10	126.6 ±4

4.2.2 TPU/MCC nanocomposites via masterbatch process

4.2.2.1 Physical Appearance of TPU Nanocomposites

Types of reinforcing fillers plays an important role to improve the properties of TPU. Besides cellulose, carbon and clay are commonly used in TPU as a filler. Carbon materials are preferred for their mechanical properties, thermal conductivity and low density.[153] Clays are able to improve thermal, mechanical and barrier and viewed as potential fillers for automotive, aerospace and packaging industries. However, incorporating fillers like carbon and clay in polymer matrix may give an effects on the appearance of polymer matrix. Hence, by using MCC as reinforcing fillers does not affect the physical appearance of composites. Figure 4.24 shows the physical appearance of TPU control and TPU/MCC (1.0, M-3.0, M-5.0). Nanocomposites films produced via solvent casting retained the transparency at low 1 wt.% loading levels for all types of MCCs and at the higher 5 wt.%.

Figure 4.24 Physical appearance of composites

4.2.2.2 Morphology of MCC in TPU Matrix

Scanning electron microscope (SEM) images was employed to study the surface morphology of the composites. Figure 4.25 (a) shows the MCC which has size in the range of 5 µm to 20 µm, Figure 4.25 (b) is TPU control without MCC. Figure 4.25 (c) (d) (e) shows the TPU/MCC 1.0, M-TPU/MCC 1.0 and M-TPU/MCC 3.0 respectively. Figure 4.25 (c) shows TPU/MCC 1.0 from SEM images the small white dot shows the dispersed within TPU but only can be seen at certain area. For masterbatch sample Figure 4.2 (d) and (e) it was observed that MCCs uniformly dispersed in the TPU matrix, which can be seen the compatibility between the MCCs and TPU matrix was performed. During the solvent exchange procedure, the suspension of MCC and coating of MCC with TPU chains to ensure the dispersion of MCC in TPU matrix. Figure 4.25 (e) M-TPU/MCC 3.0 shows the agglomeration of MCCs because of volume fraction of MCCs.

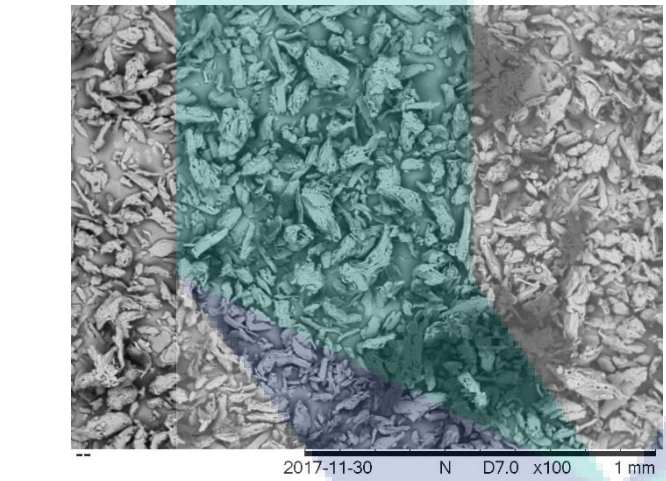

(a)

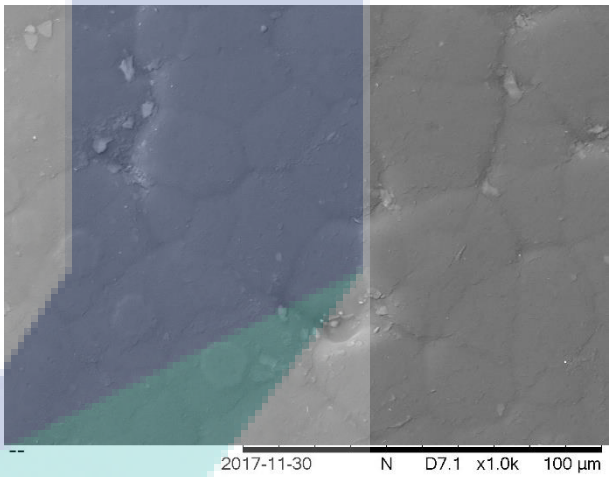

(b)

(c)

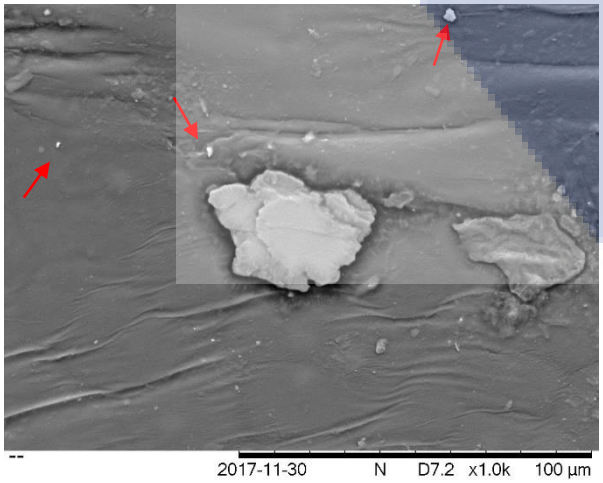

(d)

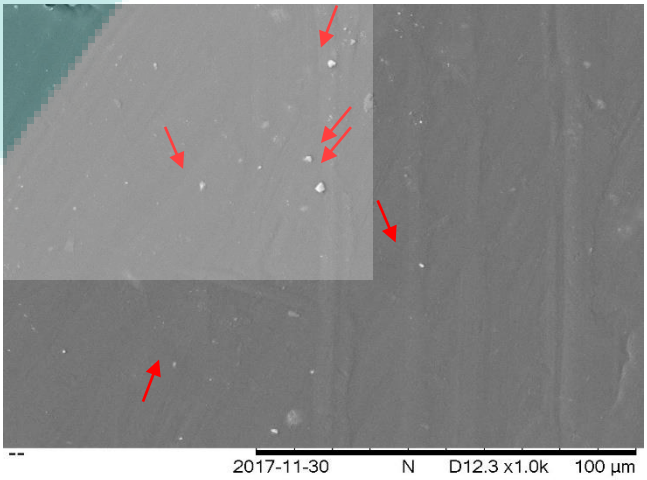

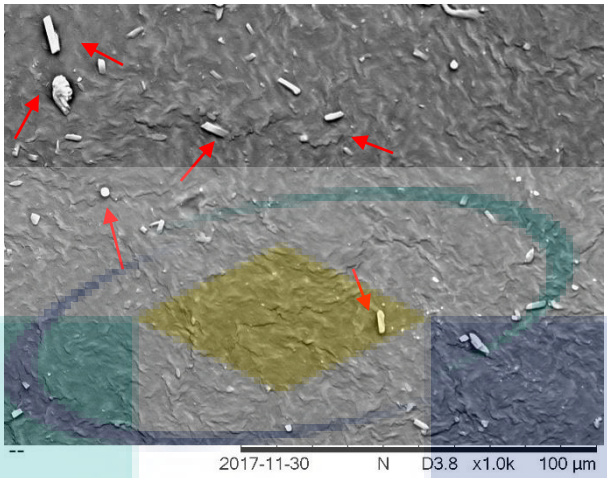

(e)

Figure 4.25 Scanning electron micrograph of the surface for (a) MCC (b) TPU control (c) TPU/MCC 1.0 (d) M-TPU/MCC 1.0 (e) M-TPU/MCC 3.0

4.2.2.2 Spectroscopic Characterisation of TPU/MCC Composites (FTIR)

Fourier transform infrared (FTIR) was used to identify the network bonding of TPU and the effect of MCC presence in TPU composites. It was expected that the hydroxyl group that presence on the surface of MCC was observed in the TPU/MCC nanocomposite film. Hydroxyl functional group can be detected at the range 3550 - 3200 cm^{-1}.[154]As shown in Figure 4.26 it can be seen the peak area of hydroxyl group for sample TPU/MCC1.0 and M-TPU/MCC1.0 has clear difference where the master batch sample has high absorbance peak area. This is due to well dispersed of MCC in TPU matrix. For M- TPU/MCC3.0 and M- TPU/MCC5.0 the peak is slightly smaller than M-TPU/MCC1.0, it caused by agglomeration of MCC, so that OH- bonding decreases.

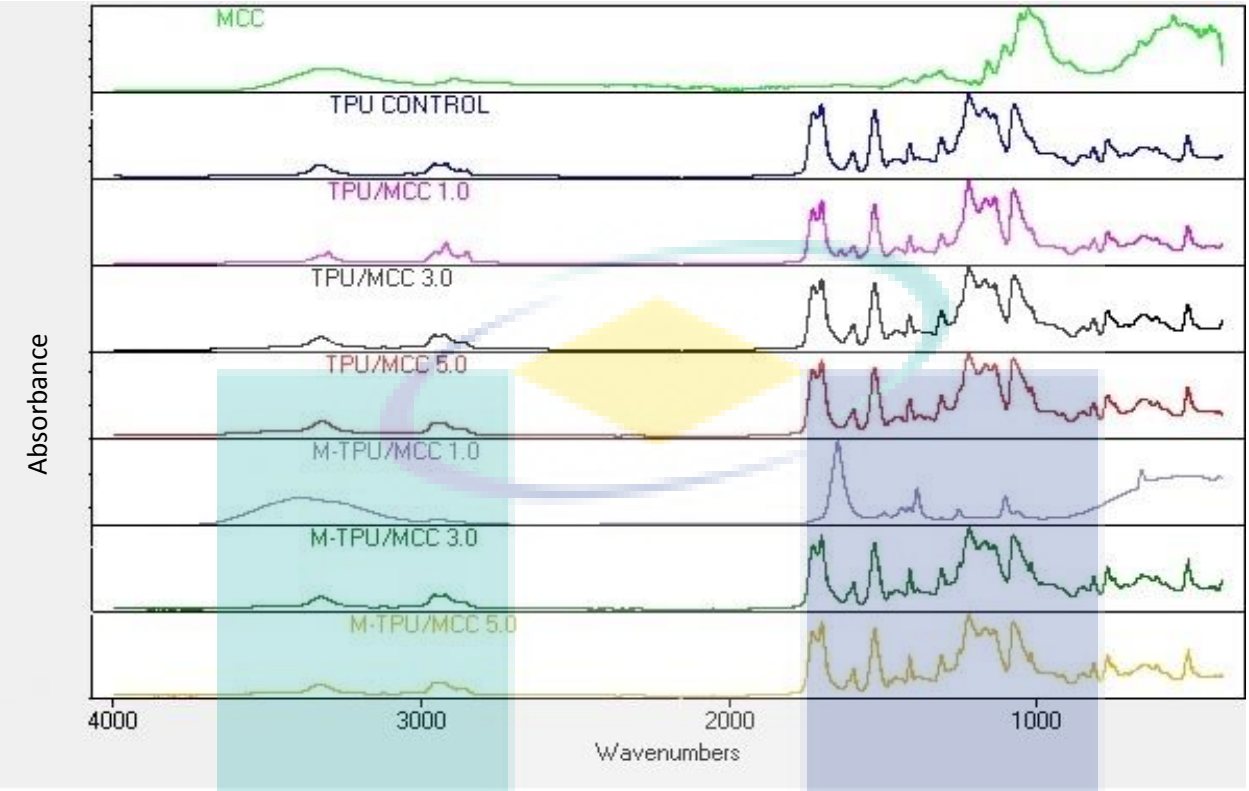

Figure 4.26 FTIR spectra for MCC, TPU Control, TPU/MCC 1.0, TPU/MCC 3.0, TPU/MCC 5.0, M-TPU/MCC 1.0, M-TPU/MCC 3.0 and M-TPU/MCC 5.0

4.2.2.3 Mechanical Properties

In the development of polyurethane nanocomposites, a significant improvement in tensile strength is important. The reinforcement effect of MCCs was investigated by measuring the tensile properties, strain and young modulus of the TPU control and its nanocomposites at room temperature. The tensile-strain curves of TPU control and its nanocomposites are shown in this discussion.

Figure 4.27 (a) shows the tensile graph with different incorporation of fillers for non-masterbatch while Figure 4.27 (b) is for masterbatch composites and values determined are summarised in Table 4.10. There are no significant changes in tensile strength with the incorporation of 1.0 wt. % of MCC upon 0 to 40% of tensile strain were observed until their failure. With increasing of MCC ratio incorporated in nanocomposites shows significant increase in ultimate strength. For example, the M-TPU/MCC nanocomposite with 5.0 wt.% of MCC has shown about 21% improvement in tensile strength (40.125 MPa

from 33.09 MPa). The enhancement of mechanical properties achieved much better with incorporation of MCC.

As discussed, the structural morphology of TPU can be influenced by the covalent-linkages between the hydroxyl groups of MCC and diisocynates. The Young modulus and tensile strain values are affected by MCC incorporation. At 5.0 wt.% of MCC, nanocomposite sample exhibits about 43% increase in tensile modulus.

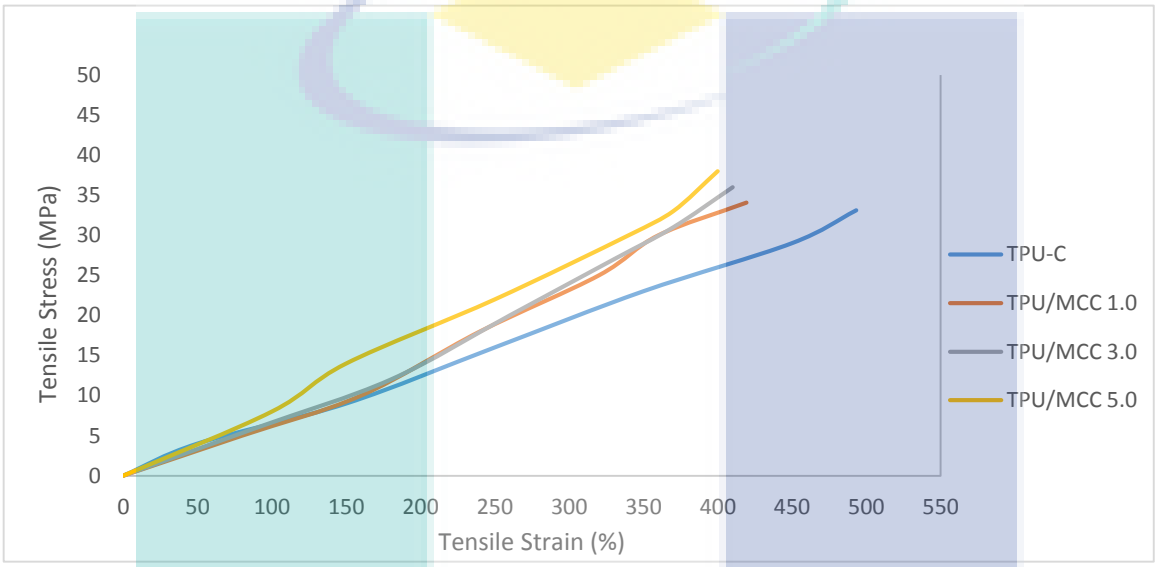

(a)

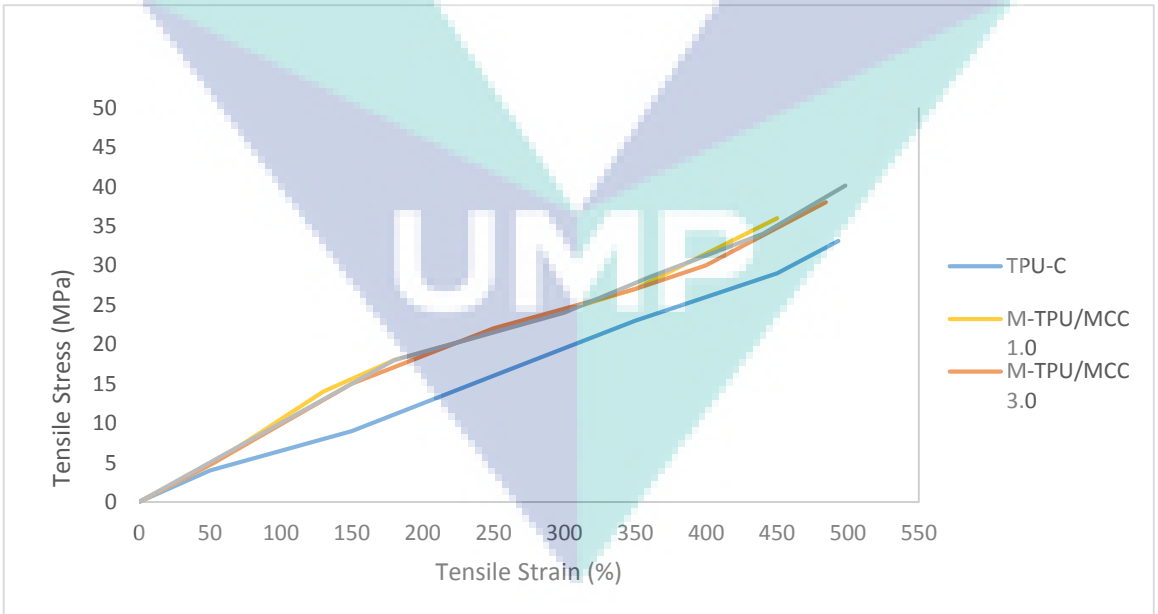

(b)

Figure 4.27 (a) Tensile curve for non-masterbatch nanocomposites (b) Tensile curve for masterbatch nanocomposites.

Table 4.11 Mechanical properties of TPU control and its nanocomposites

Sample	Tensile Stress (MPa)	Tensile Strain (%)	Modulus (MPa)
TPU Control	33.1	493.1	6.7
TPU/MCC 1.0	34.2	419.2	8.2
TPU/MCC 3.0	36.7	410.6	8.9
TPU/MCC 5.0	38.5	400.7	9.6
M-TPU/MCC 1.0	36.8	450.5	8.2
M-TPU/MCC 3.0	38.6	484.4	8.0
M-TPU/MCC 5.0	40.2	498.3	8.1

CHAPTER 5

CONCLUSION AND RECOMMENDATION

5.1 Conclusion

Cellulose nanocrystal (CNC) was successfully isolated from MCC via mixed acid hydrolysis with the assistance of ultrasonication treatment. In this study, two factors that affect the properties of CNC is manipulated which are temperature and reaction time. Among these conditions, CNC at 50°C and 70°C shows positive results towards the better properties of CNC. It can be seen through several analyses on morphology, chemical structure, thermal and dispersion stability. In these characterizations, percentage of yield produce is take into account. As the temperature increase, the percentage of yield is decreasing due to the closer to degradation conditions. Based on morphology, CNC shows the reduction in dimension and higher aspect ratio. Furthermore, the aspect ratio via mixed acid is identified to be in between CNC produced via sulphuric and phosphoric acid. Besides that, FTIR spectra shows the similar pattern on both MCC and CNC produced. It is concluded that molecular structure of cellulose is not affected by the presence of mixed acid due to stable functional group. However, hydroxyl group detected in MCC is reported to be higher due to the presence of sulphate group on surface of CNC. In addition, thermal stability is considered as one of properties which determine good CNC. Mixed acid hydrolysis has shown the improvement of the limitation in thermal behaviour of CNC isolated via sulphuric acid. Furthermore, dispersion stability of CNC in water also is observed. However, due to different method used, significant difference is resulted compared to previous study. Based on experimental results, no characterization has been made on CNC produced at 90°C/180 min as degradation occurred to that sample.

Three types of CNCs isolated via sulphuric acid hydrolysis (CNC-S), phosphoric acid hydrolysis (CNC-P) and mechanical milling method (CNC-MC) were successfully incorporated into thermoplastic polyurethane (TPU) via melt compounding method. These nanocomposites were compared with that processed via conventional solvent casting method. The thermally stable CNCs (CNC-P and CNC-MC) have demonstrated the melt processability with polyether based thermoplastic polyurethane (TPU) without affecting the optical transparency, whereas, CNC-S has shown the degradation (transurethanisation) behaviour. Remarkable reinforcement effect has been observed for nanocomposites with

all the three CNCs, in terms of improvement in tensile strength and toughness without affecting elongation. The properties enhancement has been related to the structural-morphology changes induced by CNCs, as observed from spectral analysis, thermal transition behaviour and thermo-mechanical properties of TPU nanocomposites. At very low concentrations (0.5 and 1 wt. %) the nanocomposites with CNC-P and CNC-MC have also shown improvement in creep modulus and hysteresis properties.

It can be summarised (Table 5.1) that CNC isolated via mild acid hydrolysis and an optimised mechanical milling methods, can be easily processed via large scale melt-processing techniques for reinforcing thermoplastic polyurethanes (at 0.5-1 wt. %) without affecting their physical appearance and elastic properties.

Table 5.1 Performance of TPU/CNC nanocomposites via melt compounding method.

Rating *	**1**	**2**	**3**
Optical property	TPU/CNC-S	**TPU/CNC-MC**	TPU/CNC-P
Tensile strength		**TPU/CNC-MC** TPU/CNC-P	TPU/CNC-S
Toughness		TPU/CNC-P	TPU/CNC-S **TPU/CNC-MC**
Elasticity	TPU/CNC-S	**TPU/CNC-MC**	TPU/CNC-P

*1= under average 2= average 3= good

TPU/MCC composites have been prepared successfully through the masterbatch method. The dispersibility of composite of MCC were improved due to TPU coating by solvent exchange method. The MCC as reinforcing fillers does not affect the physical appearence of nanocomposites. Next, SEM results show that MCC can be incorporated well with TPU in the film form. For FTIR results, M-TPU/MCC 1.0 has high absorbance peak compare to M-TPU/MCC 3.0 and 5.0 due to agglomeration of MCC. The incorporation of microcellulose at 5.0 wt% has improved the tensile strength of TPU up to 21%. Thus, MCC can disperse well in TPU matrix by masterbatch process

5.2 Recommendations

Based on the results of the experiments, it was obvious that mixed acid hydrolysis is highly capable in producing CNC with better properties. A few recommendations could be outlined for further study. Further characterization need to be done on crystallinity and dispersion stability via XRD and Zeta potential measurement respectively. These characterizations provide strong evidence in the ability of mixed acid hydrolysis to produce better properties of CNC. Besides that, a few factors that affect the properties which can be study in future such as cellulose sources, types of acids used, ratio of solid-liquid, ratio of acids, and pre-treatment method after acid hydrolysis (George & Sabapathi, 2015). These factors are reported to affect the properties of CNC. Therefore, this improvement will be very beneficial in the application of CNC.

Meanwhile, the processing of TPU nanocomposites film via solution casting which involved the usage of solvent should be dried longer to completely eliminates the residual of solvent. To better understand the filler-TPU interaction and structure-property relationship, further investigation into the morphology and the proposed hard segment formation at the interface of CNC can be carried out using synchontron small-angle x-ray/neutron scattering (SAXS/SANS), ideally on an in-situ tensometer to follow morphology and the cellulose I crystalline signature orientation during extension.

REFERENCES

[1] a) J. W. Xiong, Z. Zheng, X. M. Qin, M. Li, H. Q. Li and X. L. Wang, *Carbon* **2006**, *44*, 2701-2707; b) S. H. Park, K. W. Oh and S. H. Kim, *Composites Science and Technology* **2013**, *86*, 82-88.

[2] a) S. S. Ray and M. Okamoto, *Progress in Polymer Science* **2003**, *28*, 1539-1641; b) I. Siro and D. Plackett, *Cellulose* **2010**, *17*, 459-494; c) S. J. Eichhorn, A. Dufresne, M. Aranguren, N. E. Marcovich, J. R. Capadona, S. J. Rowan, C. Weder, W. Thielemans, M. Roman, S. Renneckar, W. Gindl, S. Veigel, J. Keckes, H. Yano, K. Abe, M. Nogi, A. N. Nakagaito, A. Mangalam, J. Simonsen, A. S. Benight, A. Bismarck, L. A. Berglund and T. Peijs, *Journal of Materials Science* **2010**, *45*, 1-33; d) Z. S. Petrovic, I. Javni, A. Waddon and G. Banhegyi, *Journal of Applied Polymer Science* **2000**, *76*, 133-151.

[3] F. Hussain, M. Hojjati, M. Okamoto and R. E. Gorga, *Journal of Composite Materials* **2006**, *40*, 1511-1575.

[4] M. O. Seydibeyoglu and K. Oksman, *Composites Science and Technology* **2008**, *68*, 908-914.

[5] a) Y. Habibi, L. A. Lucia and O. J. Rojas, *Chemical Reviews* **2010**, *110*, 3479-3500; b) M. A. S. A. Samir, F. Alloin and A. Dufresne, *Biomacromolecules* **2005**, *6*, 612-626; c) A. Dufresne, *Canadian Journal of Chemistry-Revue Canadienne De Chimie* **2008**, *86*, 484-494.

[6] a) L. Rueda, A. Saralegui, B. F. d'Arlas, Q. Zhou, L. A. Berglund, M. A. Corcuera, I. Mondragon and A. Eceiza, *Carbohydrate Polymers* **2013**, *92*, 751-757; b) J. Mendez, P. K. Annamalai, S. J. Eichhorn, R. Rusli, S. J. Rowan, E. J. Foster and C. Weder, *Macromolecules* **2011**, *44*, 6827-6835; c) X. D. Cao, H. Dong and C. M. Li, *Biomacromolecules* **2007**, *8*, 899-904.

[7] M. Szycher, *Szycher's handbook of polyurethanes*, CRC press, **1999**, p.

[8] R. J. Zdrahala and I. J. Zdrahala, *Journal of Biomaterials Applications* **1999**, *14*, 67-90.

[9] D. K. Chattopadhyay and K. V. S. N. Raju, *Progress in Polymer Science* **2007**, *32*, 352-418.

[10] C. W. McGary and D. D. Solomon in *Thermoplastic polyurethane anticoagulant alloy coating, Vol.* Google Patents, **1987**.

[11] D. Tabuani, F. Bellucci, A. Terenzi and G. Camino, *Polymer Degradation and Stability* **2012**, *97*, 2594-2601.

[12] C. S. Scollenberger in *Thermoplastic Polyurethane Elastomer Structure-Thermal Response Relations.*, American Chemical Society, Washington DC, **1979**.
[13] X. Zhang, R. Xu, Z. Wu and C. Zhou, *Polymer International* **2003**, *52*, 790-794.
[14] H. H. Liu, L. Zhang, Y. Zuo, L. Wang, D. Huang, J. Shen, P. J. Shi and Y. B. Li, *Journal of Applied Polymer Science* **2009**, *112*, 2968-2975.
[15] a) G. Sankar and N. Yan, *Journal of Macromolecular Science Part a-Pure and Applied Chemistry* **2015**, *52*, 47-55; b) K. D. Kavlock, T. W. Pechar, J. O. Hollinger, S. A. Guelcher and A. S. Goldstein, *Acta Biomaterialia* **2007**, *3*, 475-484.
[16] M. Szycher, *Journal of Biomaterilas Applications* **1998**, *3*.
[17] P. Krol, *Progress in Materials Science* **2007**, *52*, 915-1015.
[18] Z. S. Petrović and J. Ferguson, *Progress in Polymer Science* **1991**, *16*, 695-836.
[19] N. M. Lamba, K. A. Woodhouse and S. L. Cooper, *Polyurethanes in biomedical applications*, CRC press, **1997**, p.
[20] R. C. R. Nunes, J. L. C. Fonseca and M. R. Pereira, *Polymer Testing* **2000**, *19*, 93-103.
[21] H. Biernholtz, S. Kenig and H. Dodiuk, *Polymers for Advanced Technologies* **1992**, *3*, 125-131.
[22] L. Domka, *Colloid and Polymer Science* **1993**, *271*, 1091-1099.
[23] M. Furukawa and T. Yokoyama, *Journal of Applied Polymer Science* **1994**, *53*, 1723-1729.
[24] D. Feldman and M. Lacasse, *Journal of Applied Polymer Science* **1994**, *51*, 701-709.
[25] C. Eisenbach, A. Ribbe and A. Goldel, *Kautschuk Gummi Kunststoffe* **1996**, *49*, 406-411.
[26] O. Otterstedt, J. E. Otterstedt, J. Ekdahl, J. Backman and C. H. Andersson, *Journal of Applied Polymer Science* **1987**, *34*, 2575-2582.
[27] W. Chen, X. Tao and Y. Liu, *Composites Science and Technology* **2006**, *66*, 3029-3034.
[28] J. L. Caillaud, S. Deguillaume, M. Vincent, J. C. Giannotta and J. M. Widmaier, *Polymer International* **1996**, *40*, 1-7.
[29] A. P. Kumar, D. Depan, N. Singh Tomer and R. P. Singh, *Progress in Polymer Science* **2009**, *34*, 479-515.
[30] a) Y. K. Choi, K. I. Sugimoto, S. M. Song and M. Endo, *Materials Letters* **2005**, *59*, 3514-3520; b) L. W. Fan, X. Fang, X. Wang, Y. Zeng, Y. Q. Xiao, Z. T. Yu, X. Xu, Y. C. Hu and K. F. Cen, *Applied Energy* **2013**, *110*, 163-172.
[31] a) M. K. Liu, C. Zhang, W. W. Tjiu, Z. Yang, W. Z. Wang and T. X. Liu, *Polymer* **2013**, *54*, 3124-3130; b) N. Mahmood, A. U. Khan, K. W. Stockelhuber, A. Das, D. Jehnichen and

G. Heinrich, *Journal of Applied Polymer Science* **2014**, *131*; c) M. Ji, H. Deng, D. Yan, X. Li, L. Duan and Q. Fu, *Composites Science and Technology* **2014**, *92*, 16-26; d) H. Koerner, W. Liu, M. Alexander, P. Mirau, H. Dowty and R. A. Vaia, *Polymer* **2005**, *46*, 4405-4420; e) A. K. Barick and D. K. Tripathy, *Materials Science and Engineering B-Advanced Functional Solid-State Materials* **2011**, *176*, 1435-1447.

[32] S. Ganguly, K. Dana, T. K. Mukhopadhyay, T. K. Parya and S. Ghatak, *Transactions of the Indian Ceramic Society* **2011**, *70*, 189-206.

[33] a) A. K. Barick and D. K. Tripathy, *Polymers for Advanced Technologies* **2010**, *21*, 835-847; b) X. Y. Ma, H. J. Lu, G. Z. Lian, J. C. Zhao and T. L. Lu, *Journal of Applied Polymer Science* **2005**, *96*, 1165-1169; c) M. Barmar, M. Barikani and M. Fereidounnia, *Iranian Polymer Journal* **2006**, *15*, 709-714.

[34] D. K. Sheng, J. J. Tan, X. D. Liu, P. X. Wang and Y. M. Yang, *Journal of Materials Science* **2011**, *46*, 6508-6517.

[35] a) M. Sternitzke, B. Derby and R. J. Brook, *Journal of the American Ceramic Society* **1998**, *81*, 41-48; b) I. V. Khudyakov, R. D. Zopf and N. J. Turro, *Designed Monomers and Polymers* **2009**, *12*, 279-290.

[36] M. T. Albdiry, B. F. Yousif, H. Ku and K. T. Lau, *Journal of Composite Materials* **2013**, *47*, 1093-1115.

[37] A. C. OSullivan, *Cellulose* **1997**, *4*, 173-207.

[38] A. Payen, *Comptes rendus* **1838**, *7*, 1052-1056.

[39] a) J. Kim, S. Yun and Z. Ounaies, *Macromolecules* **2006**, *39*, 5583-5583; b) R. J. Moon, A. Martini, J. Nairn, J. Simonsen and J. Youngblood, *Chem Soc Rev* **2011**, *40*, 3941-3994.

[40] L. M. J. Kroon-Batenburg, B. Bouma and J. Kroon, *Macromolecules* **1996**, *29*, 5695-5699.

[41] a) Y. Nishiyama, P. Langan and H. Chanzy, *Journal of the American Chemical Society* **2002**, *124*, 9074-9082; b) R. H. Atalla and D. L. Vanderhart, *IPC Technical Paper Series* **1987**, *217*, 4.

[42] H. Yamamoto and F. Horii, *Macromolecules* **1993**, *26*, 1313-1317.

[43] H. Yamamoto and F. Horn, *Cellulose* **1994**, *1*, 57-66.

[44] P. Belton, S. Tanner, N. Cartier and H. Chanzy, *Macromolecules* **1989**, *22*, 1615-1617.

[45] a) M. Ioelovich, *BioResources* **2008**, *3*, 1403-1418; b) I. M. Saxena and R. M. Brown, *Annals of Botany* **2005**, *96*, 9-21.

[46] V. Favier, H. Chanzy and J. Y. Cavaille, *Macromolecules* **1995**, *28*, 6365-6367.

[47] N. Lavoine, I. Desloges, A. Dufresne and J. Bras, *Carbohydrate Polymers* **2012**, *90*, 735-764.

[48] E. Brännvall in *Aspects on strength delivery and higher utilisation of the strength potential of softwood kraft pulp fibres, Vol. Doctor of Philosophy* KTH, Royal Institute of Technology, **2007**, p. 57.

[49] a) B. G. Ranby and R. H. Marchessault, *Journal of Polymer Science* **1959**, *36*, 561-564; b) B. G. Ranby and R. W. Noe, *Journal of Polymer Science* **1961**, *51*, 337-&.

[50] R. H. Marchessault, F. F. Morehead and N. M. Walter, *Nature* **1959**, *184*, 632-633.

[51] W. Li, J. Q. Yue and S. X. Liu, *Ultrasonics Sonochemistry* **2012**, *19*, 479-485.

[52] A. Alemdar and M. Sain, *Bioresource Technology* **2008**, *99*, 1664-1671.

[53] J. F. Revol, H. Bradford, J. Giasson, R. H. Marchessault and D. G. Gray, *International Journal of Biological Macromolecules* **1992**, *14*, 170-172.

[54] M. M. Ruiz, J. Y. Cavaille, A. Dufresne, J. F. Gerard and C. Graillat, *Composite Interfaces* **2000**, *7*, 117-131.

[55] J. Araki, M. Wada, S. Kuga and T. Okano, *Colloids and Surfaces a-Physicochemical and Engineering Aspects* **1998**, *142*, 75-82.

[56] S. Camarero Espinosa, T. Kuhnt, E. J. Foster and C. Weder, *Biomacromolecules* **2013**, *14*, 1223-1230.

[57] Y. Sun, L. Lin, C. S. Pang, H. B. Deng, H. Peng, J. Z. Li, B. H. He and S. J. Liu, *Energy & Fuels* **2007**, *21*, 2386-2389.

[58] S. Y. Lee, D. J. Mohan, I. A. Kang, G. H. Doh, S. Lee and S. O. Han, *Fibers and Polymers* **2009**, *10*, 77-82.

[59] M. Jonoobi, R. Oladi, Y. Davoudpour, K. Oksman, A. Dufresne, Y. Hamzeh and R. Davoodi, *Cellulose* **2015**, *22*, 935-969.

[60] a) S. Beck-Candanedo, M. Roman, and and D. G. Gray, *Biomacromolecules* **2005**, *6*, 1048-1054; b) J. Araki, M. Wada, S. Kuga and T. Okano, *Colloids and Surfaces A: Physicochemical and Engineering Aspects* **1998**, *142*, 75-82.

[61] P. B. Filson, B. E. Dawson-Andoh and D. Schwegler-Berry, *Green Chemistry* **2009**, *11*, 1808-1814.

[62] P. B. Filson and B. E. Dawson-Andoh, *Bioresource Technology* **2009**, *100*, 2259-2264.

[63] a) Y. Y. Yue, C. J. Zhou, A. D. French, G. Xia, G. P. Han, Q. W. Wang and Q. L. Wu, *Cellulose* **2012**, *19*, 1173-1187; b) G. Morandi, L. Heath and W. Thielemans, *Langmuir* **2009**, *25*, 8280-8286.

[64] P. Satyamurthy, P. Jain, R. H. Balasubramanya and N. Vigneshwaran, *Carbohydrate Polymers* **2011**, *83*, 122-129.

[65] a) S. Iwamoto, W. H. Kai, A. Isogai and T. Iwata, *Biomacromolecules* **2009**, *10*, 2571-2576; b) Y. Habibi, T. Heim and R. Douillard, *Journal of Polymer Science Part B-Polymer Physics* **2008**, *46*, 1430-1436; c) O. van den Berg, J. R. Capadona and C. Weder, *Biomacromolecules* **2007**, *8*, 1353-1357.

[66] a) A. Hirai, O. Inui, F. Horii and M. Tsuji, *Langmuir* **2009**, *25*, 497-502; b) M. Grunert and W. T. Winter, *Journal of Polymers and the Environment* **2002**, *10*, 27-30.

[67] J. George, K. V. Ramana, A. S. Bawa and Siddaramaiah, *International Journal of Biological Macromolecules* **2011**, *48*, 50-57.

[68] a) M. F. Rosa, E. S. Medeiros, J. A. Malmonge, K. S. Gregorski, D. F. Wood, L. H. C. Mattoso, G. Glenn, W. J. Orts and S. H. Imam, *Carbohydrate Polymers* **2010**, *81*, 83-92; b) P. Lu and Y. L. Hsieh, *Carbohydrate Polymers* **2012**, *87*, 564-573; c) S. Mueller, C. Weder and E. J. Foster, *Rsc Advances* **2014**, *4*, 907-915; d) W. P. F. Neto, H. A. Silverio, N. O. Dantas and D. Pasquini, *Industrial Crops and Products* **2013**, *42*, 480-488.

[69] M. Jonoobi, A. Khazaeian, P. M. Tahir, S. S. Azry and K. Oksman, *Cellulose* **2011**, *18*, 1085-1095.

[70] M. L. Hassan, A. P. Mathew, E. A. Hassan, N. A. El-Wakil and K. Oksman, *Wood Science and Technology* **2012**, *46*, 193-205.

[71] a) N. Wang, E. Ding and R. Cheng, *Langmuir* **2008**, *24*, 5-8; b) P. Lu and Y.-L. Hsieh, *Carbohydrate Polymers* **2010**, *82*, 329-336.

[72] V. Favier, J. Y. Cavaille, H. Chanzy and A. Dufresne, *Abstracts of Papers of the American Chemical Society* **1995**, *209*, 29-Macr.

[73] a) C. Salas, T. Nypelo, C. Rodriguez-Abreu, C. Carrillo and O. J. Rojas, *Current Opinion in Colloid & Interface Science* **2014**, *19*, 383-396; b) S. Kalia, A. Dufresne, B. M. Cherian, B. Kaith, L. Avérous, J. Njuguna and E. Nassiopoulos, *International Journal of Polymer Science* **2011**, *2011*.

[74] M. A. S. A. Samir, F. Alloin, J. Y. Sanchez and A. Dufresne, *Polymer* **2004**, *45*, 4149-4157.

[75] a) B. Noble, S. J. Harris and K. Dinsdale, *Journal of Materials Science* **1982**, *17*, 461-468; b) J. F. Shackelford in *CRC Materials Science and Engineering Handbook, Third Edition, Vol.* Eds.: J. F. Shackelford and W. Alexander), CRC Press, **2000**.

[76] P. Soroushian and K. B. Choi, *Journal of Structural Engineering-Asce* **1987**, *113*, 663-672.

[77] P. Wambua, J. Ivens and I. Verpoest, *Composites Science and Technology* **2003**, *63*, 1259-1264.

[78] S. Kalia, A. Dufresne, B. M. Cherian, B. S. Kaith, L. Averous, J. Njuguna and E. Nassiopoulos, *International Journal of Polymer Science* **2011**.

[79] N. Ljungberg, C. Bonini, F. Bortolussi, C. Boisson, L. Heux and J.-Y. Cavaillé, *Biomacromolecules* **2005**, *6*, 2732-2739.

[80] A. J. de Menezes, G. Siqueira, A. A. Curvelo and A. Dufresne, *Polymer* **2009**, *50*, 4552-4563.

[81] a) M. Roohani, Y. Habibi, N. M. Belgacem, G. Ebrahim, A. N. Karimi and A. Dufresne, *European Polymer Journal* **2008**, *44*, 2489-2498; b) A. Jalal Uddin, J. Araki and Y. Gotoh, *Biomacromolecules* **2011**, *12*, 617-624.

[82] a) K. Oksman, A. Mathew, D. Bondeson and I. Kvien, *Composites Science and Technology* **2006**, *66*, 2776-2784; b) E. Fortunati, I. Armentano, Q. Zhou, A. Iannoni, E. Saino, L. Visai, L. A. Berglund and J. Kenny, *Carbohydrate Polymers* **2012**, *87*, 1596-1605.

[83] J. K. Pandey, A. N. Nakagaito and H. Takagi, *Polymer Engineering and Science* **2013**, *53*, 1-8.

[84] a) H. F. Pan, L. Song, L. Y. Ma and Y. Hu, *Industrial & Engineering Chemistry Research* **2012**, *51*, 16326-16332; b) H. Liu, D. Liu, F. Yao and Q. Wu, *Bioresour Technol* **2010**, *101*, 5685-5692; c) W. Xu, Z. Qin, H. Yu, Y. Liu, N. Liu, Z. Zhou and L. Chen, *Journal of Nanoparticle Research* **2013**, *15*.

[85] R. R. Lahiji, X. Xu, R. Reifenberger, A. Raman, A. Rudie and R. J. Moon, *Langmuir* **2010**, *26*, 4480-4488.

[86] a) P. Hajji, J. Y. Cavaille, V. Favier, C. Gauthier and G. Vigier, *Polymer Composites* **1996**, *17*, 612-619; b) V. Favier, G. R. Canova, J. Y. Cavaille, H. Chanzy, A. Dufresne and C. Gauthier, *Polymers for Advanced Technologies* **1995**, *6*, 351-355; c) N. Ljungberg, C. Bonini, F. Bortolussi, C. Boisson, L. Heux and J. Y. Cavaille, *Biomacromolecules* **2005**, *6*, 2732-2739; d) S. Eichhorn, A. Dufresne, M. Aranguren, N. Marcovich, J. Capadona, S. Rowan, C. Weder, W. Thielemans, M. Roman and S. Renneckar, *Journal of Materials Science* **2010**, *45*, 1-33.

[87] U. Siemann in *Solvent cast technology–a versatile tool for thin film production*, Springer, **2005**, pp. 1-14.

[88] a) S. Z. Li, M. M. Xiao, A. Zheng and H. N. Xiao, *Biomacromolecules* **2011**, *12*, 3305-3312; b) A. L. Goffin, J. M. Raquez, E. Duquesne, G. Siqueira, Y. Habibi, A. Dufresne and

P. Dubois, *Biomacromolecules* **2011**, *12*, 2456-2465; c) D. Ray and S. Sain, *Composites Part A: Applied Science and Manufacturing*.

[89] X. Wang, Y. A. Hu, L. Song, H. Y. Yang, W. Y. Xing and H. D. Lu, *Journal of Materials Chemistry* **2011**, *21*, 4222-4227.

[90] X. D. Cao, Y. Habibi and L. A. Lucia, *Journal of Materials Chemistry* **2009**, *19*, 7137-7145.

[91] D. Schmidt in *Vol. PhD* Cornell University, Ithaca, **2003**.

[92] a) J. R. Capadona, O. Van Den Berg, L. A. Capadona, M. Schroeter, S. J. Rowan, D. J. Tyler and C. Weder, *Nature Nanotechnology* **2007**, *2*, 765-769; b) J. R. Capadona, K. Shanmuganathan, D. J. Tyler, S. J. Rowan and C. Weder, *Science* **2008**, *319*, 1370-1374; c) J. R. Capadona, K. Shanmuganathan, S. Trittschuh, S. Seidel, S. J. Rowan and C. Weder, *Biomacromolecules* **2009**, *10*, 712-716.

[93] a) A. Dufresne, *Intern. Polymer Processing* **2012**, 557-564; b) G. Siqueira, A. P. Mathew and K. Oksman, *Composites Science and Technology* **2011**, *71*, 1886-1892.

[94] F. Schwertfeger, D. Frank and M. Schmidt, *Journal of Non-Crystalline Solids* **1998**, *225*, 24-29.

[95] D. Ishii, D. Tatsumi and T. Matsumoto, *Biomacromolecules* **2003**, *4*, 1238-1243.

[96] a) K. Oksman, A. P. Mathew, D. Bondeson and I. Kvien, *Compos Sci Technol* **2006**, *66*, 2776-2784; b) A. L. Goffin, J. M. Raquez, E. Duquesne, G. Siqueira, Y. Habibi, A. Dufresne and P. Dubois, *Polymer* **2011**, *52*, 1532-1538; c) A. J. de Menezes, G. Siqueira, A. A. S. Curvelo and A. Dufresne, *Polymer* **2009**, *50*, 4552-4563.

[97] L. P. B. M. Janssen, *Reactive Extrusion Systems*, Marcel Dekker, Inc., U.S.A., **2004**, p.

[98] Y. B. Cai, Y. Hu, L. Song, L. Liu, Z. Z. Wang, Z. Chen and W. H. Fan, *Journal of Materials Science* **2007**, *42*, 5785-5790.

[99] B. Imre, D. Bedo, A. Domjan, P. Schon, G. J. Vancso and B. Pukanszky, *European Polymer Journal* **2013**, *49*, 3104-3113.

[100] Q. J. Wu, M. Henriksson, X. Liu and L. A. Berglund, *Biomacromolecules* **2007**, *8*, 3687-3692.

[101] X. Cao, H. Dong and C. M. Li, *Biomacromolecules* **2007**, *8*, 899-904.

[102] N. Marcovich, M. Auad, N. Bellesi, S. Nutt and M. Aranguren, *Journal of Materials Research* **2006**, *21*, 870-881.

[103] M. I. Aranguren, N. E. Marcovich, W. Salgueiro and A. Somoza, *Polymer Testing* **2013**, *32*, 115-122.

[104] a) B. M. Cherian, A. L. Leão, S. F. de Souza, L. M. M. Costa, G. M. de Olyveira, M. Kottaisamy, E. R. Nagarajan and S. Thomas, *Carbohydrate Polymers* **2011**, *86*, 1790-1798; b) A. Dufresne, *International Polymer Processing* **2012**, *27*, 557-564; c) M. O. Seydibeyoglu and K. Oksman, *Compos Sci Technol* **2008**, *68*, 908-914.

[105] N. E. Marcovich, M. L. Auad, N. E. Bellesi, S. R. Nutt and M. I. Aranguren, *Journal of Materials Research* **2006**, *21*, 870-881.

[106] J. C. Liu, D. J. Martin, R. J. Moon and J. P. Youngblood, *Journal of Applied Polymer Science* **2015**, *132*.

[107] M. L. Auad, V. S. Contos, S. Nutt, M. I. Aranguren and N. E. Marcovich, *Polymer International* **2008**, *57*, 651-659.

[108] H. Liu, S. Q. Cui, S. B. Shang, D. Wang and J. Song, *Carbohydrate Polymers* **2013**, *96*, 510-515.

[109] Y. X. Wang, H. F. Tian and L. N. Zhang, *Carbohydrate Polymers* **2010**, *80*, 665-671.

[110] A. H. Pei, J. M. Malho, J. Ruokolainen, Q. Zhou and L. A. Berglund, *Macromolecules* **2011**, *44*, 4422-4427.

[111] V. M. Wik, M. I. Aranguren and M. A. Mosiewicki, *Polymer Engineering and Science* **2011**, *51*, 1389-1396.

[112] Y. Li and A. J. Ragauskas, *Rsc Advances* **2012**, *2*, 3347-3351.

[113] A. Pei, J.-M. Malho, J. Ruokolainen, Q. Zhou and L. A. Berglund, *Macromolecules* **2011**, *44*, 4422-4427.

[114] M. Roman and W. T. Winter, *Biomacromolecules* **2004**, *5*, 1671-1677.

[115] F. Fahma, S. Iwamoto, N. Hori, T. Iwata and A. Takemura, *Cellulose* **2010**, *17*, 977-985.

[116] L. Petersson, A. Mathew and K. Oksman, *Journal of Applied Polymer Science* **2009**, *112*, 2001-2009.

[117] Y. Yue, C. Zhou, A. D. French, G. Xia, G. Han, Q. Wang and Q. Wu, *Cellulose* **2012**, *19*, 1173-1187.

[118] L. Segal, J. J. Creely, A. E. Martin and C. M. Conrad, *Textile Research Journal* **1959**, *29*, 786-794.

[119] S. Camarero Espinosa, T. Kuhnt, E. J. Foster and C. Weder, *Biomacromolecules* **2013**, *14*, 1223-1230.

[120] D. Liu, T. Zhong, P. R. Chang, K. Li and Q. Wu, *Bioresource technology* **2010**, *101*, 2529-2536.

[121] A. Alemdar and M. Sain, *Bioresource technology* **2008**, *99*, 1664-1671.

[122] M. Jonoobi, J. Harun, A. P. Mathew and K. Oksman, *Composites Science and Technology* **2010**, *70*, 1742-1747.
[123] M. M. Coleman, D. J. Skrovanek, J. Hu and P. C. Painter, *Macromolecules* **1988**, *21*, 59-65.
[124] N. Wang, E. Ding and R. Cheng, *Polymer* **2007**, *48*, 3486-3493.
[125] E. Qua, P. Hornsby, H. Sharma and G. Lyons, *Journal of Materials Science* **2011**, *46*, 6029-6045.
[126] W. Chen, H. Yu, Y. Liu, P. Chen, M. Zhang and Y. Hai, *Carbohydrate Polymers* **2011**, *83*, 1804-1811.
[127] R. Li, J. Fei, Y. Cai, Y. Li, J. Feng and J. Yao, *Carbohydrate Polymers* **2009**, *76*, 94-99.
[128] S. M. Rosa, N. Rehman, M. I. G. de Miranda, S. M. Nachtigall and C. I. Bica, *Carbohydrate Polymers* **2012**, *87*, 1131-1138.
[129] F. Niu, M. Li, Q. Huang, X. Zhang, W. Pan, J. Yang and J. Li, *Carbohydrate polymers* **2017**, *165*, 197-204.
[130] H. Charreau, M. L. Foresti and A. Vazquez, *Recent Patents on Nanotechnology* **2013**, *7*, 56-80.
[131] L. Zhang, T. Tsuzuki and X. Wang, *Cellulose* **2015**.
[132] a) D. Bondeson, A. Mathew and K. Oksman, *Cellulose* **2006**, *13*, 171; b) X. M. Dong, J.-F. Revol and D. G. Gray, *Cellulose* **1998**, *5*, 19-32.
[133] a) J.-W. Rhim, J. P. Reddy and X. Luo, *Cellulose* **2014**, *22*, 407-420; b) W. Y. Hamad and T. Q. Hu, *Canadian Journal of Chemical Engineering* **2010**, *88*, 392-402.
[134] a) W. Li, J. Yue and S. Liu, *Ultrason Sonochem* **2012**, *19*, 479-485; b) Q. Cheng, S. Wang and T. G. Rials, *Composites Part A: Applied Science and Manufacturing* **2009**, *40*, 218-224.
[135] S. Park, J. O. Baker, M. E. Himmel, P. A. Parilla and D. K. Johnson, *Biotechnology for Biofuels* **2010**, *3*.
[136] D. Yang, X.-W. Peng, L.-X. Zhong, X.-F. Cao, W. Chen and R.-C. Sun, *Cellulose* **2013**, *20*, 2427-2437.
[137] H. Zhao, J. H. Kwak, Y. Wang, J. A. Franz, J. M. White and J. E. Holladay, *Energy & Fuels* **2006**, *20*, 807-811.
[138] H. Kargarzadeh, I. Ahmad, I. Abdullah, A. Dufresne, S. Zainudin and R. Sheltami, *Cellulose* **2012**, *19*, 855-866.
[139] C. M. Brunette, S. L. Hsu and W. J. Macknight, *Macromolecules* **1982**, *15*, 71-77.

[140] W. Nierzwicki and E. Wysocka, *Journal of Applied Polymer Science* **1980**, *25*, 739-746.

[141] C. L. Zhang, J. L. Hu, S. J. Chen and F. L. Ji, *Journal of Molecular Modeling* **2010**, *16*, 1391-1399.

[142] E. Kontou, G. Spathis, M. Niaounakis and V. Kefalas, *Colloid and Polymer Science* **1990**, *268*, 636-644.

[143] G. Edwards, P. Halley, G. Kerven and D. Martin, *Thermochimica Acta* **2005**, *429*, 13-18.

[144] W. P. Yang, C. W. Macosko and S. T. Wellinghoff, *Polymer* **1986**, *27*, 1235-1240.

[145] D. J. Martin, G. F. Meijs, P. A. Gunatillake, S. J. Mccarthy and G. M. Renwick, *Journal of Applied Polymer Science* **1997**, *64*, 803-817.

[146] F. S. Yen and J. L. Hong, *Macromolecules* **1997**, *30*, 7927-7938.

[147] Y. I. Tien and K. H. Wei, *Polymer* **2001**, *42*, 3213-3221.

[148] a) D. J. Martin, G. F. Meijs, P. A. Gunatillake, S. J. McCarthy and G. M. Renwick, *Journal of Applied Polymer Science* **1997**, *64*, 803-817; b) D. J. Martin, G. F. Meijs, G. M. Renwick, S. J. McCarthy and P. A. Gunatillake, *Journal of Applied Polymer Science* **1996**, *62*, 1377-1386.

[149] R. W. Seymour and S. L. Cooper, *Macromolecules* **1973**, *6*, 48-53.

[150] A. F. Osman, G. A. Edwards, T. L. Schiller, Y. Andriani, K. S. Jack, I. C. Morrow, P. J. Halley and D. J. Martin, *Macromolecules* **2012**, *45*, 198-210.

[151] B. Finnigan in *The morphology and properties of thermoplastic polyurethane nanocomposites, Vol. Dissertation/Thesis* St. Lucia, Qld. U6 - ctx_ver=Z39.88-2004&ctx_enc=info%3Aofi%2Fenc%3AUTF-8&rfr_id=info:sid/summon.serialssolutions.com&rft_val_fmt=info:ofi/fmt:kev:mtx:book&rft.genre=dissertation&rft.title=The+morphology+and+properties+of+thermoplastic+polyurethane+nanocomposites&rft.DBID=21P&rft.au=Finnigan%2C+Bradley&rft.date=2005-01-01&rft.externalDBID=n%2Fa&rft.externalDocID=b22396457&paramdict=en-US U7 - Dissertation, **2005**.

[152] A. Dufresne, J.-Y. Cavaillé and W. Helbert, *Polymer Composites* **1997**, *18*, 198-210.

[153] Z. Ge, F. Ye and Y. Ding, *ChemSusChem* **2014**, *7*, 1318-1325.

[154] M. Amin and K. Najwa, *The University of Queensland* **2016**.